The Thesis Committee for Robert H. Bush III
Certifies that this is the approved version of the following thesis:

Characteristics of Radially Propagating Smoldering Combustion in a Sawdust Bed

APPROVED BY
SUPERVISING COMMITTEE:

Supervisor:

Janet Ellzey

Amara Holder

Characteristics of Radially Propagating Smoldering Combustion in a Sawdust Bed

by

Robert H. Bush III, B.S.

Thesis

Presented to the Faculty of the Graduate School of

The University of Texas at Austin

in Partial Fulfillment

of the Requirements

for the Degree of

Master of Science in Engineering

The University of Texas at Austin

December 2015

Dedication

I would like to dedicate this to my parents. They have always been a source of encouragement and stability when I needed it most. A debt of gratitude is also extended to my friends who have remained consistent in their support and prayer when experimental pursuits seemed most stressful.

Acknowledgements

I would like to thank my advisor Dr. Ellzey for her consistent direction and invaluable depth of knowledge, Amara Holder for being willing to provide her industry and experimental knowledge for both experimental work and editing the contents of this thesis, and Dr. Hildebrandt-Ruiz for her insight into physical chemistries and parallel experimental pursuits that could support future work.

An incredible debt of gratitude is owed to the undergraduates that contributed to the experimental work over these years Jeremy King, Brad Resh, Elizabeth Anderson, and Jonathon Vineyard.

A special thanks to Aaron at Precision Craft Woodworks for providing sawdust with very little lead time and always being accommodating to the need for homogenous samples.

Abstract

Characteristics of Radially Propagating Smoldering Combustion in a Sawdust Bed

Robert H. Bush III, M.S.E

The University of Texas at Austin, 2015

Supervisor: Janet Ellzey

In this thesis, experimental work on smoldering of sawdust beds is presented and discussed. Extensive study has been done on wood burning cookstoves with an emphasis on performance characterization and optimization. Few studies, however, have focused on the smoldering process with the goal of understanding the propagation of the front and the production of emissions. In this study, photographs, temperature and emission measurements on smoldering sawdust clearly showed the evolution of the combustion process: an initial conversion of the raw sawdust to char followed by the conversion of sawdust to ash. In general, the char front propagated symmetrically in the radial direction while the ash front was not symmetric, and typically followed paths where oxygen was most readily available. Further analysis was accomplished by observing the characteristics of the sawdust bed before transition to flaming occurred. Contrary to expected results, flaming did not occur as the air flow was increased, but rather once it was decreased, suggesting that flaming is determined by a balance between generation of volatiles and dilution by incoming air. Experiments with vitiated air, in which the oxygen content of air

is diluted by adding nitrogen, were conducted to determine a limit at which combustion was no longer self-sustaining. Experiments showed that vitiated air with 7% oxygen in the supply air did not support self-sustaining combustion.

Finally, a comparison between poplar and walnut was conducted to show the effect of wood species. Comparison of temperature, hydrocarbon, and carbon monoxide outputs identified characteristic differences between the poplar and walnut species.

Table of Contents

List of Tables

List of Figures

Chapter 1: Introduction

Wood has been a long standing source of fuel for humanity. As such, it has been utilized to produce heating for industrial production, residential heating, and individual cooking needs. In developing and underdeveloped nations, wood as a fuel source tends to attract more use due to its abundance in supply and regional accessibility as compared to alternative fuel sources. Globally, over two billion homes use some form of biomass: dung, agro crop residue, or wood [1]. Biomass, as a source of fuel for individual and residential use, has also seen a rise in the developed countries of central and northern Europe [2], with wood being a commonly selected fuel [3]. Utilizing this resource as a fuel source is seen as mostly sustainable as it is renewable and is considered carbon neutral.

Consideration for the use of wood as a fuel source extends beyond the CO_2 footprint. The study of the health effects from using wood cook stoves has begun to take on new life with regard to the emission properties. Particulates, carbon monoxide, and hydrocarbon emissions impact individual health and the environment [2]. The particulate matter considered dangerous to human health consists of anything under ten micrometers (PM_{10}) in diameter [4], and anything under $PM_{2.5}$ is considered significantly dangerous to the point of causing illness leading to death. Furthermore, hydrocarbon and carbon monoxide build-up in improperly ventilated homes, for areas where biomass combustion is a staple resource, further endangers the health of the residents. These homes are relatively more prevalent in underdeveloped and developing nations globally than that of regions of economic prosperity [1]. Carbon monoxide can cause loss of consciousness and death if exposure to levels exceeding 6400 ppm or 3200 ppm lasts for longer than 15 or 30 minutes, respectively [5].

Unburnt hydrocarbons also contribute to the global warming potential more substantially, on a volumetric basis, than that of the reduced CO_2 emissions resulting from biomass combustion. Methane, a majority constituent within unburnt hydrocarbon emission in incomplete wood combustion, has 25 times more global warming potential effects, over a 50 year period of time, than that of CO_2 [6].

The physical and chemical properties of wood can vary significantly based on the physical form, whether it be logs, briquettes, compressed sawdust pellets, or loose sawdust. Sawdust combustion, like all biomass, can be controlled to maintain intense heat or smolder by increasing or decreasing air-flow. This option provides the user with either higher heat outputs or longer heat sources, depending on the individual usage.

Combustion of biomass may occur either as high temperature flaming combustion or lower temperature smoldering. Wood smoldering and pyrolytic effects occur below 300°C [7]. Piloted ignition of wood occurs about 350°C, and spontaneous ignition occurs at approximately 600°C. Devices, such as cook stoves, in which the production of heat over long periods of time is desirable, are generally operated in the smoldering regime. Seen from the combustion reactions observed within this report, and other studies [8], smoldering combustion stoves tend to produce useable cooking heat for 3-5 hours depending on the rate of air flow and stage of combustion in the stove.

The smoldering combustion process for wood and sawdust has had some experimental study with respect to emissions and health effects, as discussed previously. Much of the work has focused on the performance of cook stoves [8] [9] [10] with the goal of increasing efficiency and decreasing emissions. In contrast, however, much of the fundamental understanding of smoldering biomass, particularly, sawdust is lacking. The intent of this thesis is to expand the understanding of radially propagating smoldering combustion in packed beds of sawdust. The knowledge from this study of smoldering

combustion characteristics will further develop the relationship between hydrocarbon and carbon monoxide gases, the stages of combustion, along with characteristics of combustion within ovens utilizing sawdust combustion.

Chapter 2: Background

In this chapter, the basic characteristics of the sawdust will be presented along with a general discussion of smoldering combustion.

2.1 Wood Composition

Basic wood consists of 50% cellulose ($C_6H_{10}O_5$), 25% hemicellulose impregnated with 25% lignin [11]. The latter two constituents have multiple variations of chemical make-up, but all three are made up of carbon, hydrogen, and oxygen atoms. The characteristics of pyrolysis for the constituent parts are thoroughly characterized by Yang et al. [12].

Three species of wood were used in the current study: mesquite, poplar, and walnut. Early experimentation utilized mesquite sawdust while a permanent source of sawdust was being secured. The mesquite sawdust was studied, in greater detail, in the thesis of Jenny Lo [13]. All sawdust was obtained from local lumberyards or woodworking shops. The poplar and walnut samples were generated by sanding and planing in cabinet production. Samples of poplar and walnut were sent to Galbraith Labs (Knoxville, TN) for proximate and ultimate analysis to characterize the constituents of poplar and walnut Table 1.

Species of Wood	H	C	N	O
Poplar	8.0%	58.9%	0.5%	34.1%
Walnut	6.0%	47.1%	0.2%	48.4%

Table 1: Ultimate Analysis for Constituents of Studied Sawdust Species

The ultimate analysis is based on a weight percentage of C, H, O, N, and S. Sulfur was not of measureable quantity, less than 0.05%, for the significant figures in which this data is presented for either wood sample. Both species were dried before ultimate analysis for 48 hours in 110°C drying oven. Methods for the analyses adhered to ASTM standards.

Species of Wood	Volatile Matter	Fixed Carbon	Ash	L.O.D.
Poplar	88.3%	10.9%	0.6%	2.8%
Walnut	87.9%	10.4%	1.0%	6.5%

Table 2: Proximate Analysis for Constituents of Studied Sawdust Species; Loss on Drying (L.O.D.)

Proximate analysis gives the weight fraction of moisture and volatiles which include the tar, char, and ash. The proximate data is accomplished using the same methods for ultimate analyses, except for the loss on drying (L.O.D.) which was acquired using the sample as received, to determine the amount of moisture in the sample. It should be noted that a pre-dried sample was sent and sealed in plastic bag, as received. Effects of re-hydration are assumed to have occurred to some degree during transport.

2.2 SMOLDERING COMBUSTION

General combustion requires a fuel, an oxidizer and an ignition source. When these three elements are combined in the correct proportions, a combustion reaction will occur. For complete combustion of a hydrocarbon with air, the fuel is entirely consumed by the oxygen in the air and the products are only carbon dioxide and water. However, even a pure hydrocarbon flame will have some amount of products associated with incomplete combustion.

Wood, in contrast to a conventional hydrocarbon, has non-reacting mineral constituents that do not combust within any environment, no matter how well balanced the oxidizer proportion may be [14]. These resulting minerals are termed ash. Incomplete combustion yields products that are considered environmentally caustic: carbon monoxide (CO), nitrous oxide compounds (NOx), unburnt hydrocarbons (HC), and particulate matter.

Combustion of wood particles is further broken down into two distinct processes: flaming and smoldering. Self-sustained smoldering combustion will be the focus of this study. The process of self-sustained smoldering involves an ignition source, after which the combustion process is sustained by exothermic oxidations of the fuel. Smoldering combustion is characterized by two main fronts. The initial front converts the raw wood species into a carbonaceous "char" [15] by either a pyrolytic, endothermic reaction (Rxn 1) or an exothermic fuel oxidation (Rxn 2) [15].

$$fuel \rightarrow char + volatiles \qquad (Rxn\ 1)\ Endothermic\ Pyrolysis$$
$$fuel + oxidizer \rightarrow char + volatiles \qquad (Rxn\ 2)\ Exothermic\ Thermal\ Oxidation$$
$$char + oxidizer \rightarrow ash + volatiles \qquad (Rxn\ 3)\ Exothermic\ Char\ Oxidation$$

The process of char conversion requires a higher activation energy, than that of the wood, and therefore occurs when the bed has either transitioned to flaming or enough heat has been generated by the exothermic reactions to drive the char to ash reaction (Rxn 3).

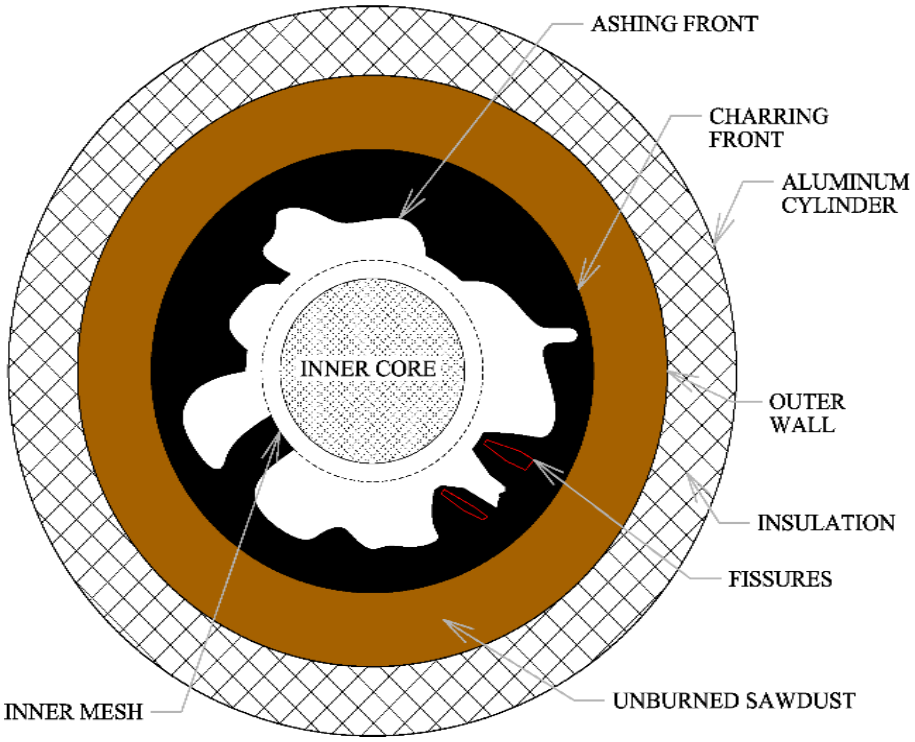

Figure 1: One-Dimensional Sketch of Charring and Ashing fronts

Figure 1 illustrates the defining characteristics of the smoldering combustion observed in the current study. The fuel is an unburned packed sawdust bed. As heat propagates radially outward, the unburned sawdust is converted to char. This charring front continues to propagate outward from the inner core where further oxidative reactions begin to convert the char to ash. As the bed experiences significant mass loss, fissures form which provide additional pathways for airflow, and further oxidative reactions to occur. The detailed characteristics of these fronts are discussed in section 4.3.

2.3 Factors Influencing the Design of Smoldering Combustion Chamber

As discussed in the introduction, the wood stove is commonly used throughout the world. The purpose of the current study is not to design a stove or analyze the performance of a particular design. Rather, the purpose is to provide more fundamental insight into the

characteristics of smoldering of sawdust. Therefore a simple and easily replicable geometry was chosen, an annular bed with a central core through which air flowed. This geometry, however, is similar to some "practical" stoves that use sawdust as a fuel.

There are a variety of means to initiate a combustion front in a sawdust bed, and the initial conditions potentially have important effects on the smolder propagation. In practical applications the bed may be ignited directly by a flame from a match or by exposure to a hot coal. In the second method, flaming does not occur and it was determined that this was more repeatable for the experiments. Therefore, all smoldering fronts were initiated through exposure to a hot coil. In some cases, flaming occurred accidently and the effect of this phenomenon is also discussed.

Chapter 3: Methods

3.1 Introduction to Methods

This chapter discusses the development of the testing apparatus and data collection methods utilized in the smoldering combustion process. The use of a combustion chamber was necessary to determine the effects and stages of combustion given different combustion environments. These data would then inform the type of combustion taking place given varying air-flow and speciation.

3.2 Combustion Chamber Design

The combustion chamber was developed by a previous graduate student, Jenny Lo [13]. The design was originally influenced by Dahlman and Forst's cookstove [8]. In principle the design was an aluminum cylinder, filled with sawdust, around a mesh inner cylinder creating an annulus for an induced airflow.

3.2.1 Combustion Chamber Modifications

The modifications made, were to utilize a steel combustion chamber with insulation wrap. This reduced any conductive heat loss to the environment. However, it was confirmed in previous experimental setups by Jenny Lo, with the first iteration of the combustion chamber, that the sawdust acts as a natural insulation barrier, and that adding insulation did not significantly alter the temperature measurements [13]. The insulation therefore provided a safety measure to ensure that the heat generated by the stove was isolated from the lab environment and operators.

The dimensions of the combustion chamber can be seen in Figure 2 and Figure 3.

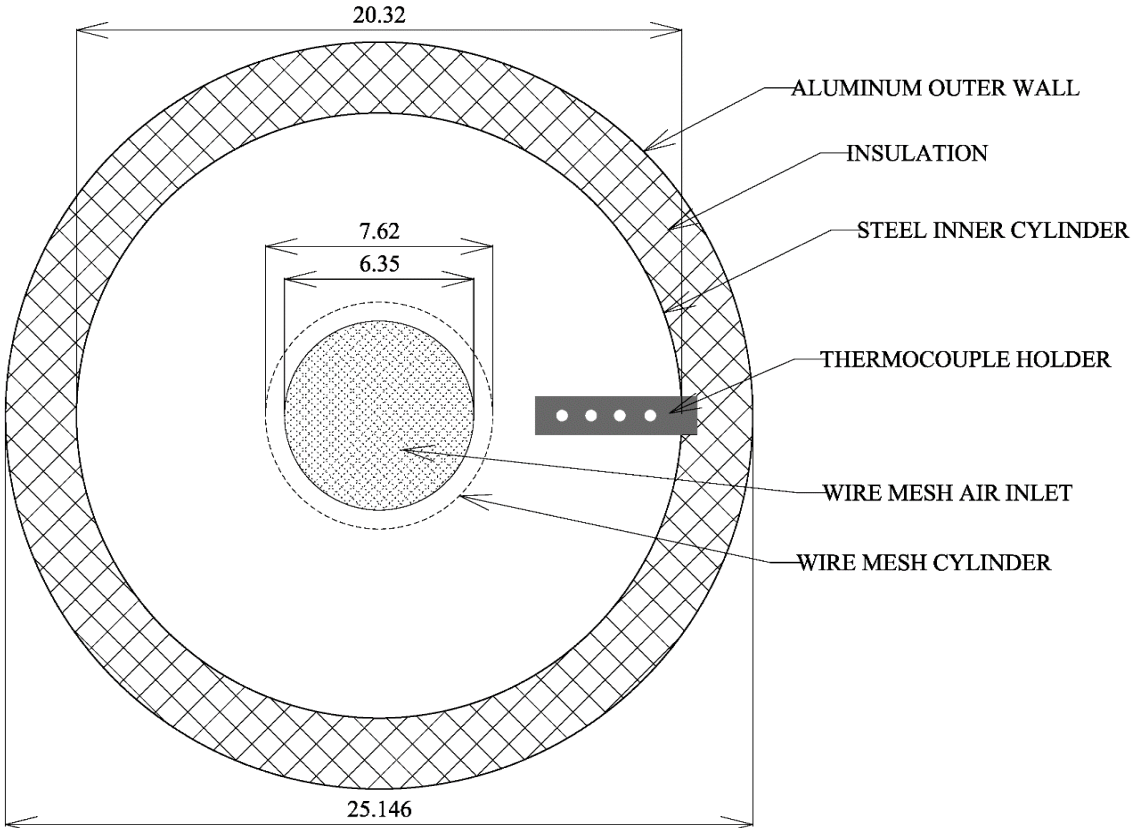

Figure 2: Top View of Experimental Apparatus; all dimensions in centimeters.

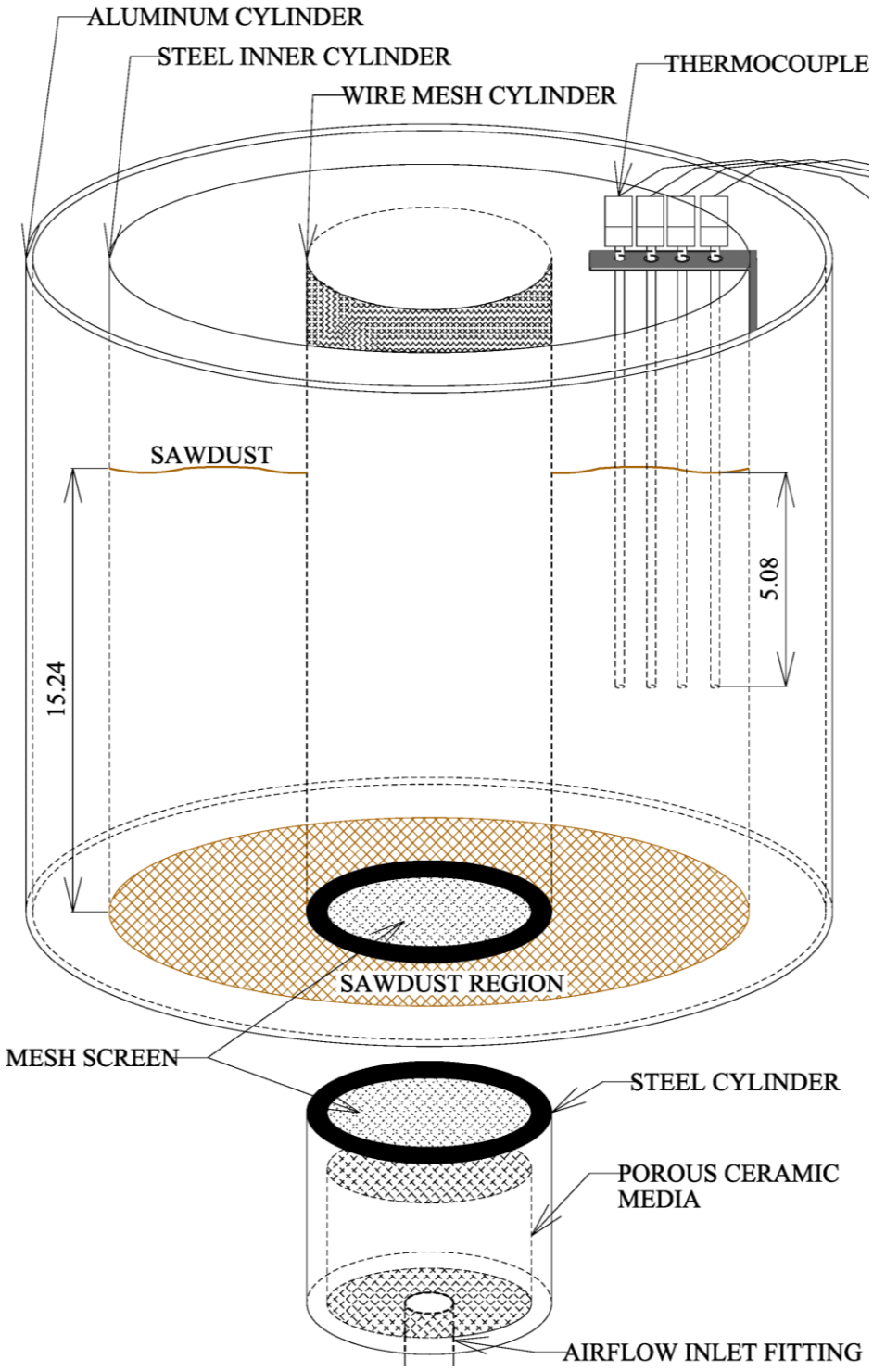

Figure 3: Isometric View of Experimental Apparatus with detached airflow inlet cylinder; all dimensions in centimeters.

Seen in Figure 2, the inner radius of the annulus, where the air enters the combustion chamber, is a 6.35 cm diameter, stainless steel mesh. This was made to ensure the ash did not block the diffuser area of the air inlet. Another mesh was spot welded in a 7.62 cm diameter cylinder that extended vertically through the chamber, seen in Figure 2 and Figure 3. This mesh was used to ensure that the sawdust compaction maintained the structure around the inner diameter of the annulus, as well as provide a region to remove an ignition coil without disturbing the sawdust bed.

Heat tape, Omega 624 watt dual-element heating tape, was wrapped around a two inch stainless steel cylinder to initiate the smoldering front. The heat tape was attached to a 120 volt AC variac to control the temperature output of the heat tape. The coil acted to imitate smoldering ignition at the point of contact with the sawdust and mesh interface.

The use of an inner steel cylinder within the aluminum outer cylinder was also incorporated within this iteration of combustion chamber. This afforded the experiments an insulation barrier around the steel cylinder between the outer aluminum cylinder. Once the smoldering front was established, an aluminum chimney was added to reduce the effects external airflow conditions could have on the smoldering front.

A chimney was attached to the top of the combustion chamber to mitigate the effects of external air flows. The chimney also forced the emissions into a more concentrated focal point from which samples were drawn, to help with the external HC and CO measurements.

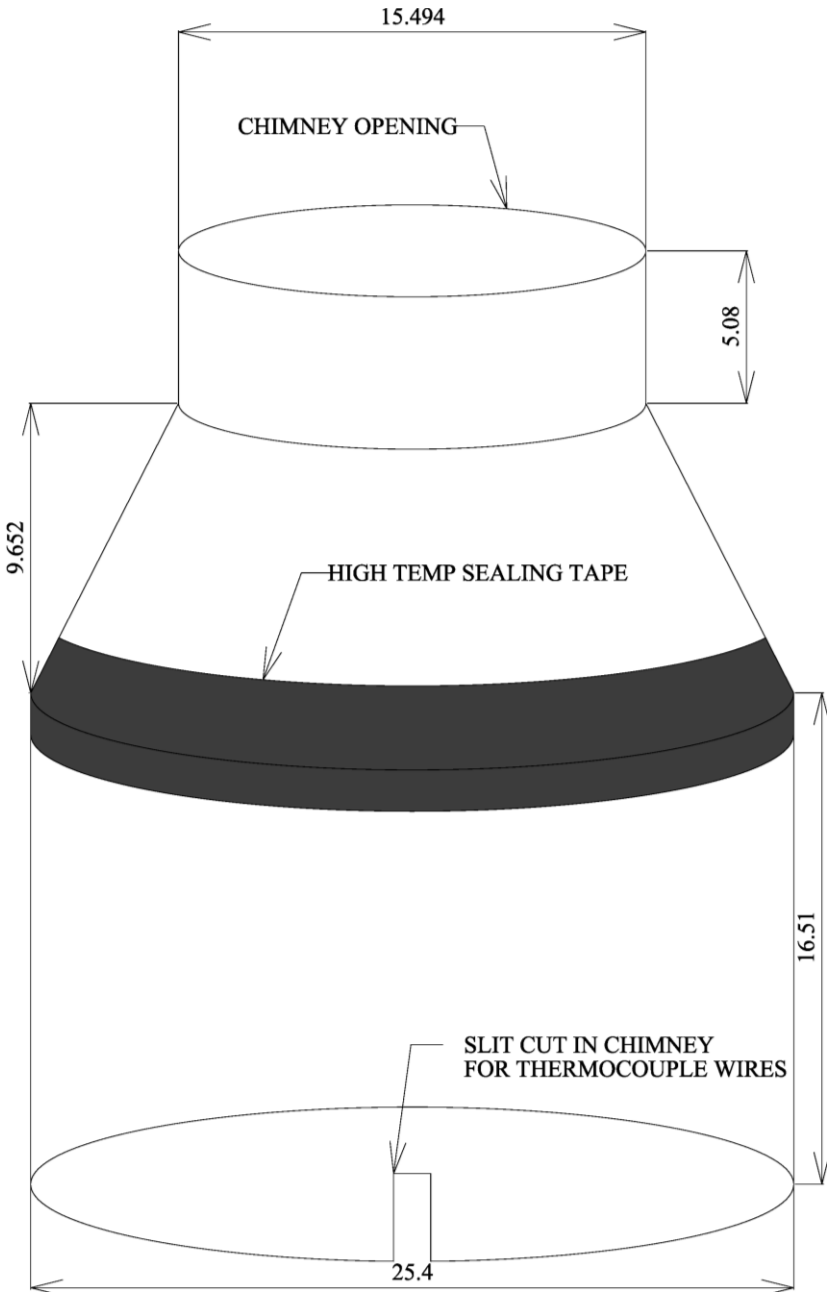

Figure 4: Chimney Top for combustion chamber; all dimensions in centimeters.

The chimney top was just slightly larger in diameter than the combustion chamber so that it could be easily installed over the stationary combustion chamber, after the ignition coil was removed.

3.2.2 Combustion Inlet Air

The combustion inlet air used for the project was measured using a digital airflow controller, Omega FMA-2607A, 0-10 SLPM. This connected through the airflow inlet fitting as seen in Figure 3. During the transition to flaming experiments, discussed in section 3.5, the incoming air also used a manual needle valve to control the air flow beyond those levels allowed by the digital controller.

The air was maintained at a relatively constant temperature from ignition to completion, varying by less than one degree Celsius. However, from day to day, the temperature of the inlet air could vary from 24 to 29 °C.

Latter experimentation required the analysis of smoldering with modified oxygen content, as discussed in section 3.6.4. This was accomplished by introducing an added load of 100% compressed nitrogen, from AirGas, into the inlet stream. By utilizing a three-way tee fitting, a rotometer, and the previously discussed Omega flow-controller, the nitrogen was added at varying ratios. This served to modify the effects of the stoichiometric fuel-air ratios by reducing the oxygen supply through increased nitrogen supply.

3.3 Sawdust Formulations and Experiments

The sawdust speciation in early experimentation was based on what was left over from the previous study of sawdust smoldering. This was untreated mesquite wood acquired from Berdoll Sawmill. Intermediate and final experiments were taken utilizing poplar or walnut from Precision Craft Woodworks of Austin, Texas. All sawdust was dried with a 120W lamp inside a wooden box lined with radiant barrier insulation. The sawdust was left in the drying oven at minimum of 24 hours. Results of sawdust drying can be seen in section 4.2.1.

The sawdust, when added to the combustion chamber, was added in 500 mL quantities, and compacted using a 5.08 cm diameter glass tube with a capped end. The

sawdust was added using a 500mL beaker. When added, the sawdust was uncompressed in the beaker as this would reduce human variations in quantity between operators. The layers were spread evenly and tamped to ensure the sawdust was compacted in the tightest possible arrangement. The layers were added until a depth of 15.2 cm of sawdust had been achieved. The theoretical volume of space the sawdust could fill was 4.25 Liters. Based on the aforementioned dimensions of the combustion rig and the diameter of the wire mesh. The volume was determined using equation #1.

$$V = \pi h(r_1{}^2 - r_2{}^2) \quad [1]$$

Where r_1 is the size of the outer radius, and r_2 is the radius of the inner circle within the annulus.

3.3.1 Sawdust Sizing

An identifying characteristic of the sawdust selection was the particle sizing. It was necessary to determine the particle size, because this composition effects the density of compaction which can affect the smoldering propagation. Based on the photo and temperature cross-referencing accomplished in early experimentation section 3.4.3, 'Charring and Ashing Front', the density of compaction contributes to the speed of propagation of the oxidative front through fissures or cracks in the sawdust bed, which further supplies oxidizers to drive the smoldering front. Ohlemiller's study of buoyant forces within vertically propagating smoldering reactions eludes to the significance of compaction densities as to the propagation of smoldering [16]. The more porous the material, the more effectively oxygen is transported to the smoldering front, inducing oxidative reactions further driving the proceeding reactions. The same assumptions were tested within the radial propagation of smoldering. This concept will be further discussed in section 4.3.

The process of identifying particle size was first accomplished by characterizing a random sample of the mesquite sawdust at micro-scale measurement, utilizing a Scanning Electron Microscope (SEM). This required dabbing, within a randomly selected sample tray, an adhesive disk to apply to a mount. From there the particles on the disk were coated with a nano-powder of gold to create a contrast between the adhesive and the particles of interest. This mount was inserted within the SEM and from there multiple photographs were taken across the span of the disk to try and get a full characterization of the sample. These pictures can be seen in Appendix A.

Once the range of particle sizes were determined from the SEM measurements, sieve trays were ordered to quickly characterize composition of the entire sample within the packed bed of the combustion chamber. The sieves were ordered from Shanghai Shangshai Bolting Cloth Manufacturing Co., Ltd.. The sieves were stainless steel and the mesh adhered to the ASTM E11 for the size of aperture. Sieve sizes for analysis can be seen in Table 3.

Sieve Mesh Number	Sieve Opening (Microns)
5	4000
8	2380
12	1680
45	354
50	297
60	250
80	177
120	125
170	88
270	53

Table 3: Sieve Sizes for Particle Sizing

These tray sizes afforded a standardization of the sizing process. The trays were first weighed individually. The particle size was determined by placing the trays stacked

in descending size order, from largest to smallest in mesh size. After stacking the trays, an empty bowl was placed at the bottom of the trays to have a final catch for the remaining particles below 53 microns.

The particle size distributions were standardized based on bin size, which is the range between the selected and the previous trays mesh openings, as discussed by Hinds [17]. The process of standardizing by bin size started by taking the difference between the lower and upper bound of the selected tray range. After which, the mass percent was divided by the calculated range to produce the average frequency per mm of the particle sizes within the bin. The standardization can be seen in equation 2.

$$\frac{\frac{m}{M} * 100}{(Tr_{pr} - Tr_{sel})} = Frequency\ of\ Particle\ Diameter/bin \qquad [2]$$

Where m is the mass of sawdust in the selected tray, M is the total mass of the sample before sieving, Tr_{sel} is the mesh size of the selected tray, and Tr_{pr} is the size of the mesh for the previous tray.

Sawdust samples were placed in the same location in the oven and dried for 24 hours. Sawdust was added to the topmost tray and then a sheet of metal was added to act as a lid to the top tray. The trays were then hand shaken to ensure that the particles were given as much mixing and shifting as possible. Since particles naturally separate themselves vertically from largest descending to smallest particles on the bottom, this method was determined an effective first mix. After hand shaking, each tray was stirred with a metal probe to sift through and manually mix any remaining unseparated particles. This secondary mixing was performed before each tray was measured. The imprecise mixing process and the potential for human error within the manual mixing done with the metal probe should be improved upon in subsequent experiments. Improvements to the mixing process can be made utilizing an industrial sieve shaker.

The sample was determined by the amount in a randomly selected tray from the drying oven. The total mass of the sawdust in the randomly selected trays varied from 109 grams up to 163 grams. Each tray was measured individually to determine the separated mass. The imprecision of the scale was a limitation of the sawdust drying measurements. The measurements for the lower particle sizes lacked the precision necessary to achieve measureable amounts. These results however were expected to be at, or below, one gram. Therefore, the proportionality of the particles would likely not be effected by more than the standard deviation.

The particle sizes can be seen in section 4.2.1.

3.4 EARLY EXPERIMENTATION

The equipment used on this project was developed from knowledge gained in early experimentation. The project was influenced by the earlier work of Lo et al. [13] and modifications in the apparatus and equipment were made as needs evolved.

3.4.1 National Instruments Data Acquisition and Processing

Utilizing National Instruments' (NI) LabVIEW programming environment and NI hardware an array of eight thermocouples were used to establish the radial symmetry of the smoldering front. Type E thermocouples were connected to an NI CB-68LP also known as a data acquisition device (DAQ).

The DAQ was connected to the computer through the NI PCI6024E, which was connected using the factory installed onboard bay extensions for the computer. This PCI was then read in the LabVIEW software environment where the data from the eight thermocouples was written into a LabVIEW proprietary software packaging file called a .TDMS file. The TDMS file could be packaged or unpackaged in the LabVIEW environment, but was also readily viewable in Microsoft Excel with the use of a NI

downloadable extension for windows machines. The data was concatenated in such a way that each thermocouple was read simultaneously for a given timestamp, then output to the TDMS file two times every second. This ensured precision of measurement without creating a file too large to manage.

LabVIEW is a visual coding environment, the detailed back-end of the circuit had to be designed from scratch and can be seen in Appendix B. However, a front-end virtual interface (VI) seen in Figure 5, was created for a wide array of user experience and background with NI software.

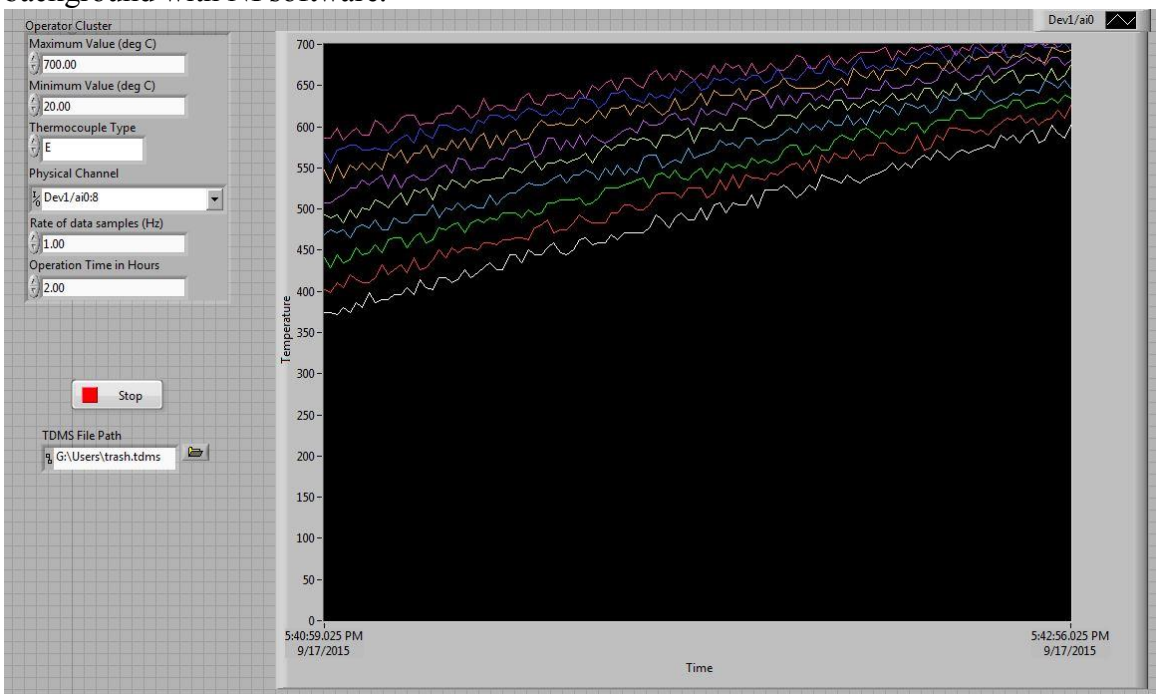

Figure 5: Front-End of National Instruments LabVIEW Virtual Interface

The back-end was written with the intention that the user would not change the rate of data collection once established. The front-end allows the user to specify the type of thermocouple, the duration the VI should run to collect data, the number of thermocouples and the specific channel they are connected to on the DAQ, and the expected temperature

ranges. These upper and lower limits of temperature were programmed with the intention to attenuate the error readings that sometimes were encountered when the thermocouple wires were nudged or pulled during the course of data acquisition.

A common error occurred when the use of the VI without all of the proprietary DAQ based VI's having been properly installed. This meant that the VI could not properly process the acquired information. The resolution was often to create the necessary subVI routines from scratch, or to ensure that the install routine was fully successful. Along with this error, if the created control (.ctl) files were not present, the VI user interface would not load correctly, which would not render the VI useless, but would not allow the unfamiliar user access to running the VI routine.

3.4.2 Radial Symmetry Verification

Jenny Lo provided radial symmetry verification within her report [13]. In the study of the sawdust smoldering process, radial symmetry of the smoldering front was furthered by cross-comparing the temperature responses and video capture utilizing the Logitech b910 webcam.

3.4.3 Charring and Ashing fronts

One of the significant accomplishments of early experimentation was the confirmation of slopes and peaks with respect to thermocouple response and the cross-referenced visual data. This was done by utilizing the same apparatus in Figure 3, in conjunction with a time-synced webcam, to produce visual cues of where the front positions corresponded with a temperature inclination or peak. In confirming these results, the time of analysis was reduced from 4-5 hours, down to 2 hours per test. This was done by observing that when the thermocouple response started to decline, the thermocouple became exposed to the convective heat present in the chamber, and was no longer

influenced by the exothermic reactions taking place along the ashing front. The solid bed had compacted or fallen away from the thermocouple and therefore no longer represented the temperatures of the smoldering solid. However, a relatively slow rate of temperature increase can be influenced by the retarded rate of decomposition of the sawdust bed, with respect to the volume, in the area surrounding the thermocouples. This resulted in an insulation near the thermocouples that registered the effects of the surrounding smoldering combustion through conductive heat transfers through the bed, rather than a typical temperature profile that indicates exposure of the thermocouple tips. This analysis can be confirmed in Section 4.3 and 4.6.

3.5 TRANSITION TO FLAMING

This section of the report will discuss the further development of the testing procedure to produce consistent smoldering combustion. The confirmation of the transition point from smoldering to flaming was assumed to be based on a potential airflow. This assumption was informed by earlier experiments when it seemed like transition was happening based on increasing airflow through the central annular core. After multiple tests a confirmed transition point was resolved, along with new assumptions on what effects transition to flaming.

3.5.1 Rig Modifications

To determine the transition to flaming, it was necessary to modify the experimental rig to try and reduce the amount of sawdust wasted in each experiment. The reduced sawdust volume afforded more tests with the same blend of sawdust. The modified pipe was reduced from a diameter of 20.3 cm to 15.2 cm schedule 40 steel pipe. The height of the pipe was cut to 22.9 cm, to be slightly higher than the existing rig height at 20.3cm. This made it easier to suffocate the flaming when transition occurred. The sawdust was

filled to a height of 15.2cm. The steel pipe was placed inside of, and axially centered with, the existing combustion chamber. The ignition and airflow setup was then maintained in the same environment as discussed in section 3.2.1.

The webcam was placed over the top of the combustion rig looking at an 80-90 degree angle depending on whether the chimney was used (90 degrees when chimney was placed over the top). Tests were performed with and without the addition of the chimney top to confirm whether external airflows and the open environment would directly affect the transition to flaming.

3.5.2 Testing Procedure for Transition to Flaming

Transition to flaming tests, first started by verifying the volume of sawdust being analyzed. The sawdust was filled to a height of 15.2cm, and the volumes of added sawdust varied from 3300-3700 mL. This was largely due to compaction densities, but could also be due to the drying effects and variation of average particle sizes.

The heat coil was removed after the charring front was established. Upon removal, air flow was initiated through the central core. Airflow was increased in increments of 0.25 liters per minute (lpm), every 2-3 seconds, from 0 lpm to 10 lpm. Once at 10 lpm, the digital flow-controller could not be used. A needle valve was placed in parallel with the digital flow controller so as to allow for the maximum flow rate from the air supply, approximately 50 lpm. The needle valve was slowly opened over the period of one minute, equating to approximately half a turn every five seconds. Once the needle valve had been fully opened, the airflow would then be turned back down, on the needle valve, until fully dependent on the digital flow controller. Then the decrease would continue using the same 0.25 lpm every 2-3 seconds from 10 to 0 lpm.

If transition occurred at any point during the test, a 0.635 cm thick steel plate was placed over the top of the combustion chamber to extinguish the flames. Once the flames were extinguished, if enough fuel remained in the testing bed, a second attempt at flaming was made using the same procedure as stated before, utilizing the continued combustion process. The second attempt was made to assess whether the effects of an already established charring would make a difference on when and if the combustion process transitioned. The results of the transition to flaming and the information gleaned from these tests can be seen in section 4.5.

3.6 Final Experimental Analysis

Experience gained with early experiments led to the development of a hybrid of the data collection processes found in the European (EN-13240) and US (EPA: Method 5G and Method 28) Emission Collection Standards [9] [18]. Furthermore, the analysis resulted in the development of a temperature, CO, and HC measurement process to afford perspective on the smoldering combustion process. The process of sustaining a pyrolytic reaction required the use of nitrogen to modify the fuel-air mixture to produce a combustion that would not transition to an oxidative reaction. If transition did occur, the study of the oxidative response, and slope of the temperature within this oxidative reaction, was compared to the case of the previously studied responses where the pyrolytic reactions were sustained.

3.6.1 Carbon Monoxide analysis Standardization

In order to compare results, a standard location for the CO measurements was required. It was determined that the sample should be drawn as close as possible to the outlet of the chimney. A fixed metallic probe with a thermocouple attached to the probe was placed over the outlet of the chimney. A rubber tube with a fixed condensation

chamber was attached to the end of the probe and provided a removable connection for a portable, handheld CO analyzer, the TPI 707 Carbon Monoxide Analyzer. The analyzer was calibrated by the manufacturer, using 1001 ppm CO/3% Oxygen/Balance Nitrogen.

The collection of data was taken by averaging the readout on the CO analyzer over the course of twenty seconds. A reading was recorded ten times to average out a fluctuating CO readout. In addition, the CO analyzer outputs a peak from the period of analysis. These two data points, the average and the peak, were seen to be a consistent separation, and offered the same general trend line. It was decided to use the average CO readout with respect to final analysis.

CO measurements were taken every 10 minutes after the chimney hood was added. The duration of the measurements continued until the experiment is complete.

3.6.2 Hydrocarbon analysis Standardization

Measurement of HCs required extensive addition to the emission collection process. The HC analyzer used for the experiment was a Rosemount Model 400A Hydrocarbon Analyzer [19]. The foremost design constraint was to ensure that the analyzer would not process anything within the emission product that could serve to cause malfunctions within the system. The method selected to ensure that no condensable or particulate matter could pass though the sample line was based on the experimental setup by Ortega [9]. This was first introduced as an option based on the experimental setup established by Yelverton et al. [20] with regard to the EPA study of emissions within diesel gensets. The experimental design within Yelverton et al.'s project utilized a cold box and thimble filter to reduce the condensed matter within the sample stream. The cold box was made up of a dry impinger train submerged within an ice bath. The impinger train within the experimental setup can be seen in Figure 6. The impinger train was utilized to settle out

or condense particulate matter or tar, respectively, within the sample gas (referred to as condensables). The impingers were submerged within a chilled water bath that was initially chilled using a continuous flow chilling machine, a ThermoFisher ThermoFlex 5000 Recirculating Chiller. This machine required a closed loop flow system which meant that a copper tubing in a serpentine arrangement was used to create maximum surface area exposure within the chilled water bath. Due to the inconsistency of the machinery, the chilled water bath was ultimately achieved by pouring ice directly into the bath in which the impingers were submerged.

Entering the impinger train was a strand of copper tubing which served as a probe within the emitted smoke. The entry of the tube was placed directly over the chimney's axial center. The copper tubing was also wrapped with 624 watt heat tape. The heat tape covered the majority of the exposed outer surface of the copper and was directly plugged into a 120 VAC source. The copper was kept near 200 degrees Celsius to ensure that the temperature difference between the walls of the impinger and the entering gas was significant enough to cause condensation.

The selection of three impingers in-line was based on Method 202 of the EPA's Dry impinger method [21]. The impinger design was modified based on the capabilities of the University of Texas Glass Shop. The individual glass pieces were procured from ACE Glass, item 7648.

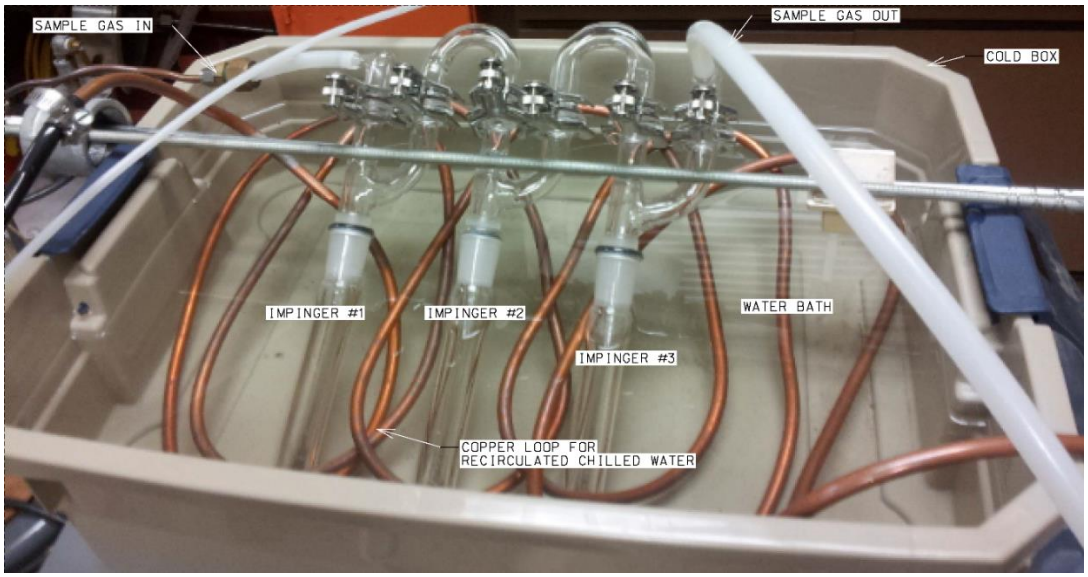

Figure 6: Impinger train within Cold Box.

Figure 7: Impinger Train Side View

As seen in Figure 6 and Figure 7, Impinger #1 and #3 have inner cylinders that were designed to be structurally similar. These impingers have one millimeter slits cut into the sidewall of the glass at staggered intervals for the bottom four centimeters to allow for the air to flow out and spread along the outer tube walls which are in contact with the chilled water. Impinger #2 was constructed to include one millimeter holes which provided a different flow effect. The modified impinger #2 also served as a secondary filter for any macro particles still in the sample gas.

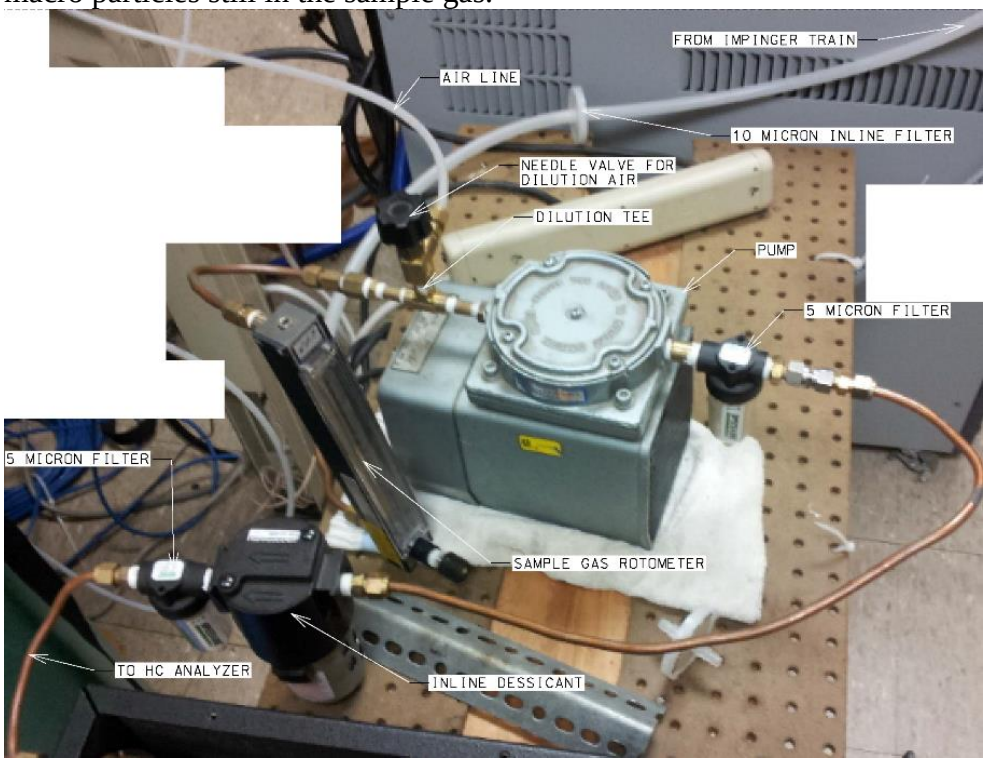

Figure 8: Pump, Dilution, and Filter Arrangements between Impingers and HC Analyzer

The arrangement of the devices following the Impinger train can be seen in Figure 8. The gas flowed through a polypropylene, 50 mm diameter, 10 micron pore size, in-line, disposable air filter, produced by Whatman. This filter served to remove any remaining macro-particles and tars that could stand to damage the HC analyzer.

Following the in-line filter was a 150-mm Cole-Parmer Correlated Rotometer, which afforded flow rates up to 16.737 lpm. This flowmeter preceded a three way tee in which a standard air-line was attached with the same flowmeter and a needle valve near the tee. These flowmeters acted as a control for the point of dilution within the three way tee. The dilution for the region of study was considered unnecessary after two preliminary tests in which the dilution of the sample gas was gradually reduced to zero, and the HC analyzer showed no issue with the analyte.

The sample gas was drawn off from the chimney utilizing a Gast DOA-P135-AA diaphragm pump. The pump flow-rate was metered by the rotometer mentioned above.

A five micron Speedaire, 4ZL08, Compressed Air Filter was at the pump outlet to ensure that no particles were in the flow. Due to the temperature change through the diaphragm pump, an in-line desiccant dryer, Wilkerson X06-02-000, was also added to ensure no condensation entered the sample chamber of the HC analyzer. One more five micron Speedaire filter was added after the desiccant, before the sample gas entered the HC analyzer.

The analyzer could only support pressures between 3-5 PSI. So, the bypass needle valve within the instrument was kept open slightly to ensure the pressure within the system was not too high. The analyzer was calibrated using a calibration gas of 100 ppm methane, balance air. The fuel mix for the analyzer was a 60% Helium/40% Hydrogen compressed gas mixture from AirGas. The air supplied to the analyzer utilized an Airgas zero grade air.

3.6.3 Forced Convection through Modified Air Supply

The preliminary data of CO and temperature were taken on multiple experiments of the poplar sawdust. Visual data was collected with time-synced video capture.

Airflow was supplied at different flow rates to determine the effects of modified convective forces on the smoldering fronts. Airflows were varied from 3 to 10 lpm, an airflow velocity of 0.011 to 0.037 m/s within the core. The use of air was intended to control the inherent variability of no flow convection conditions. Standard airflow rates could be applied across any species or compaction density.

The ignition coil was removed after the charring front moved approximately 0.5 centimeters from the ignition coil and mesh interface, or just enough that it was visually verified to be propagating on all sides of the mesh. This distance is determined by visual cues of the charring front, and typically occurs between 7 to 10 minutes. If the front was allowed to propagate too far from the ignition coil, before being removed, the sawdust bed was far more likely to transition to flaming, which is further discussed in section 4.5.3. Following the removal of the ignition coil, airflow was then introduced. Temperatures and CO data were collected over the course of two hours.

3.6.4 Forced Convection with Vitiated Air

To understand the effects of oxygen concentration, vitiated air, in which nitrogen accounted for a larger percent of the gas, was used.

The nitrogen was added by first observing the chemical balance necessary to increase nitrogen in the supply air, inherently reducing the effective oxygen presence. A simple estimation of the constituent oxygen in the supply air can be seen in equation 3.

$$Percent\ of\ Oxygen\ in\ Air\ Supply = \frac{x * (0.22)}{x + y} \quad [3]$$

Where x is the molar amount of air, and y, the amount of nitrogen. In the case of 3 lpm of air supplied, 6.45 lpm of nitrogen was added to result in a 14% reduction of O_2 from 21% down to 7%. The addition of nitrogen utilized the setup in section 3.2.2. A case of reduced air and nitrogen flowrates was also utilized in the same proportions to ensure the

convection with nitrogen was not acting as a source of cooling on the bed. This case utilized 1 lpm of air supplied, 2 lpm of nitrogen was added to again result in a 14% reduction of O_2 from 21% down to 7%. The nitrogen proportions in the supply was further varied to find the point in which the combustion process achieved exothermic reactions through oxidation, without entirely extinguishing the smoldering front, as in the cases of the aforementioned vitiation. This was achieved by supplying nitrogen at 1.5 lpm with 1.5 lpm air. Effectively, reducing the constituent oxygen percentage by nearly half, 11% of the supplied air. The method of finding this range was accomplished by increasing the nitrogen percentage until the value that produced an exothermic combustion was achieved. However, precision in the control system of nitrogen and air mixing, and its proportional addition as a homogenous stream, can could be improved upon. Adding a mixing chamber, before the inlet to the combustion chamber, could serve as an insurance to the quality and homogeneity of the supplied air. The experiments were initially taken over two hours, however, some were taken over three to three and half hours to better understand the delayed response time of the exothermic effects.

Further effects of the oxygen suppressed combustion process were analyzed with respect to whether a transition had taken place before the introduction of the air supply. This transition was induced by leaving the ignition coil in the inner core, too long, allowing the front to propagate beyond the 0.5 cm distance.

3.6.5 Speciation and Smoldering Combustion

Data were collected on two different wood species, poplar and walnut, to determine the effect of species properties on the smoldering process. This was accomplished by gathering the data from the unmodified air and vitiated air tests for both the poplar and walnut, and comparing the results. Both wood samples were prepared for testing in the

same way, utilizing the drying oven, measuring the particle size through sieve testing, compacting the sawdust in the combustion chamber, and finally data collection methods through the aforementioned instruments.

Chapter 4: Results and Discussion

4.1 INTRODUCTION

In this chapter, results and discussion are presented for experiments on smoldering sawdust. Early experiments provided information that led to changes in experimental setup. The data are presented in the same order as the presentation of the experimental methods in Chapter 3.

A number of tests were taken across the proceeding results that included temperature, mass loss, CO, and HC measurements during the analysis. Table 4 shows the measurements taken, species analyzed, airflow variations, and section in which the results are discussed.

Species	Air [lpm]	N_2 [lpm]	Temp	Mass Loss	CO	HC	Section Discussed
Poplar	3.0	0.0	X				4.2.2
Poplar	3.0	0.0	X				4.2.2
Poplar	3.0	0.0	X				4.2.2
Poplar	3.0	0.0	X				4.2.2; 4.6.1.1
Poplar	3.0	0.0	X	X			4.3; 4.4
Mesquite	3.0	0.0	X	X			4.3.1; 4.3.2
Poplar	Varies	0.0					4.5
Poplar	Varies	0.0					4.5
Poplar	Varies	0.0					4.5
Poplar	Varies	0.0					4.5
Poplar	Varies	0.0					4.5
Walnut	Varies	0.0					4.5
Walnut	Varies	0.0					4.5
Walnut	Varies	0.0					4.5
Poplar	Varies	0.0					4.5
Poplar	3.0	0.0	X		X		4.6.1.1
Poplar	3.0	0.0	X		X		4.6.1.1
Poplar	6.0	0.0	X		X		4.6.1.1
Poplar	10.0	0.0	X		X		4.6.1.1
Poplar	3.0	0.0	X		X		4.6.1.1
Poplar	3.0	0.0	X	X	X	X	4.6.1.1; 4.6.3
Poplar	3.0	6.0	X				4.6.1.2
Poplar	3.0	6.0	X		X		4.6.1.2
Poplar	1.5	1.5	X		X		4.6.1.2
Poplar	1.0	2.0	X		X		4.6.1.2
Poplar	1.5	1.5	X	Partial	X	X	4.6.1.2; 4.6.3
Walnut	3.0	0.0	X	X	X	X	4.6.2.1; 4.6.3
Walnut	1.5	1.5	X	X	X	X	4.6.2.2; 4.6.3

Table 4: Index of Test Iterations, Airflow Compositions, Data Collected, and Section Discussed

4.2 Sawdust Sizes and Heat Propagation

As described previously, the sawdust was obtained from local woodworking or lumber enterprises therefore there was no specification of particle size or distribution

although it is believed that these are important to the smoldering process. It was deemed necessary to document these characteristics which are presented in this section.

4.2.1 Sawdust Sizing and Drying Experiments

Sawdust size distribution was determined using multiple sieves. The sawdust particle sizes were first compared on a percent by mass basis, as shown in Table 5. To determine the effect of drying, a comparison of dried and undried is also included.

	Test1	Test2	Test3	Test4	Test6	Average Size (dried)	Standard Deviation	Test 5 undried
Total Mass	167 g	109 g	130 g	168 g	127 g			150 g
Mesh Aperature								
4 mm	1%	14%	7%	3%	4%	6%	5%	5%
2.38 mm	7%	12%	7%	4%	17%	9%	5%	12%
1.68 mm	11%	7%	8%	6%	13%	9%	3%	10%
.354 mm	78%	66%	60%	64%	50%	64%	10%	50%
.297 mm	0%	0%	7%	9%	6%	4%	4%	9%
.250 mm	1%	0%	3%	6%	4%	3%	2%	4%
.177 mm	2%	2%	5%	5%	4%	4%	2%	6%
.125 mm	0%	0%	2%	1%	2%	1%	1%	2%
.088 mm	0%	0%	2%	1%	1%	1%	1%	1%
.053 mm	0%	0%	0%	0%	0%	0%	0%	1%

Table 5: Dried Particle Size Concentrations with Undried Comparison of on basis of Percent of total Mass. Left side of the table is size of mesh opening.

Table 5 shows the percent by mass of individual tests conducted on different days. The largest mass percent, across dried samples, is in the range of .354-1.68 mm. The standard deviation is based on the dried experiments and their respective averages over the five individual tests for the specific tray size. The data illustrate that the largest average deviation in particle size for dried sawdust was in the range of .354 to 1.68 mm. That

implies that particles were larger than .354 mm, and smaller than 1.68 mm. This is likely due to the large margin between the mesh size of 1.68 mm and .354 mm.

Since the size range collected on each sieve vary, the results were normalized based on the bin size. The bin size is the difference between the previous and next aperture opening. The frequency of particles per mm of particle diameter within a bin is shown in Table 6.

	Test 1	**Test 2**	**Test 3**	**Test 4**	**Test 6**	**Average Frequency/bin**	**Std Dev**	**Test 5 undried**
Bin Range								
20-4 mm	0.1	0.9	0.4	0.2	0.2	0.4	0.3	0.3
4-2.38 mm	4.4	7.4	4.3	2.3	10.7	5.8	2.9	7.4
2.38-1.68 mm	16.3	10.5	11.0	7.9	19.1	12.9	4.1	14.3
1.68-.354 mm	58.7	49.8	45.2	48.6	37.4	48.0	6.9	37.7
.354-.297 mm	0.0	0.0	121.5	150.7	110.5	76.5	63.9	152.0
.297-.250 mm	12.8	0.0	65.5	117.5	83.8	55.9	43.9	85.1
.250-.177 mm	24.7	25.1	73.8	67.2	53.9	48.9	20.6	82.2
.177-.125 mm	0.0	0.0	29.6	23.6	30.3	16.7	13.8	38.5
.125-.088 mm	0.0	0.0	41.6	16.6	21.3	15.9	15.5	36.0
.088-.053 mm	0.0	0.0	0.0	0.0	0.0	0.0	0.0	19.0

Table 6: Frequency of particles weighted by bin size with mass mean diameter of each test and the average test. Standard deviation is calculated across the 5 dry sawdust samples

On a normalized basis, as shown in Table 6, the mass distribution appears more evenly distributed over the various bin size. The standard deviation for bin sizes .354-.297 mm and .297-.177 mm are higher due to tests 1 and 2 having little to no quantifiable mass compared to the other three tests. The undried sample does not fall within standard deviation of the average dried samples frequency below 1.68 mm. The frequencies are more concentrated within the smaller bins than the larger.

The results of the average particle frequency within each bin range are shown in Figure 9.

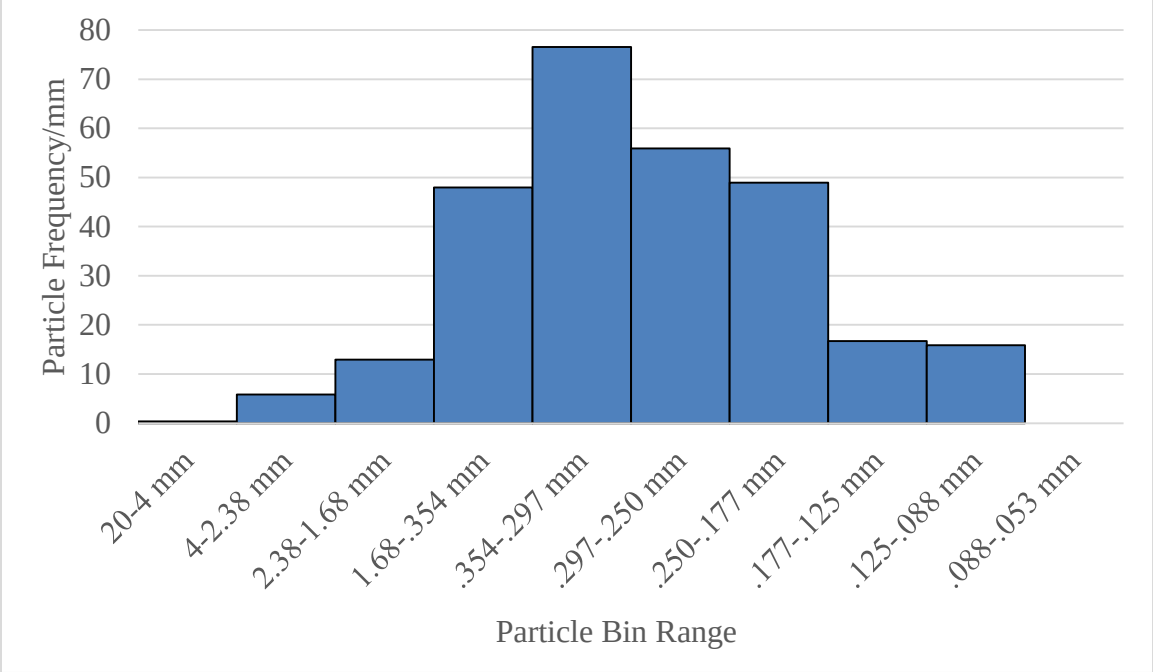

Figure 9: Average particle frequency weighted for bin size for aperture ranges in dry sawdust sieve tests.

The bin weighted particle frequency shown in Figure 9, indicates a nearly normal distribution across the bin ranges. The highest frequency of particles per mm with respect to the diameter of particles observed during sieving is between .354 and .297 mm. This indicates that ~80% of the sawdust will likely be between the sizes of .177-1.68 mm for tests using the same poplar population.

When drying the sawdust, the mass loss over a 24 hour period was on average 5.5% of mass. After one week of drying the mass loss only decreased 5.9% of original mass. Therefore, it was decided that 24 hours of drying was sufficient for these experiments.

4.2.2 General Behavior of Smoldering Front

Smoldering experiments were conducted using the poplar sawdust characterized above. Air flow of 3 lpm was introduced into the central core as described in section 3.2.2. This volumetric flow translates to an average velocity in the core of 0.011 m/s.

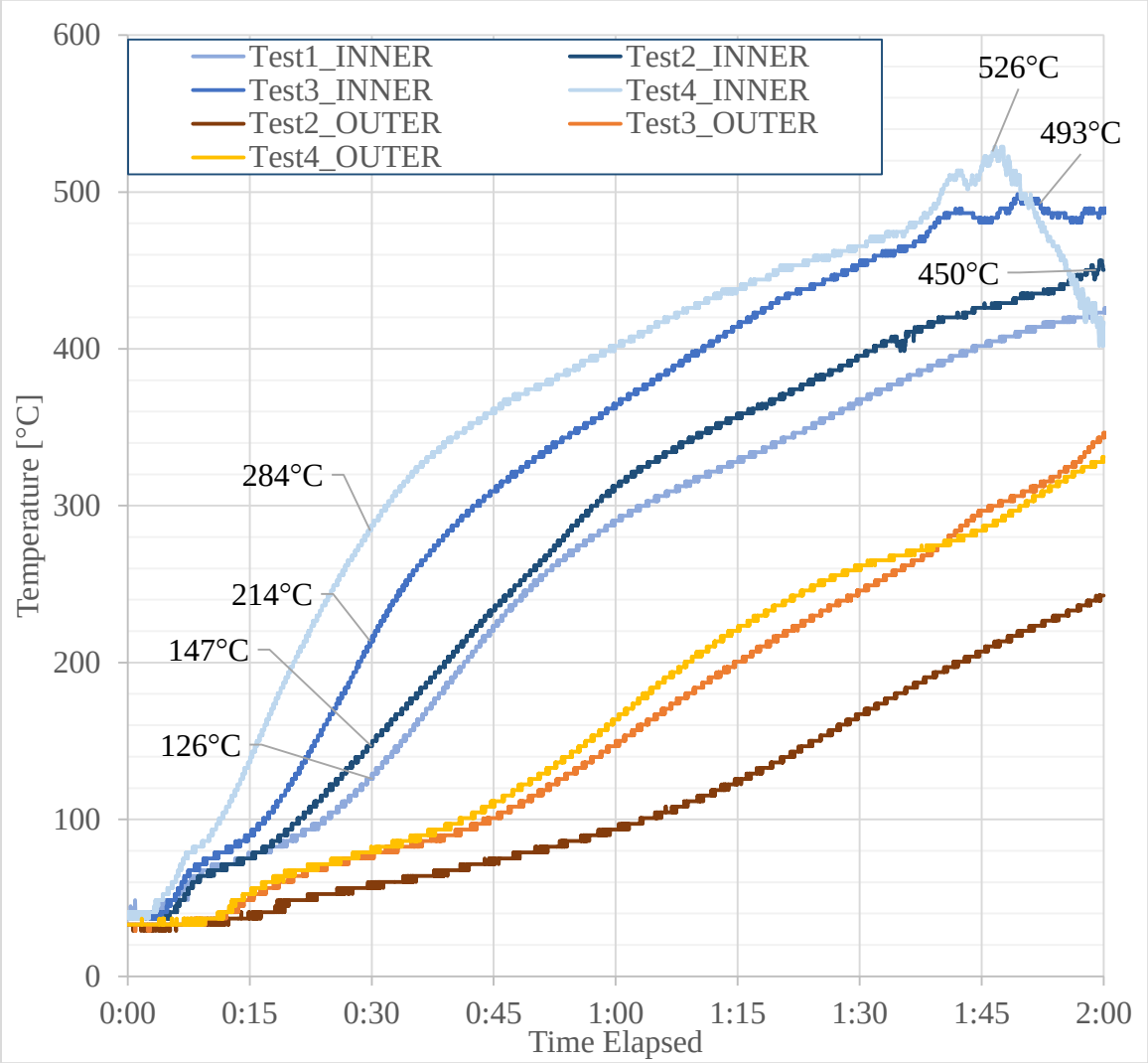

Figure 10: Comparison of Temperature Response for Tests with Different Sawdust Sizes. Left and bottom axes refer to the temperature and time elapsed, corresponding to the lines.

In Figure 10, temperatures are represented across two locations in the bed and are shown as a function of time. The terms inner and outer refer to the thermocouple closest to the central core and furthest from the core, respectively as discussed in section 3.2.1. The Test numbers refer to Table 5. Due to extreme noise within the outermost thermocouple for Test 1, these temperature data were not included. Temperature at the innermost thermocouple, between the start of collecting data and approximately 10-15 minutes (mins), increase rapidly due to the heating by the ignition coil. After the coil is removed, the temperature between 0:15-1:00 at the innermost thermocouples increases slowly for a few minutes after which it increases more rapidly.

Figure 10 shows that there is significant variation among the temperatures of the different tests. At 30 mins, the temperature difference is 162°C, from the lowest measured temperature, 126°C, to the highest, 287°C. The peak temperatures varied between the three tests from 450°C to 526°C. Test 1 was stopped before the peak temperature was reached. Although there is significant variation in the temperature profiles, these do not correspond to the differences in particles size distributions.

4.3 CHARRING AND ASHING FRONTS

The data in this section are presented to illustrate some of the phenomena observed during the smoldering combustion process. This is done by providing visual and temperature data to develop specific characteristics of these different phenomena.

As discussed in section 2.2, the charring front is the leading front, followed by the ashing front. Photos taken at several times during the smoldering process (Figure 12) indicate that the charring front propagates symmetrically in the radial direction. More detailed examination of the videos shows that ashing tended to occur near fissures in the char bed and therefore did not follow a radial pattern. The onset of charring is characterized

by an increasing slope in the temperature profile, followed by visual observations that show a blackening of the raw sawdust. This example of the temperature indications, preceding the charring front, is evident in Figure 12.

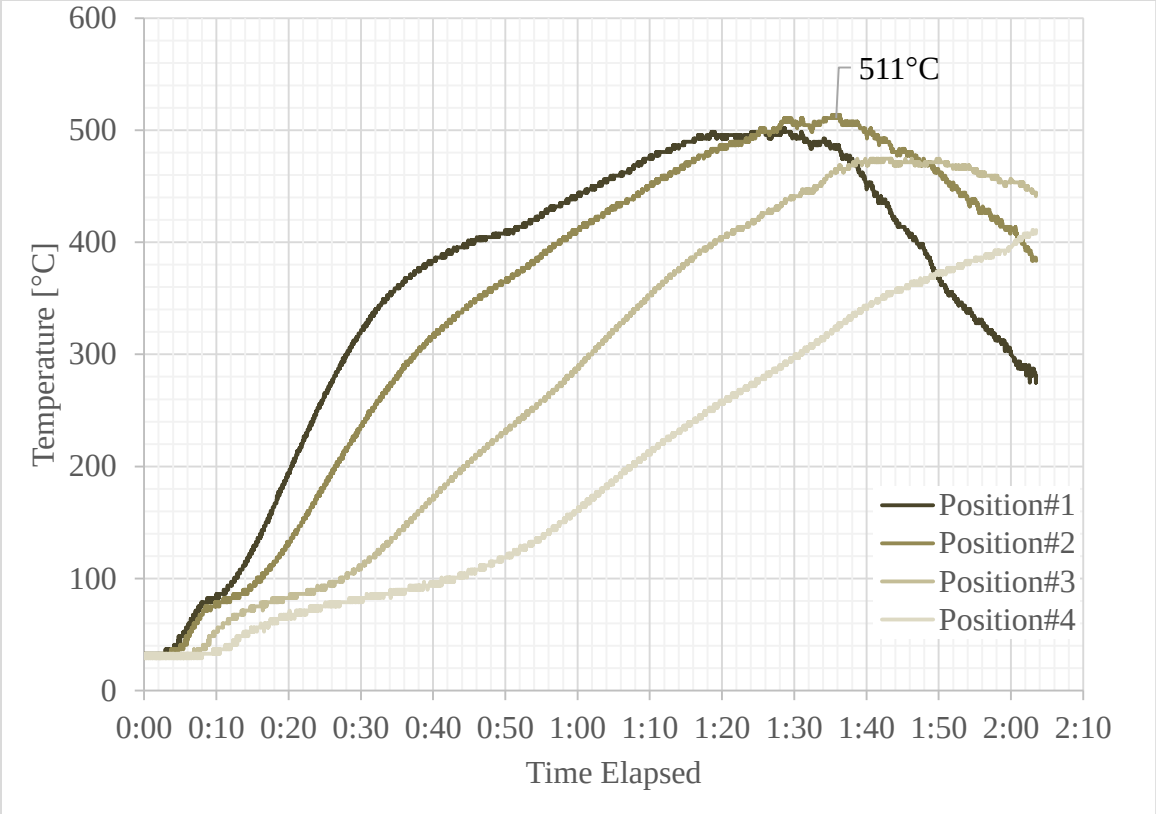

Figure 11: Full Temperature Profile of Poplar Packed Bed with 3 lpm air and no chimney

The temperature profile in Figure 11 is the cumulative temperature profile for the analysis of the charring and ashing fronts in Figure 12 and Figure 13. The plot is broken into a profile for the range of the char front, Figure 12, and the ashing front, Figure 13.

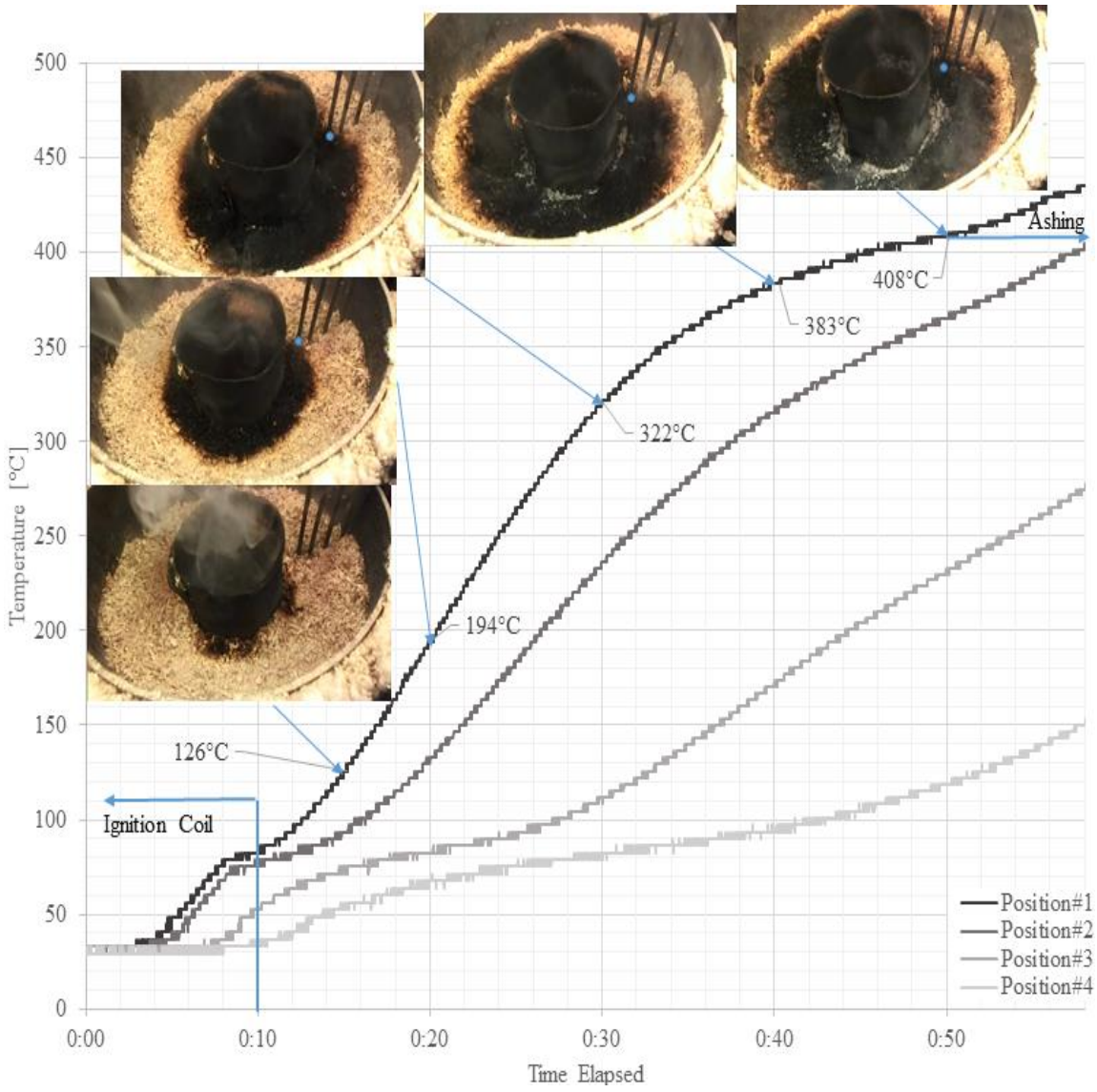

Figure 12: Charring front propagation and the associated temperature response taken in poplar sawdust packed bed with 3 lpm of airflow and no chimney. Position#1 indicates the innermost thermocouple. Thermocouple positions are in ascending order towards outermost.

The temperature increase before 10 mins is associated with the heating effects of the ignition coil. Near 15 mins the temperature profile begins its inclined slope, at which

point the charring front does not appear to have come into contact with the thermocouple position#1.

The still frame, in Figure 12, does not show what the time between 15 and 17 mins indicates in the video. The transition of the char front along the surface happens very rapidly during this time span, within the video. The assumption for visual data, hereafter, is that surface visuals may not indicate the exact location of the front with respect to the thermocouple position. The thermocouple is registering the heat flux of the bed surrounding the thermocouple and is not indicative of any specific particle within the bed. Therefore, the visual data is an approximation of the underlying effects within the bed.

Figure 12 indicates that at 20 mins, the charring front is near the thermocouple in position#1 as indicated by the blue dot. At this position we see the temperature has already begun to rise and the slope is relatively constant. This is attributed to the preheating of the sawdust bed and the forward moving heat flux of the oxidative charring front.

All slopes are calculated using a straight line approximation between two points. Between 20 and 30 mins the slope of the temperature profile is ~13°C/min. This incline is associated with the charring front moving through the position#1 of thermocouple array as it propagates outward. At 30 mins, the leading edge of the front has entirely passed through the thermocouple position, and the slope between 30 and 40 mins is ~6°C/min. The decreased slope is characteristic of a change in combustive effects within the bed. The fuel (raw wood) conversion, through oxidative effects, has now transitioned almost entirely to char. This indicates two possibilities: as the fuel is converted to char, the energy remaining within the particle is also decreasing resulting in a flatter positive slope; or as these reactions proceed, they consume some of the solid mass creating a more porous material through which the air can flow, thus providing an overall cooling effect.

The ashing front and its associated temperature response can be seen in Figure 13.

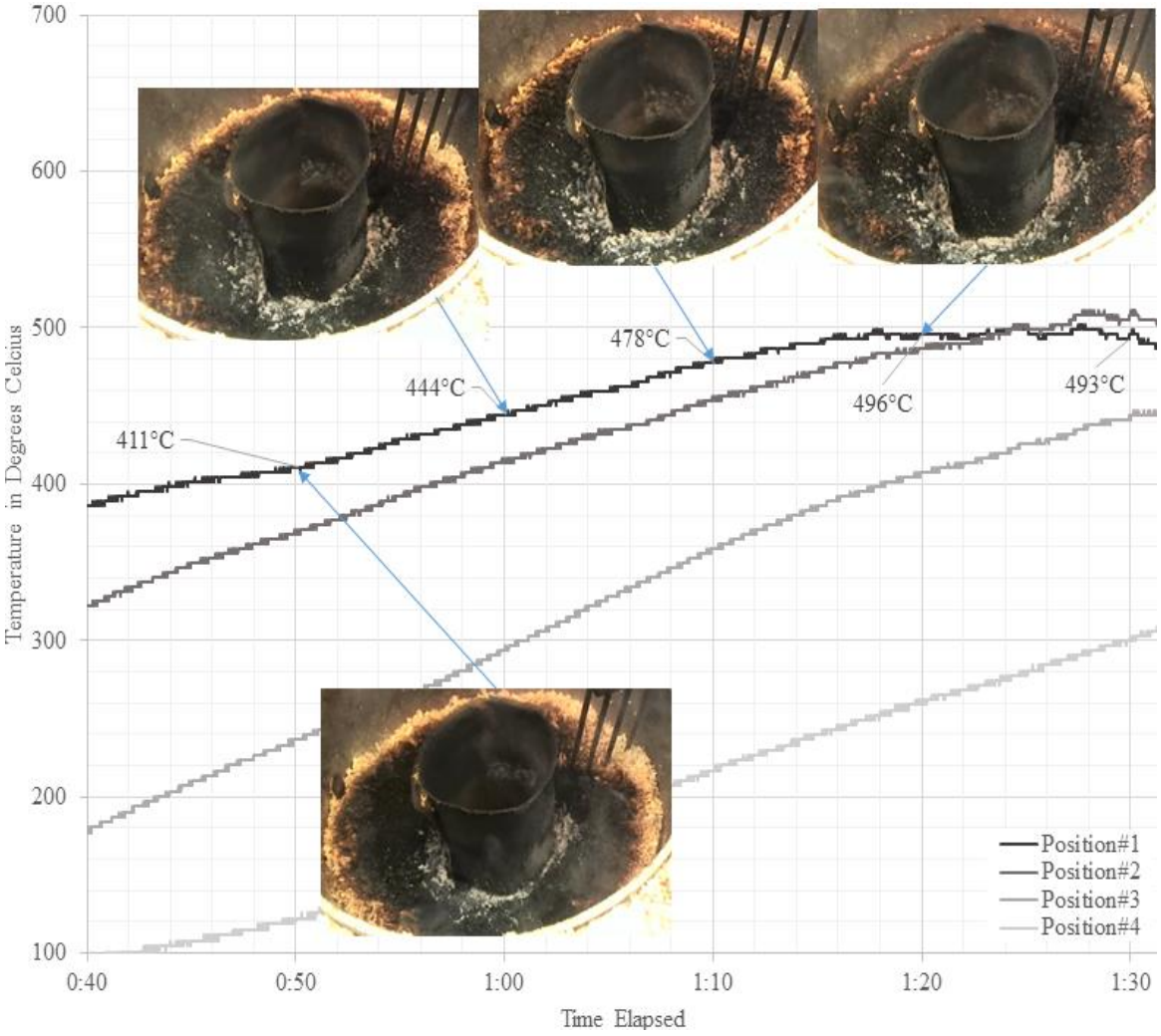

Figure 13: Ashing front propagation and the associated temperature response taken in poplar sawdust packed bed with 3 lpm of airflow and no chimney. Position#1 indicates the innermost thermocouple. Thermocouple positions are in ascending order towards outermost.

A further decreasing slope is seen between 40 mins and 1 hr and 10 mins, as the slope decreases to a range of ~3°C/min. The time of the arrival of the front at the thermocouple is not as clearly defined due to the lack of contrast between the background char and the black thermocouple. This time frame also indicates the ashing front where the char is converted to ash. This exothermic combustion reaction is the process of fully using

the energy potential. Between 1 hr and 10 mins and 1 hr and 20 mins the slope begins to significantly flatten out to ~1.5°C/min. This suggests that the amount of heat, from the char being converted to ash, is also decreasing. The flattening slope also indicates the approach to the peak temperature response within the profile, which will give way to a decreasing slope of ~0.5°C/min, seen between 1 hr and 20 mins and 1 hr and 30 mins.

4.3.1 Charring and Ashing Propagation in Initially Transitioned Bed

Smoldering of sawdust from mesquite wood was also studied. The initial condition resulted in a transition to flaming while the ignition coil was still in the mesh cylinder. The thermocouple arrangement was labeled positions 1-4 on the left hand side (LHS) and 1-4 on the right hand side (RHS), with position#1 being the innermost thermocouple ascending to the outermost couple at position 4.

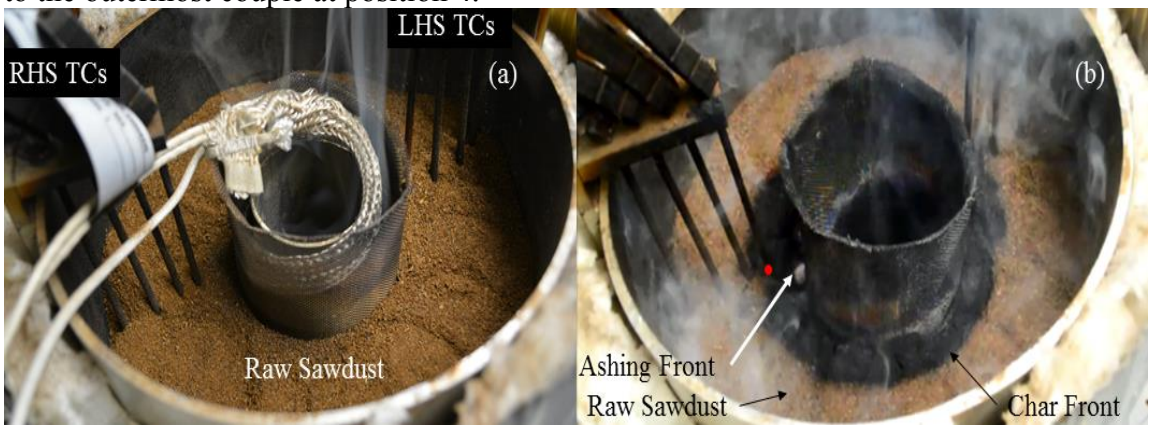

Figure 14: Comparison between (a) the initialized sawdust bed and (b) the charring front after 15 mins in mesquite sawdust bed with 3 lpm of air. The red dot in (b) indicates the RHS TC that is visible at char surface.

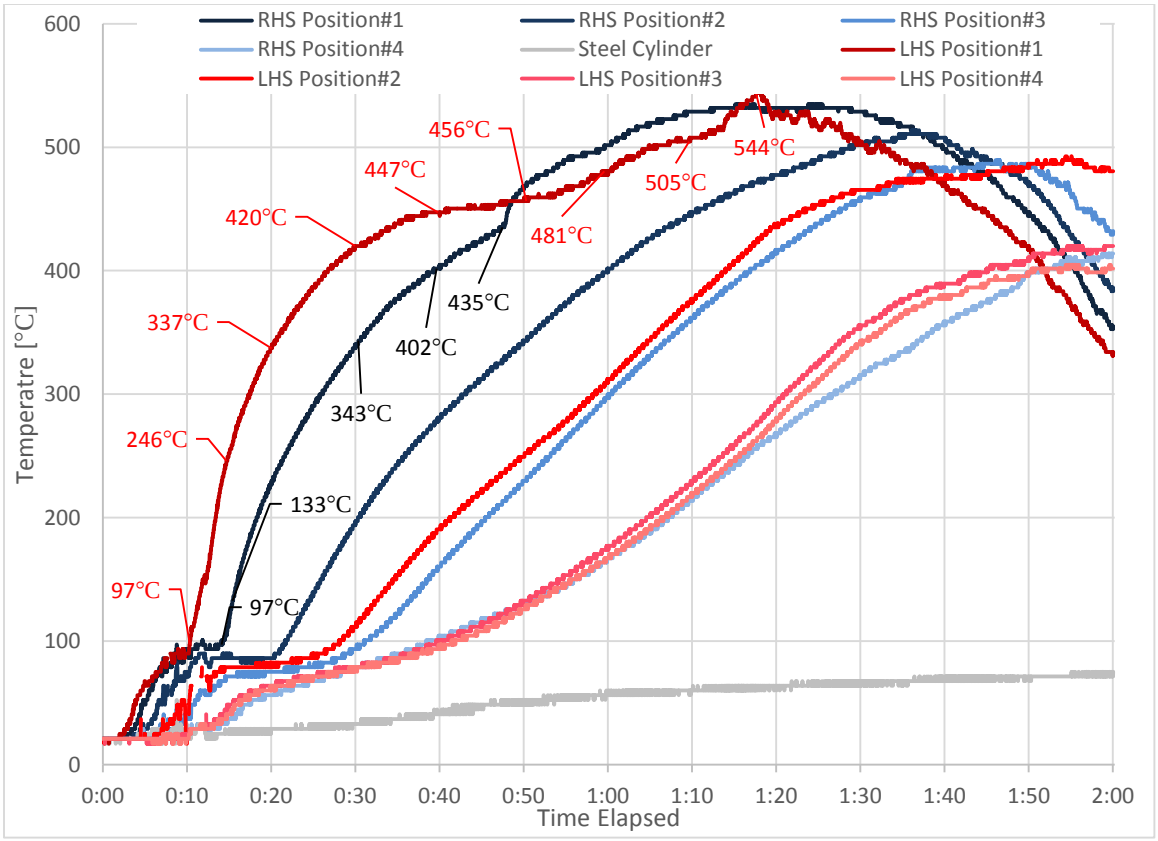

Figure 15: Temperature of right and left hand side temperature data for mesquite sawdust; Postion#1-4 corresponds to innermost to outermost thermocouples; LHS (red temperatures) and RHS (black temperatures) refers to camera left and right sides, respectively, for the webcam captured images

Seen in Figure 15, the temperature before 10 mins indicates the ignition coil's heating of the sawdust bed. After which, the slopes of positions#1 for the RHS and LHS rapidly increase in temperature. This is due to the flaming that occurred before the ignition coil was removed. This transition during initialization more evenly pre-heated the bed. This also influenced the propagation of the charring front indicated by a much more dramatic slope, as compared to the poplar, of ~25°C/min for the LHS between 10 and 20 mins and ~17°C/min for the RHS. The transition to flaming forced a rapid rise in temperature, and quickly transitioned the innermost sawdust to an ashing front, which promoted a far higher

temperature response. The range of 10 to 30 mins is the previously discussed indication of the charring front moving through the first position of the thermocouple on the LHS temperature profile in Figure 15, and the range of 15 to 45 mins shows the same behavior for the RHS. In Figure 14 (b), at 15 mins the char front can be seen as having passed through the RHS thermocouple array (the left side of the picture) as the temperature, 133°C, is in the middle of the increasing slope in Figure 15.

The ashing front, again, moves behind the charring front. This can be seen in Figure 16.

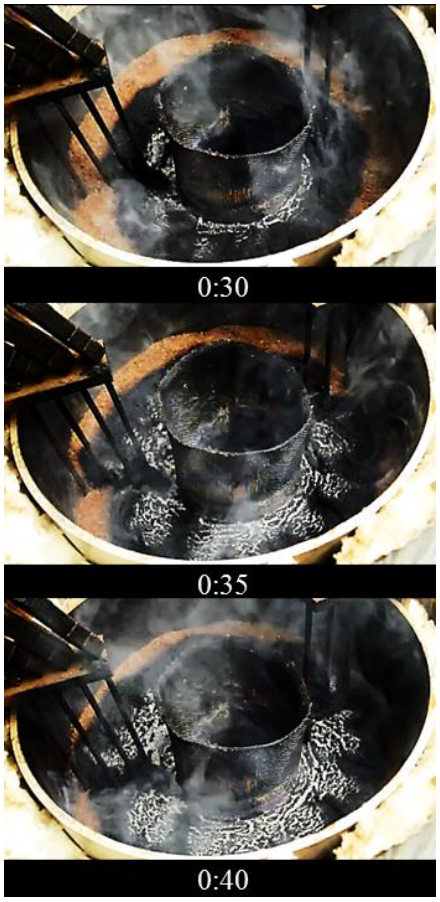

Figure 16: Ashing Front, Radial Propagation in Mesquite Sawdust with 3LPM air and initial condition of flaming at 25 mins, 30 mins, and 35 mins

The highest temperatures during the smoldering process are observed during the ashing phases, seen in Figure 15 compared with Figure 16. This is supported by Raglan's findings [14], that charring begins in wood around 250°C by changing color to a dark brown, and continues to visually change until black, around 300°C. The higher temperature, when char is converted to ash, is supported by noting that the char has a heating value of 28-32 MJ/kg, compared to raw wood's 18-20 MJ/kg [22].

The ashing front does not propagate symmetrically in the radial direction. Rather it propagates in finger-like channels, as shown in Figure 17. As the bed becomes more porous due to significant mass consumption and some bed shrinkage, the channels, termed fissures, form providing an easy pathway for the flow of air.

Figure 17: Fissures within Smoldering Front for Mesquite Sawdust Bed. Picture shown 40 mins after ignition

These fissures represent voids in the packed bed that allow the flow of air that supports a rate of higher temperature reaction. Figure 16 shows the propagation of the

ashing front along these fissures. The size of the fissures are on average 0.5 cm wide and can extend from the inner mesh to the outer wall, radially, but are typically only 5-8 cm in length. The fissures were observed in every smoldering test, although when using the chimney the visibility of the bed is masked due to smoke.

Lo [13] observed in similar experiments that the temperatures did not significantly vary between airflow conditions between 0-0.16 m/s. However, the results from Figure 15 indicate that asymmetries develop due to fissures that formed near thermocouples thus promoting rapid ashing and higher relative temperature profiles.

The initial transition to flaming ultimately did not change the overall characteristics of the bed. However, it did change the observed time that temperature responses, and the subsequent charring and ashing fronts, occurred. The pre-heated bed served to increase the slope of the temperature rise for the innermost thermocouples, and observed peak temperatures, between the non-transitioned and transitioned cases, were 511°C and 544°C for poplar and mesquite, respectively. A difference of 6%, as discussed in section 4.2.2, does not suggest flaming at initialization changed the characteristics of the combustion, any more than the particle size variations could have.

4.3.2 Long-term Behavior of Smoldering Bed

In this section, the results are presented for cases in which the bed of mesquite sawdust, from Figure 15, smoldered until all of the mass was consumed. The first position of the LHS and RHS of the thermocouple arrangement both have a strongly negative slope at 1 hr and 30 mins. The photo in Figure 18 shows the bed has shrunk such that the thermocouple is exposed. Therefore, it is no longer measuring the temperature of the smoldering bed, but rather the temperature of the air within the chamber.

Figure 18: Example of exposed thermocouple after 1 hr and 30 mins since ignition in mesquite sawdust bed

Since the angle of the camera did not provide visual data for the position#1, RHS thermocouple, the left hand thermocouple is the only one that is seen exposed to the air in Figure 18.

The assumption that an exposed thermocouple corresponds to a negative temperature slope is further validated when comparing the results after 2 hrs. At 2 hrs, positions 1-3 have a negative temperature slope for the right side (Figure 15), and position#1 and 2 have a negative slope for the left side. With position#1 of the left side being the most evidently exposed in Figure 19.

Figure 19: Example of exposed thermocouple after 2 hrs since ignition in mesquite sawdust bed.

Although difficult to discern in Figure 19, the videos reveal that the bottom of the thermocouples are exposed and are indicated by red circles in the figure.

Since the primary interest in this study was to examine the effects in the smoldering bed, subsequent experiments were reduced in time from 4 to 5 hrs to about 2 hrs, the period of time in which the thermocouples were still in contact with the bed.

4.3.3 Presence of Embers in Ashing Fronts

Once the ashing wave had fully established itself, the potential for an ember to form was also possible. These embers are points of intense heating and could lead to a transition to flaming if other conditions exist, such as being surrounded by a volatile mixture. The recorded location and time of an ember formation can be seen in Figure 20.

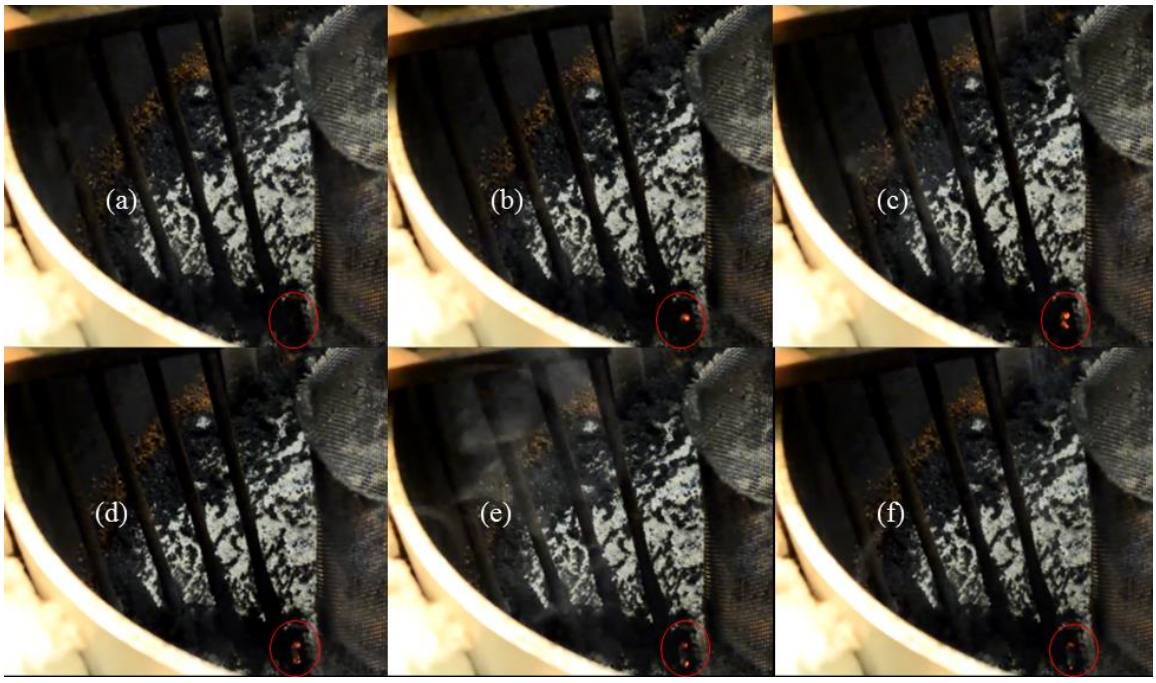

Figure 20: Presence of ember near LHS position#1 thermocouple in mesquite sawdust bed at time 1 hr and 17 mins.

The ember was visually measureable over the span of 11 seconds.

4.4 Mass Loss and Temperature Response

As discussed in Ohlemiller [23], convective effects increase as the sawdust bed becomes more porous. Ohlemiller's assertion was with regard to vertically propagating smoldering combustion although similar effects are observed in the current radially propagating front.

Temperature and mass loss data was collected for a smoldering of a bed of poplar sawdust with an initial volume of 5800 mL. This is the same experiment as discussed in section 4.3. Airflow was introduced and maintained at 3 lpm into the central core. The results of the mass loss and video data can be seen in Figure 21 and Figure 22.

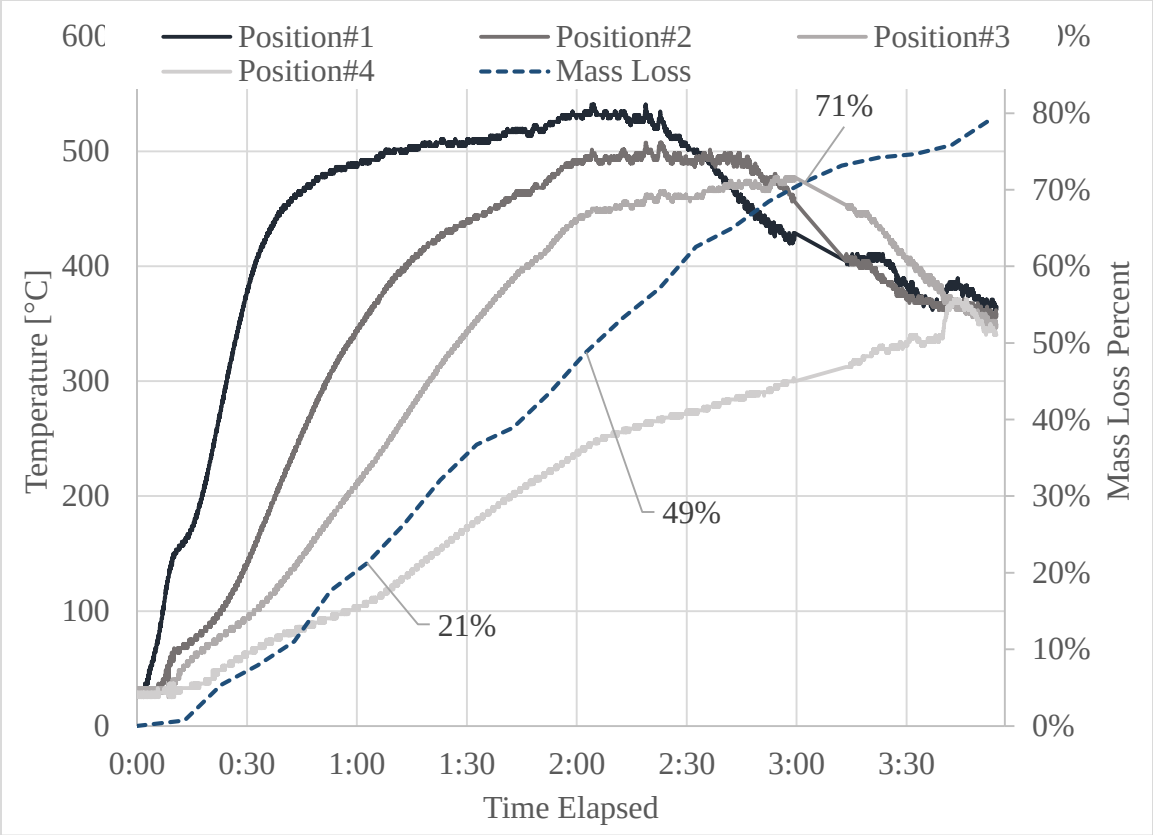

Figure 21: Temperature and Mass Loss data for Poplar Sawdust with airflow of 3 lpm and no chimney; Positions 1-4 correspond to the innermost to outermost thermocouple, with position#1 being innermost. Mass loss data corresponds to the right vertical axis.

The bed became less dense, evidenced when comparing the mass loss percent differences at 1 hr, 18.3%, and at 1 hr and 30 mins, 31.1%, and the relatively smaller decreased volume of the sawdust bed between the two time differences as shown Figure 22.

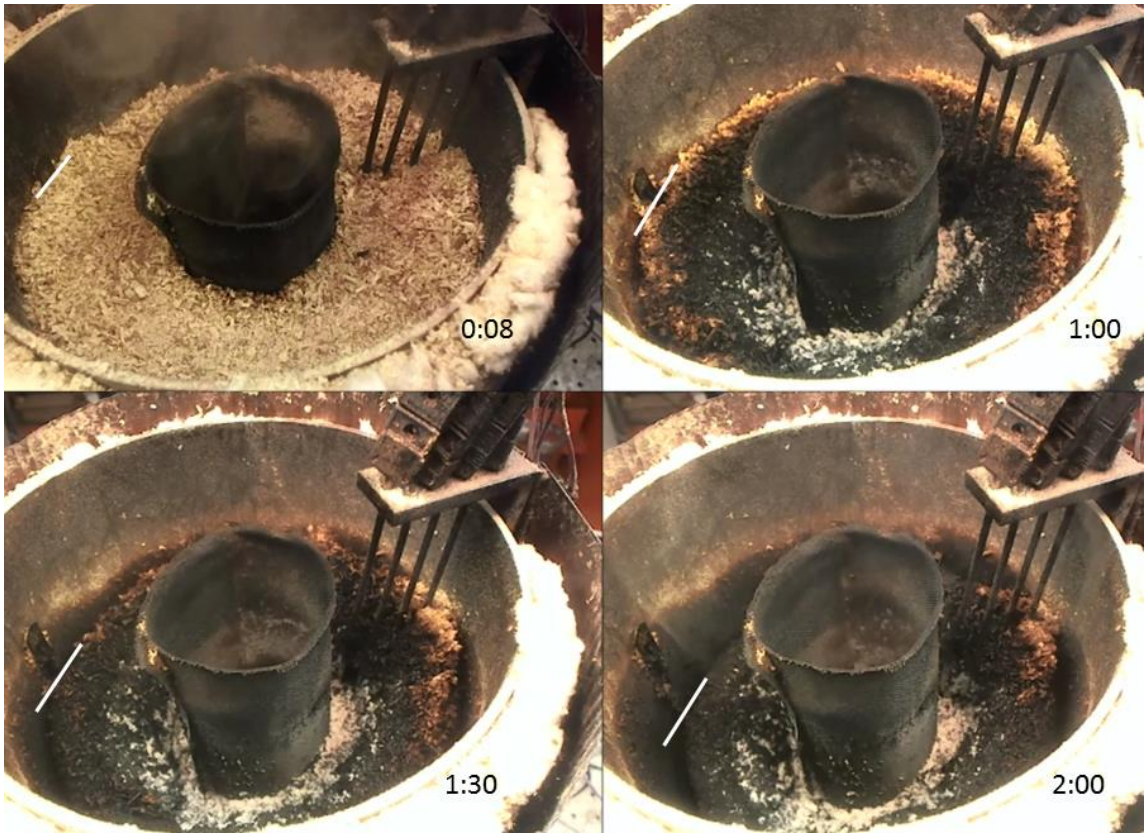

Figure 22: Time Stamped Photos of Mass Loss Experiment with Poplar Sawdust

At later times, however, there is significant volume shrinkage. In Figure 22 a white line indicates the position of the top of the sawdust bed showing the shrinkage between the various timestamps. The results are in agreement with those of Ohlemiller [16] who also showed significant bed shrinkage. The bed density decreases as the char reacts and turns to ash [14]. The height of the bed around the inner mesh decreases from the decreased structural integrity of the ash due to the extensive mass loss. This porous region initially creates pathways for oxygen to be transported to the outward expanding smoldering front. Due to the initial increased porosity within the ashing front, the driving force for the propagating smoldering wave is likely the oxidative effects. This oxidation, and subsequent ashing, creates more pathways of transport for the supply air to perpetuate the front and

create higher temperature oxidative reactions within the outer portions of the packed bed. However, eventually the bed becomes so porous that it does not have sufficient structural integrity, leading to a decreased volume, which serves to decrease porosity and inhibit oxygen transportation to the outer portions of the sawdust bed.

4.5 TRANSITION TO FLAMING

Based on early experiments, in which transition to flaming was observed in various cases, a study was undertaken to determine the conditions under which flaming occurred. The results of these experiments are shown in Table 7.

Date	Species	Chimney	Transition to Flaming	Second Attempt
6/2/2015	Poplar	No	None	No
6/3/2015	Poplar	No	None	No
6/4/2015	Poplar	Yes	Yes	Yes
6/8/2015	Poplar	Yes	Yes	Yes
6/9/2015	Poplar	Yes	Yes	Yes
6/16/2015	Walnut	Yes	Yes	Yes
6/17/2015	Walnut	Yes	Yes	Yes
6/18/2015	Walnut	Yes	Yes	Yes
6/19/2015	Poplar	Yes	Yes	Yes

Table 7: Results of Transition to Flaming Experiments with varying airflow

The airflow was increased to 50 lpm (1.8 m/s) and then decreased back down at which point it was entirely shutoff, as described in section 3.5.2. From Table 7, the results show that transition to flaming occurred in all cases except in the two cases in which there was no chimney. In some cases, after the flaming had been extinguished, a second attempt at flaming was made to establish whether the effects of an already charred, or transitioned, bed would exhibit different transition properties.

Preceding the first transition to flaming, the charring wave front was seen to propagate radially as previously discussed in section 4.3. The smoke was too thick to identify intermediate processes within the front before transition.

4.5.1 First Transition to Flaming

The different stages of flame position within the transition process can be seen in Figure 23.

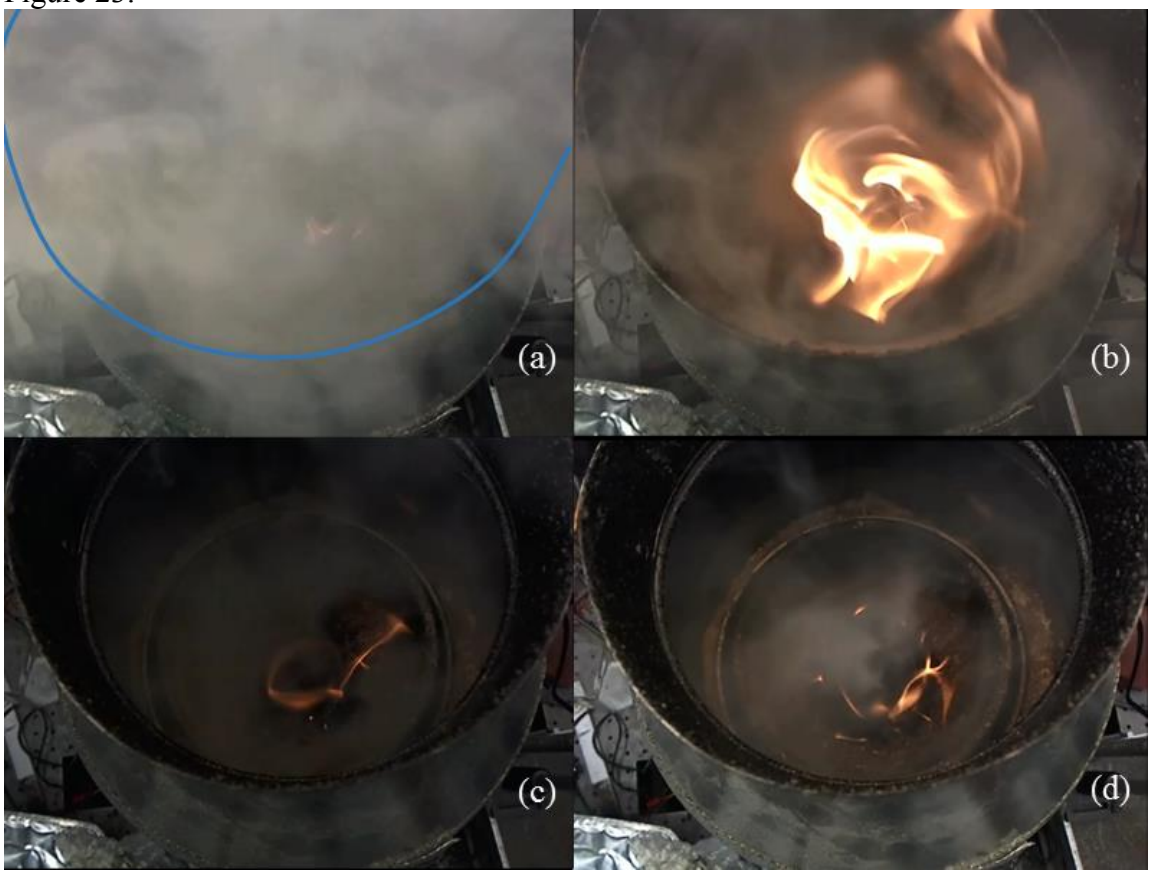

Figure 23: Transition to Flaming; Phases of Flame Position in Walnut Sawdust Bed

The point where transition occurred was after the airflow was entirely shutoff. In every instance the combustion effects began within the throat of the core (seen in (a) of Figure 23), and traveled upward along the vertically rising smoke present within the

chamber (seen in (b) of Figure 23). Initial flares typically filled the space of the chamber. After the initial flaming, a retraction of the flame reduced the flame to just above the core outlet (seen in (c) of Figure 23). Subsequent flaming tended to follow the trajectory of the rising smoke through to the chimney. A low flame also propagated radially along the surface of the unburnt wood (seen in (d) of Figure 23).

As airflow increases, the exothermic, oxidative smoldering reactions accelerate, driving high levels of heat production. Transition does not occur at this point because the airflow is sufficient to keep the volatile concentration low. When the airflow is subsequently decreased to zero, the HCs are no longer diluted and are in a high temperature environment leading to flaming.

Figure 24: Transition to Flaming Ember in Air Flow of Walnut Packed Bed. This was taken during the second attempt at transition due to the density of smoke obfuscating the field of view for the first transition. The embers are present for the first transition, but are not shows.

The results are further supported from initial transition experiments without the chimney. During these experiments, transition did not occur, but the experimental procedure was the same. The previously discussed implications of adding the chimney seem to confirm that when there was no chimney, air was entrained from the outside. Thus, diluting the mixture such that the conditions for flaming were not reached.

4.5.2 Second Transition to Flaming

During the second attempt at transition, within the same packed bed, a similar result was achieved. These attempts offered a contrast between transitions in a bed of unburnt sawdust versus transition in a mostly charred bed, seen in Figure 25.

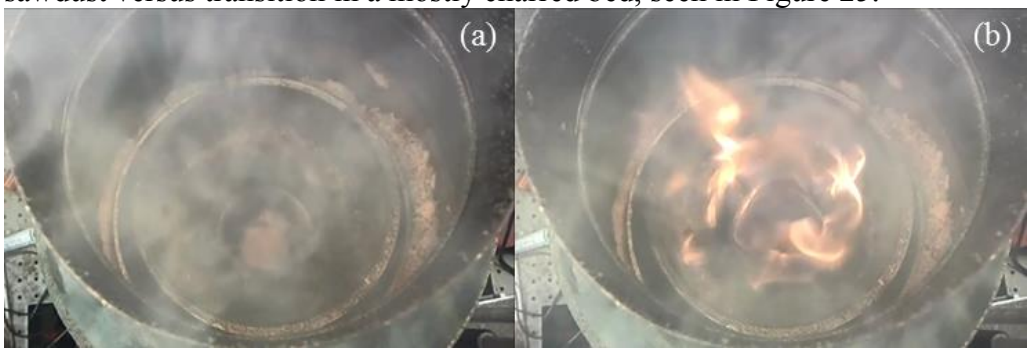

Figure 25: Second Transition to Flaming; Phases of Flaming in Walnut Sawdust Bed.

The transition began in the throat of the core, like the first attempt at transition (seen in (a) of Figure 25). However, consistently in the second attempts at transition, the flame did not fill the chamber in the same way. The flame was less robust and tended to move upward along the vertically rising smoke (seen in (b) of Figure 25). This suggests that the characteristics inside of the chimney chamber just before transition had less volatile build-up than that of the first transition. The cause is assumed to be from the lack of fuel to create an equal HC concentration within the chamber, as compared to the first attempt at transition. As the sawdust bed loses fuel to convert, the volatile gases released are reduced.

This is supported across all tests where transition to flaming occurred. The characteristics of the transition of a charred bed were not significantly different to that of the first transition. The flame radially propagated along the surface of the, now, char bed, and followed the vertically rising smoke upward through the mouth of the chimney.

4.5.3 Other Causes of Transition to Flaming

During the experiments in which smoldering was the intended combustion characteristic throughout the process, transition was known to occur during the removal of the ignition coil, as stated in section 3.6.3. The cause of this flaming seemed to be linked to the temperature of the ignition coil reaching or exceeding the auto-ignition point of the volatile gases being released from the smoldering. Methane is one of the majority gases within the volatile mixture produced by the smoldering. Methane's auto-ignition temperature has been experimentally verified to be around 600 °C [24]. When the ignition core was pulled, embers were attached to the heat tape outer sheath that was in contact with sawdust. This would imply that embers were present while the heat tape was still within the mesh cylinder. Therefore, embers were enough to initiate a transition with the volatiles present in the smoldering sawdust bed implying that transition was possible while the mesh was still in place.

To mitigate any future issues with transition while the core was still in place, the core was pulled as soon as a full 360 degree radial front was observed. This reduced any spontaneous transition because the amount of volatile production was not enough to cause flaming when removing the coil.

4.6 Final Experimental Analyses

Final experiments were taken using two different species of wood, poplar and walnut. The effects of wood species on smoldering combustion emissions, and

temperatures within the combustion chamber, are further discussed in this section. Tests were also conducted using vitiated air in which the percentage of oxygen (O_2) was reduced. These experiments were based on the assumption that pyrolytic conversions of the raw wood to char could be producing higher levels of volatiles in the form of HCs or hydrogen based fuels, based on studies of wood gasification [6] [7].

4.6.1 Poplar Experimental Analysis

In this section, data for smoldering of poplar with air and vitiated air are presented. Temperature, CO, and HC data are reported for various cases as shown in Table 8 in which blue shaded cells refer to standard airflows, whereas the red shaded cells refer to vitiated air flows.

Test Iteration	Air [lpm]	N2 [lpm]	CO	HCs
Test 1	3.0	0.0	Yes	No
Test 2	3.0	0.0	Yes	No
Test 3	3.0	0.0	Yes	No
Test 4	6.0	0.0	Yes	No
Test 5	3.0	6.0	No	No
Test 6	3.0	6.0	No	No
Test 7	10.0	0.0	Yes	No
Test 8	1.5	1.5	Yes	No
Test 9	1.0	2.0	No	No
Test 10	3.0	0.0	Yes	No
Test 11	1.5	1.5	Yes	Yes
Test 12	3.0	0.0	Yes	Yes

Table 8: Index of Poplar Test Iterations, Airflow Compositions, and Data Collected

4.6.1.1 Poplar with Air

The experiments on poplar smoldering used the same sawdust as described in section 4.2.1. Airflows were varied from 3 to 10 lpm, corresponding to an average airflow

velocity of 0.011 to 0.037 m/s within the core, respectively. The thermocouple arrangement was the same as described in sections 4.3 and 4.4. The temperature profiles, as measured by the innermost thermocouple for all tests, are shown in Figure 26.

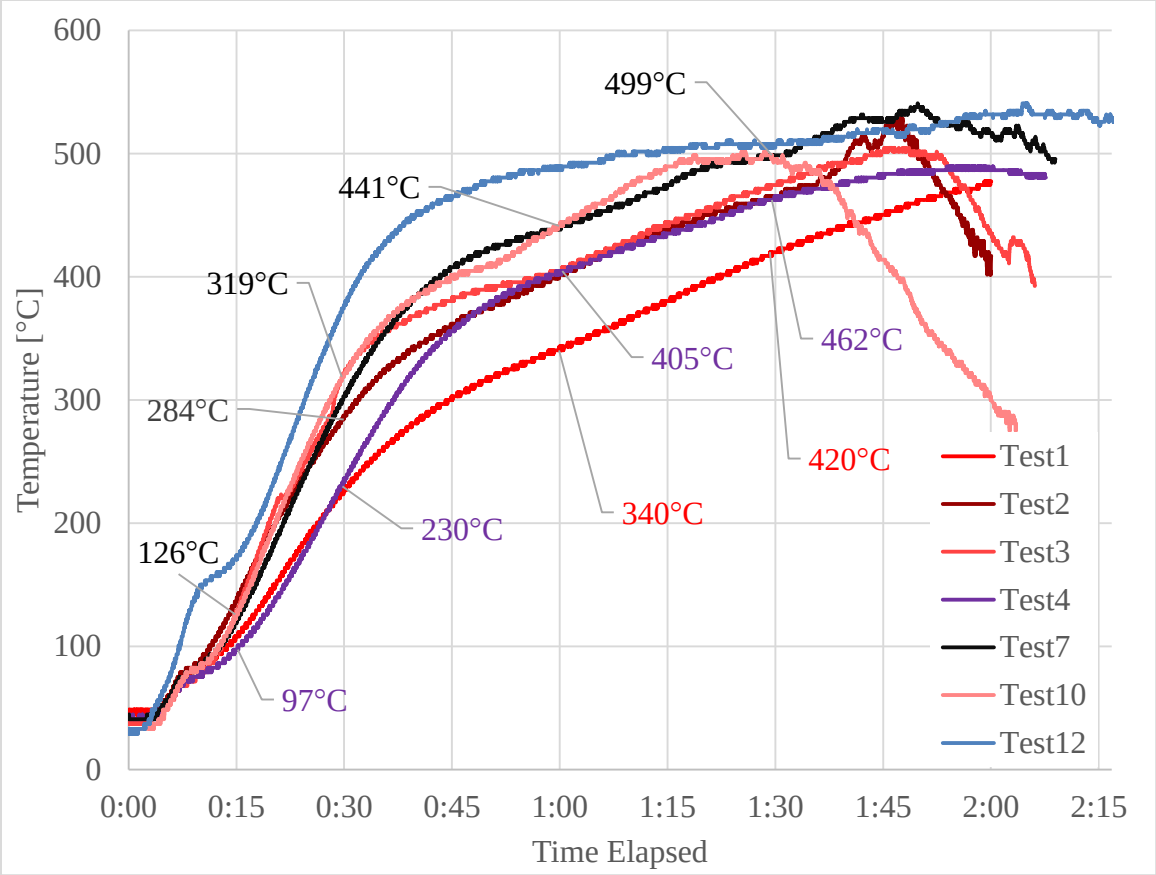

Figure 26: Temperature at innermost thermocouples for various cases. Test1-3, 10, and 12 were taken with 3 lpm, Test4 with 6 lpm, and Test7 with 10 lpm.

In Figure 17, the trends are fairly consistent for all cases. The temperatures at fifteen mins varied from 97°C for Test 4 (6 lpm case) to 126°C for Test 2 (a 3 lpm case) which amounted to a difference of 26%. The difference at this location can be attributed to inconsistent bed heating from the ignition coil, or slight variations in the ignition coil placement in proximity to the innermost thermocouple.

The temperature slopes along the profiles of the respective tests were compiled in Table 9 for the temperature profile slopes, over 15 minute intervals, from Figure 26.

Range of Time	**Test 1 Inner**	**Test 2 Inner**	**Test 3 Inner**	Test 1 Outer	Test 2 Outer	Test 3 Outer
0:15-0:30	**8**	**10**	**13**	2	2	2
0:30-0:45	**5**	**5**	**4**	1	2	3
0:45-1:00	**2**	**3**	**2**	2	4	3
1:00-1:15	**3**	**2**	**3**	3	4	3
1:15-1:30	**3**	**2**	**2**	3	3	3
	Test 4 Inner	**Test 7 Inner**	**Test 10 Inner**	Test 4 Outer	Test 7 Outer	Test 10 Outer
0:15-0:30	**9**	**12**	**13**	2	3	2
0:30-0:45	**8**	**7**	**5**	2	1	1
0:45-1:00	**3**	**2**	**3**	2	2	4
1:00-1:15	**2**	**2**	**3**	3	4	5
1:15-1:30	**2**	**2**	**0**	2	4	4

Table 9: Temperature Profile Slopes for Position and Test Iteration in °C/min over 15 min time ranges in Poplar Sawdust Beds

The effects of increased airflow did not appear to contribute to a significantly different slope at the first thermocouple position between 15 and 30 mins: 9 and 12°C/min for 6 lpm and 10 lpm, respectively, as compared to the range of 8-13°C/min for the 3 lpm tests.

Between 30 mins and 45 mins at the first thermocouple position, 6 lpm and 10 lpm show a decrease in slope of 1 and 5°C/min, respectively. In contrast, the 3 lpm cases show slopes 3, 5, 9, and 8°C/min for tests 1, 2, 3, and 10, respectively. A correlation does not strongly appear between the data sets, in this range.

The slopes stayed fairly constant between 45 mins and 1 hr and 30 mins between 2-3°C/min. This is indicative of the ashing front moving through the thermocouple positions and the char within the bed beginning its final conversion.

The temperature profiles in Figure 26 indicate that the variations in airflow do not produce a large disparity between temperature responses and their respective peaks. Outliers within this assertion exists, as seen in Test 1, but are considered anomalous with regard to the comparison of the average peak temperatures for 3 lpm.

The CO comparisons were taken for Tests 1, 2, 3, 4, 7 and are shown in Figure 27.

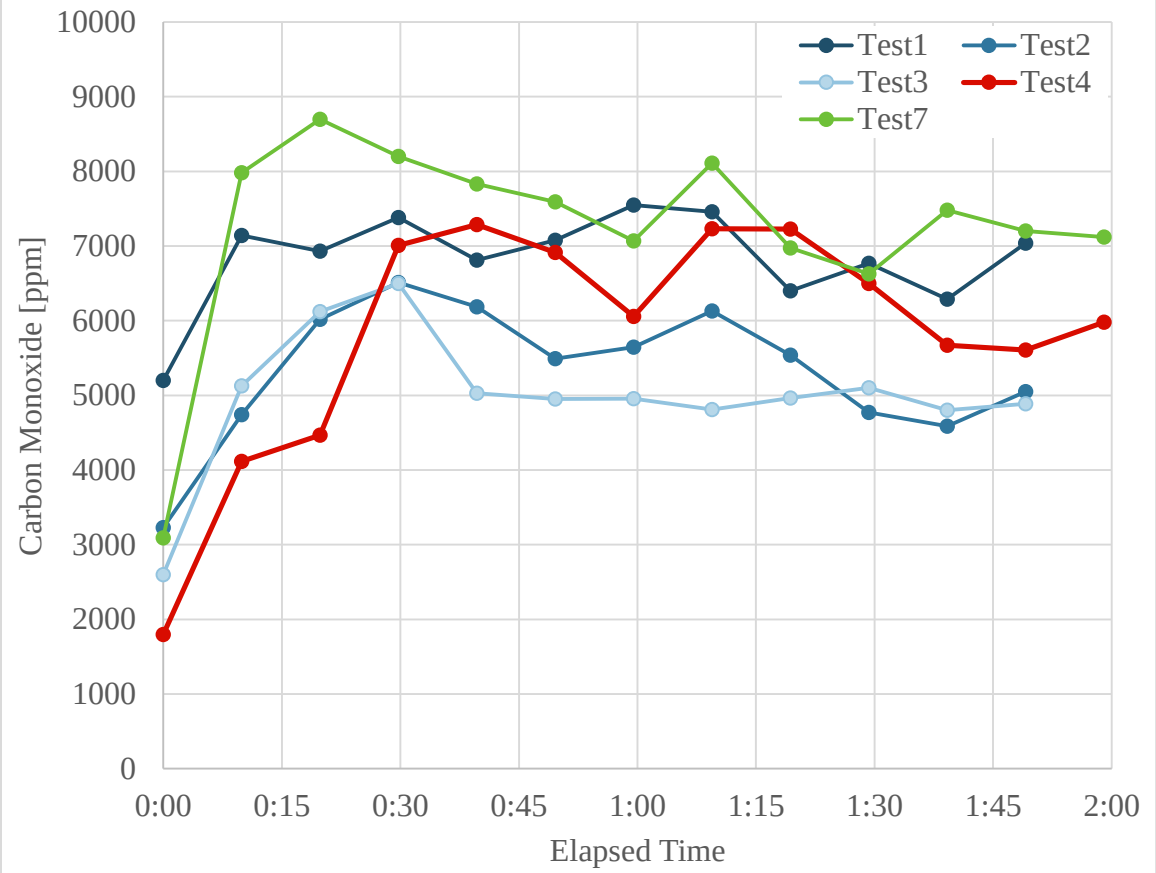

Figure 27: Standard Airflow CO Comparison; Test1-3 were taken with 3 lpm, Test4 with 6 lpm, and Test7 with 10 lpm.

Due to different airflow rates, the gases are diluted in varying amounts. Therefore, the measurements reveal trends but cannot be compared in absolute quantities. When observing the CO concentrations in Figure 27, Test7 (10 lpm), had the highest output of CO with a peak of ~8600 ppm and an average of ~7200 ppm. Test1 had the highest overall

output of the 3 lpm cases with an average CO output of ~6800 ppm. The 6 lpm case followed similar trends to that of the 10 lpm case, but produced an average of ~6200 ppm.

Each test did, however, have a peak CO output, and a general trend that could be interpreted in terms of smoldering fronts. As the raw sawdust is converted to char, between 15 mins and 45 mins, the CO output peaks. The majority of the bed has been converted to char at approximately 1 hr to 1 hr and 15 mins, as seen in the video data associated with each test. At this point, the CO for the respective tests also begins to decline. This was determined by the ashing front becoming the majority of the bed, as observed in the accompanying video data for the respective test. This is a reasonable result considering that the char to ash conversion is the final step in the combustion process and no further conversion takes place.

For Test 12 temperature, HC, and CO data were taken for a ~15 cm deep bed of poplar with 3 lpm airflow. The initial mass was 860 grams and the bed was filled with 6000 mL of sawdust. The ignition coil was pulled at 8 mins, and airflow was introduced at 9 mins. HC, mass loss, and CO data were all collected at thirteen mins, once the chimney was in place. The data for HC, CO, and temperature are shown in Figure 28. Mass loss data are presented with the temperature response in Figure 29.

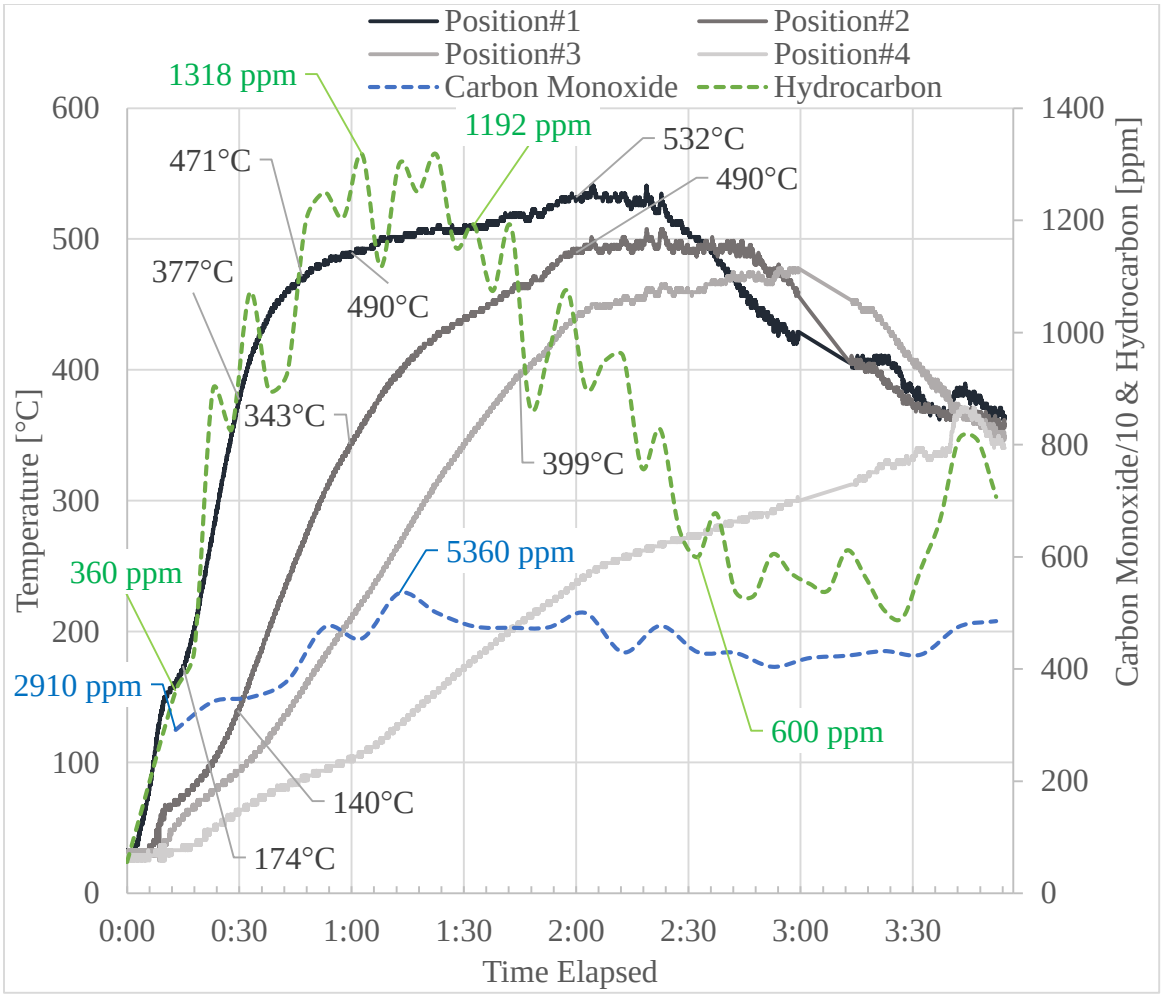

Figure 28: Test12 temperature, CO, and HC data for poplar sawdust with airflow of 3 lpm and chimney; Positions 1-4 correspond to the innermost to outermost thermocouple, with position#1 being innermost. HC and CO data corresponds to the right vertical axis. CO has been reduced by a factor of 10.

The slope of the temperature between 15 and 30 mins for thermocouple position#1 is ~13°C/min, between 30 and 45 mins ~7°C/min, between 45 mins and 1 hr ~1°C/min, and between 1 hr and 2 hrs ~1°C/min. For position#2 the slope between 30 mins and 1 hr, ~7°C/min, indicates the conversion of raw wood to char ~3cm radially from the mesh interface. The slope between 1 hr and 2 hrs is ~2-3°C/min. The slope for position#2 between 2 hrs and 2 hrs and 45 mins is ~0°C/min. After 2 hrs and 45 mins, the temperature

profile begins to decline which indicates the exposed thermocouple reading the air temperature within the chamber. Based on observations of the video, the solid bed remained intact around position#1 for about 2 hrs 30 mins, thus accounting for the sustained high temperature during this time.

A small increase in temperature at 3 hrs and 45 mins is associated with the outer structure of the sawdust bed, collapsing in towards the entirely ashen inner radii that has reduced in volume to the point of no longer supporting the outer char layers. This was confirmed in the associated video data, but due to the lack of contrast in still photos it is not readily identifiable. This collapse introduces unburnt sawdust along the wall, and char that has yet to convert to ash, into a more oxygen rich area of the chamber. The thermocouples register the temperature rise of the char conversion, which is associated with the temperature increase.

HC emissions increased rapidly between 13 mins and 1 hr at a slope of ~21ppm/min. The HC emission peaked at ~1 hr, ~1300 ppm, and maintained its high concentration for ~25 mins with an average emission of 1210 ppm over the time span. This high concentration is also near the same time (confirmed in video data) as the charring front propagates beyond 5 cm of the 6.3 cm radius from the mesh to the wall. This can be interpreted as the majority of the bed having transitioned from raw wood to char. After 1 hr and 30 mins, the HC begins to decrease at the rate of ~10ppm/min, to a concentration of 610 ppm at 2 hrs and 30 mins. From this time to 3 hrs and 25 mins, the concentration is an average of 563 ppm. At 3 hrs and 45 mins, the HC emissions jumped to ~810 ppm. After 3 hrs and 45 mins the concentrations begins to fall, again. This jump is also associated with the outer wall of the bed collapsing into the inner radii, converting some of the unburnt sawdust, and un-transitioned char, into their respective next phase of transition.

Data for CO emissions are shown as the average over 20 seconds, as discussed in section 3.6.1. The CO emissions increased from ~2100 ppm to ~5300 ppm from 13 mins to 1 hr and 13 mins. This value of 5300 ppm is the highest recorded average concentration of CO over the length of the test. After 1 hr and 13 mins, a decreasing slope corresponds to the transition from primarily charring of unburnt sawdust, to the conversion of char to ash.

The HC and CO data are highest in concentration during the transition of raw sawdust to char. As the char front propagates to the point of 80-90% of the bed's surface, the emission profiles for HC and CO reach a maximum, after which the emissions begin to decline. The temperature profile for Test 12's case tend to plateau near the peak temperature longer than other 3 lpm cases from Figure 26. This was from the bed maintaining its structure around the thermocouples, and a slower ashing front. This slower ashing front can also be ascertained from the relationship between temperature slope and the propagation of the char to ash conversion, as discussed in section 4.3.

At 3 hrs and 30 mins, the bed begins to collapse which results in a relatively sizable increase in HC emission ~300ppm (from 500 to 800 ppm), and a relatively marginal change in CO production ~500 ppm (from 4200 to 4700 ppm).

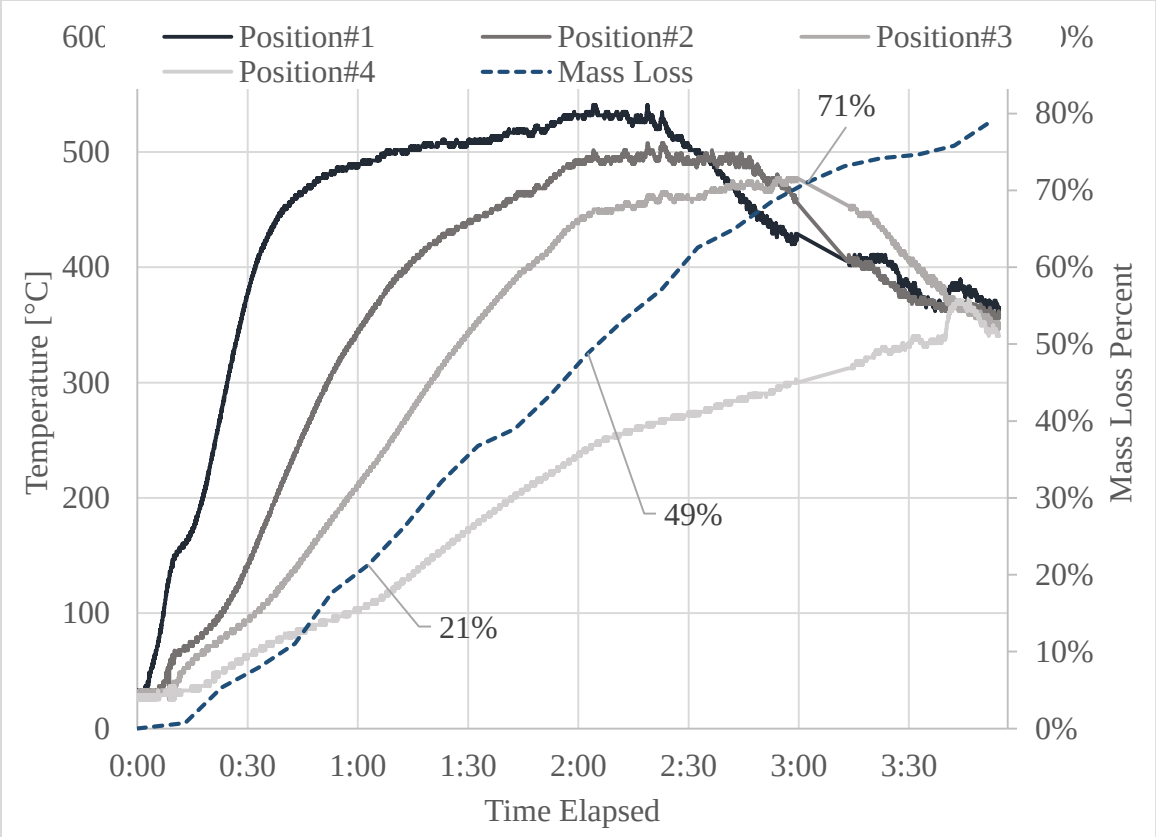

Figure 29: Temperature and mass loss data for poplar sawdust with airflow of 3 lpm and chimney; Positions 1-4 correspond to the innermost to outermost thermocouple, with position#1 being innermost. Mass loss is expressed in mass percent on right vertical axis.

The average mass loss rate calculated from the curve in Figure 29 over the entire experiment is ~5 grams/min. The decrease is relatively constant from 30 mins to 3 hrs. Before 30 mins, the lower mass loss rate is attributed to the removal of the ignition coil, and the establishment of the charring front as indicated by the temperature profile at position#1. The reduced slope after 3 hrs is attributed to the majority char bed, giving way to a characteristically ashen bed. The ash bed is considered at, or near, the final state of the smoldering combustion's conversion of the sawdust and the conversion processes are slowing.

4.6.1.2 Poplar with Vitiated Air

The results for the vitiated air involved first finding the appropriate reduction in O_2, without entirely suppressing the smoldering combustion. This was done by varying the proportion of airflow and N_2 to obtain a vitiated airflow result, as discussed in section 3.6.4. As shown in Table 8, Tests 5, 6, 8, 9, and 11 used a vitiated air supply. Airflows were taken at 6 lpm N_2 combined with 3 lpm of air for an oxygen constituent of 7%, for tests 5 and 6. Tests 8 and 11 utilized a ratio of 1.5 lpm of N_2 to 1.5 lpm of air resulting in an 11% constituent O_2. Test 9 used 2 lpm of N_2 and 1 lpm of air also resulting in 7% O_2. The latter test was taken to verify that the effects of air speed were not causing the resultant combustion characteristic. The comparison of the temperature profiles can be seen in Figure 30.

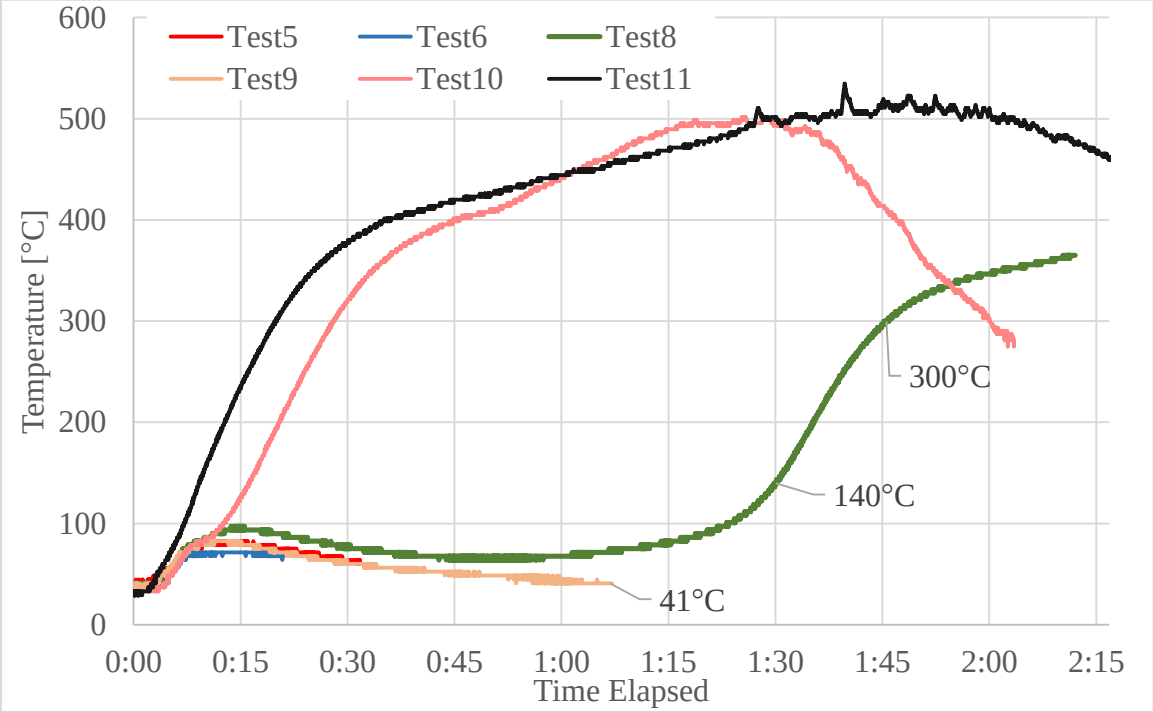

Figure 30: Vitiated Airflow Temperature Comparison for Inner Thermocouples. Test 5-6 were taken with 6 lpm N_2 and 3 lpm Air (7% O_2), Test 8 and 11 with 1.5 lpm N_2 and 1.5 lpm air (11% O_2), and Test 9 with 2 lpm N_2 and 1 lpm Air (7% O_2). Test 10 was a base case taken with 3 lpm of air.

The vitiated airflow with an O_2 content of 7% (Tests 5, 6, 9) resulted in a declining temperature after the vitiated air was added. Initially the temperature increased as associated with a self-sustaining combustion reaction just after the ignition coil was pulled out at ~8-10 mins. Once the vitiated air was introduced at ~15 mins, the temperature for the three cases decreases to just slightly above the ambient air within the chamber at ~40°C. The endothermic reaction, which does not rely on oxygen, is assumed to be the heat sink, along with the convective cooling from the vitiated air supply. A 7% constituent oxygen within a vitiated air supply is therefore concluded to not contain enough oxygen to support the exothermic reactions to produce the temperatures necessary for self-sustaining smolder front.

In the case of the 11% O_2, Tests 8 and 11, the oxygen supply was sufficient to support the propagation of the self-sustaining smoldering combustion. However, two cases occurred that produced dramatically different profiles. Test8 produced a temperature profile that declined between 15 mins and 1 hr and 15 mins, similar to the 7% oxygen case. However, the thermocouple began to register a temperature rise after 1 hr and 15 mins. Test 11 followed the temperature profile that was more characteristic of the controlled airflow cases.

After viewing the video, it was concluded that Test 8's temperature response was anomalous. The delayed temperature increase is not attributed to the effects of vitiation, but rather the lack of symmetry at ignition. The initial front propagated first in a direction 90 degrees tangentially offset from the thermocouple position. That front propagated radially outward, towards the wall. Once it had moved ~4 cm from the mesh interface, it then began to propagate tangentially from the initial direction to produce a geometric symmetry similar to standard airflow tests. Due to a lack of contrast between the chimney

smoke and the front propagation in still images, the illustration of the front propagation is shown in Figure 31.

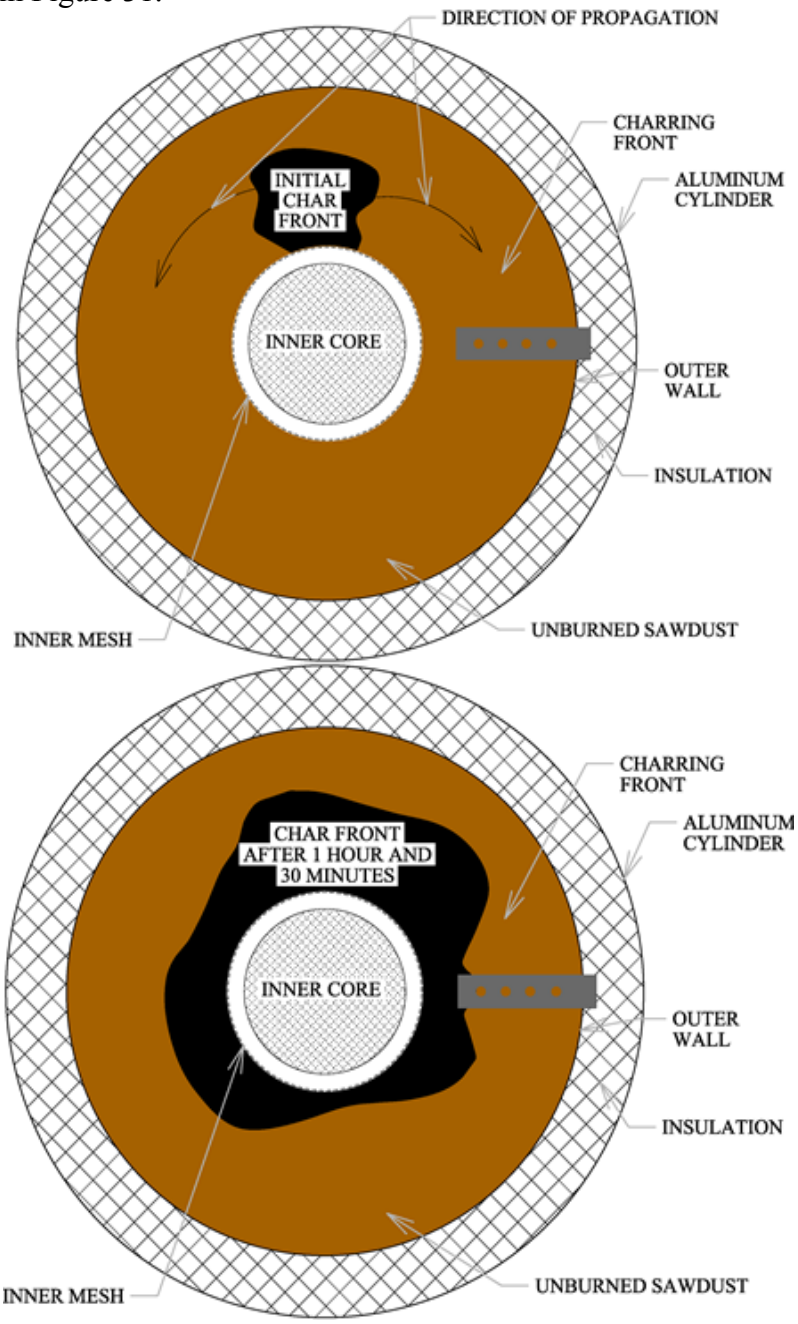

Figure 31: Illustration of char propagation in anomalous case for the initial front with vitiated air supply of 1.5 lpm N_2 and 1.5 lpm air in poplar sawdust bed.

At around 1 hr and 15 mins, the front began to approach the thermocouple array for position#1 of the array. At 1 hr and 30 mins, the charring front began to move through the thermocouple position and the temperature profile began to respond accordingly with an inclined slope of ~11°C/min for the temperature response, which suggests a relatively comparable speed of propagation, as compared to the unmodified airflow cases.

For Test 11 (11% oxygen in air supply), the temperature profile followed the same trend as the base airflow cases for position#1, as compared to Test 10 in Figure 30. The period of rapid increase in temperature occurred ~6 mins earlier than in Test 10. Furthermore, the vitiated airflow case in Test 11 lacked the typical flattening slope that is characteristic of the ignition coil removal. It is notable that the temperature at the removal of the ignition coil, ~145°C, is higher than in previous cases ~100°C. This is a likely reason for the faster temperature rise. It is also noteworthy that decreasing the percentage of O_2 from 22% (in air) to 11% did not modify the fuel or char conversion processes during smoldering combustion. The HC and CO emission data for Test 11 are shown in Figure 32.

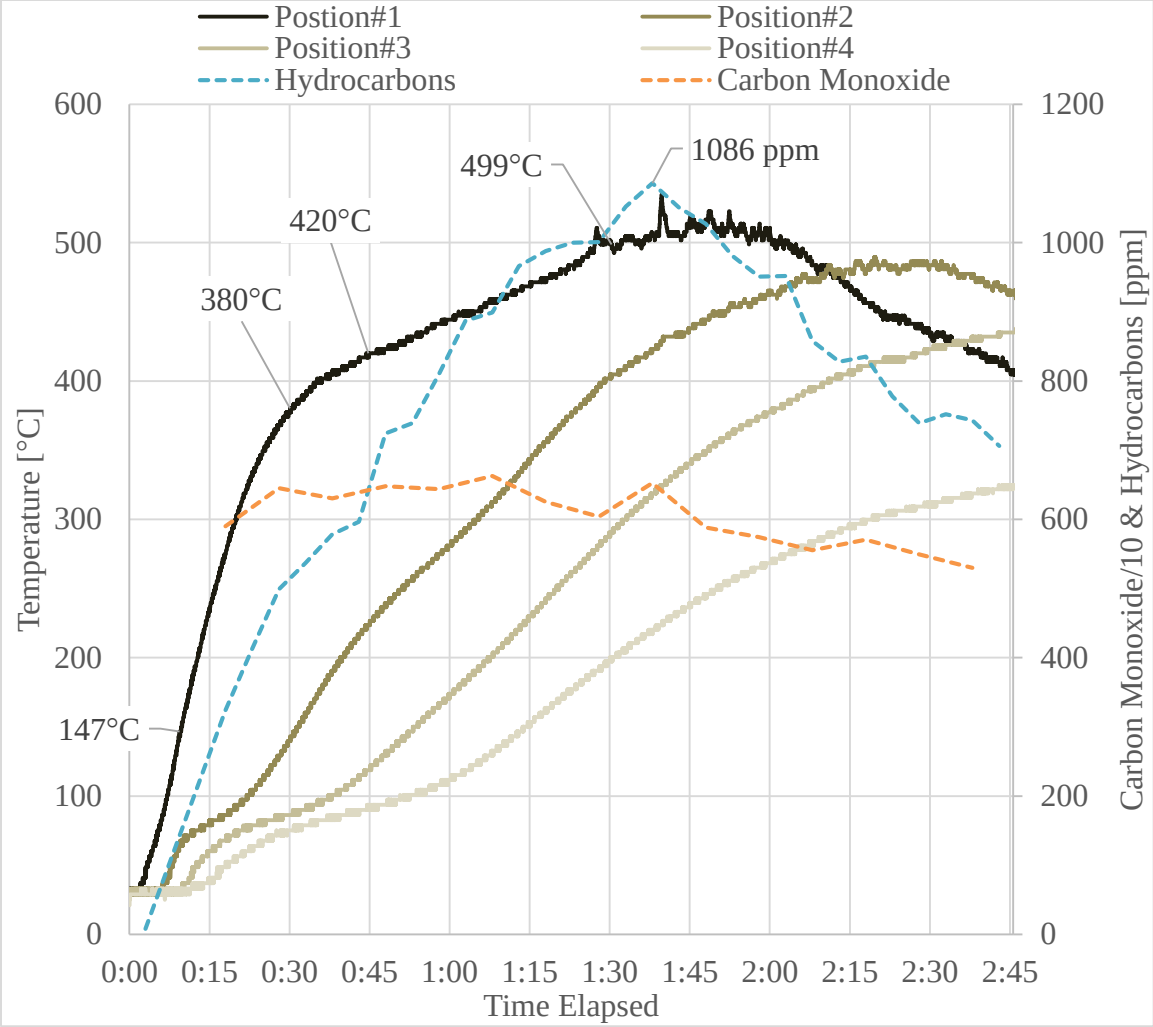

Figure 32: Test11 temperature, CO, and HC data for poplar sawdust with chimney and vitiated airflow of 1.5 lpm N_2 and 1.5 lpm air; Positions 1-4 correspond to the innermost to outermost thermocouple, with position#1 being innermost. HC and CO data corresponds to the right vertical axis. CO has been reduced by a factor of 10.

Test 11 showed similar trends for all thermocouples. The slope of the initial temperature response between the ignition coil removal at ~9 mins and 30 mins is 11°C/min, which is typical of the values of position#1 of the thermocouple array for cases using "pure" air as shown in Table 9. The slope between 30 mins and 45 mins is ~3°C/min which also is typical of the air cases. Between 45 mins and 1 hr and 30 mins the slope is

~2°C/min. This result compared equivalently with the Tests 2, 3, 4, 7, and 10. Test 12 had a slightly reduced slope of ~1°C/min, over this time span, which is attributed to the unique decomposition of the sawdust bed discussed in section 4.6.1.1.

The HC concentration followed a general trend of increasing at a rate of ~8-9 ppm/min until a peak of 1086 ppm at a time of 1 hr and 37 mins. The HC concentration then began to decrease at ~5-6 ppm/min from the peak value. The increase and subsequent peak of the HC concentration corresponds to a transition of the bed to be majority char. Once the bed is no longer converting the raw wood to char, the HC concentration experiences a downward trend corresponding to the bed transition to mostly ash. The characteristics of the trends between the conversion processes and the HC emission are not unique to the vitiated or "pure" air results.

CO concentrations were averaged over 20 seconds. Concentrations were highest at 30 mins and between 1 hr to 1 hr and 15 mins at 6450 and 6625 ppm, respectively. The minimum measured CO, at 2 hrs and 48 mins, is 5299 ppm. The values decreased after the peak at approximate 1 hr and 15 mins as the bed trended towards a majority ash composition. The CO data did not seem to follow a broader trend within the smoldering combustion conversions.

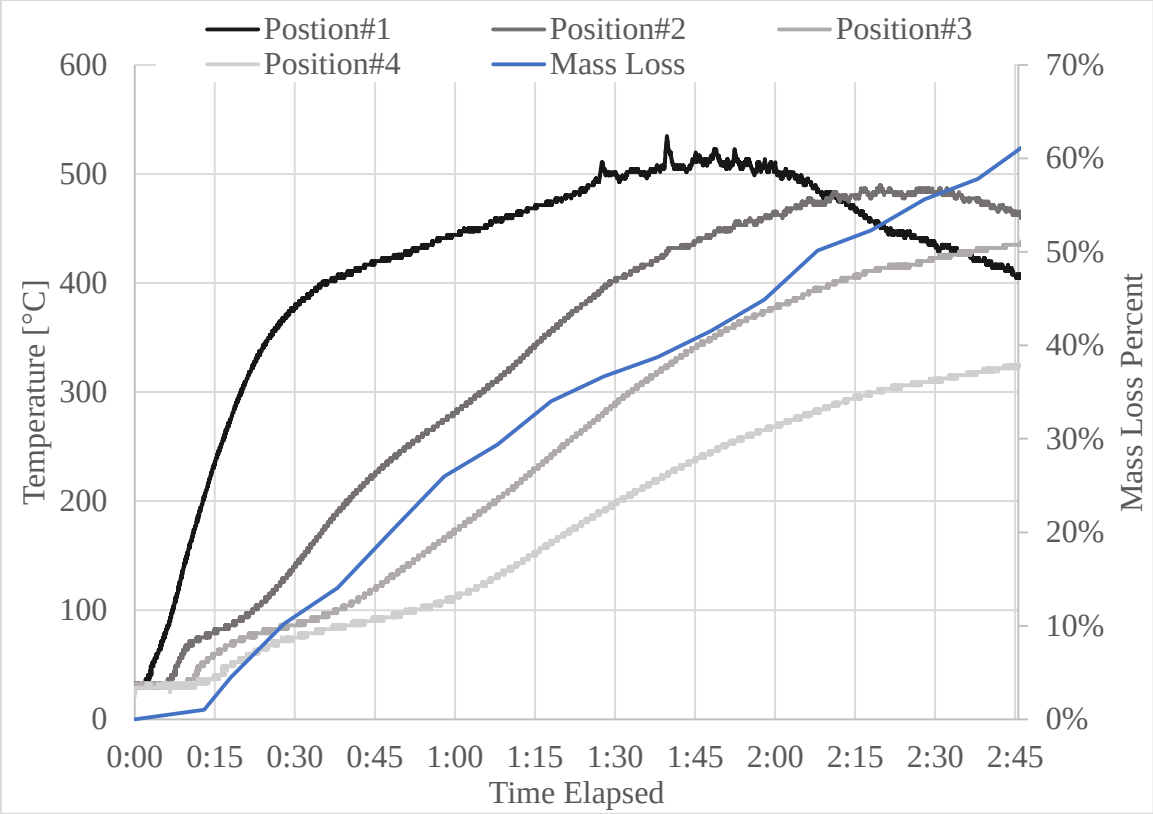

Figure 33: Temperature and mass loss data for poplar sawdust with chimney and airflow of 1.5 lpm N_2 and 1.5 lpm air; Positions 1-4 correspond to the innermost to outermost thermocouple, with position#1 being innermost. Mass loss is expressed in mass percent on right vertical axis.

The average mass loss over the course of the experiment was ~3 grams/min. The decrease was consistent from 13 mins to 2 hrs and 48 mins. The bed lost mass at a similar rate to that of the non-vitiated airflow case, ~3 grams/min, over the same time span.

Vitiated supply air did not produce any trends that limited the smoldering combustion process between the range of 11% and 21% constituent O_2 of the supply air. Furthermore, if the constituent oxygen content was reduced to 7% of the air supply, oxidative reactions did not occur resulting in a lack of exothermic heat to self-support the smoldering reaction.

4.6.2 Walnut Experimental Analysis

In this section, data for smoldering of walnut sawdust is presented. Temperature, CO, and HC data are analyzed similarly to those presented for poplar sawdust. Based on the results from the earlier experiments with poplar, the smoldering of walnut sawdust was conducted at two conditions: with "pure" air at 3 lpm and vitiated air of 1.5 lpm N_2 with 1.5 lpm air.

4.6.2.1 Walnut with Air

Smoldering of walnut sawdust was studied with 3 lpm of air which corresponds to a velocity of 0.011 m/s within the inner core. The initial mass of the sawdust within the packed bed was 387 grams and the bed was filled with 6000 mL of sawdust at a depth of ~15cm. The thermocouple arrangement was consistent with previous testing. The ignition coil was removed after 8 mins and airflow was introduced at 9 mins. The chimney was added after the addition of airflow between 9-10 mins. The results of the temperature, HC, and CO data are shown in Figure 34.

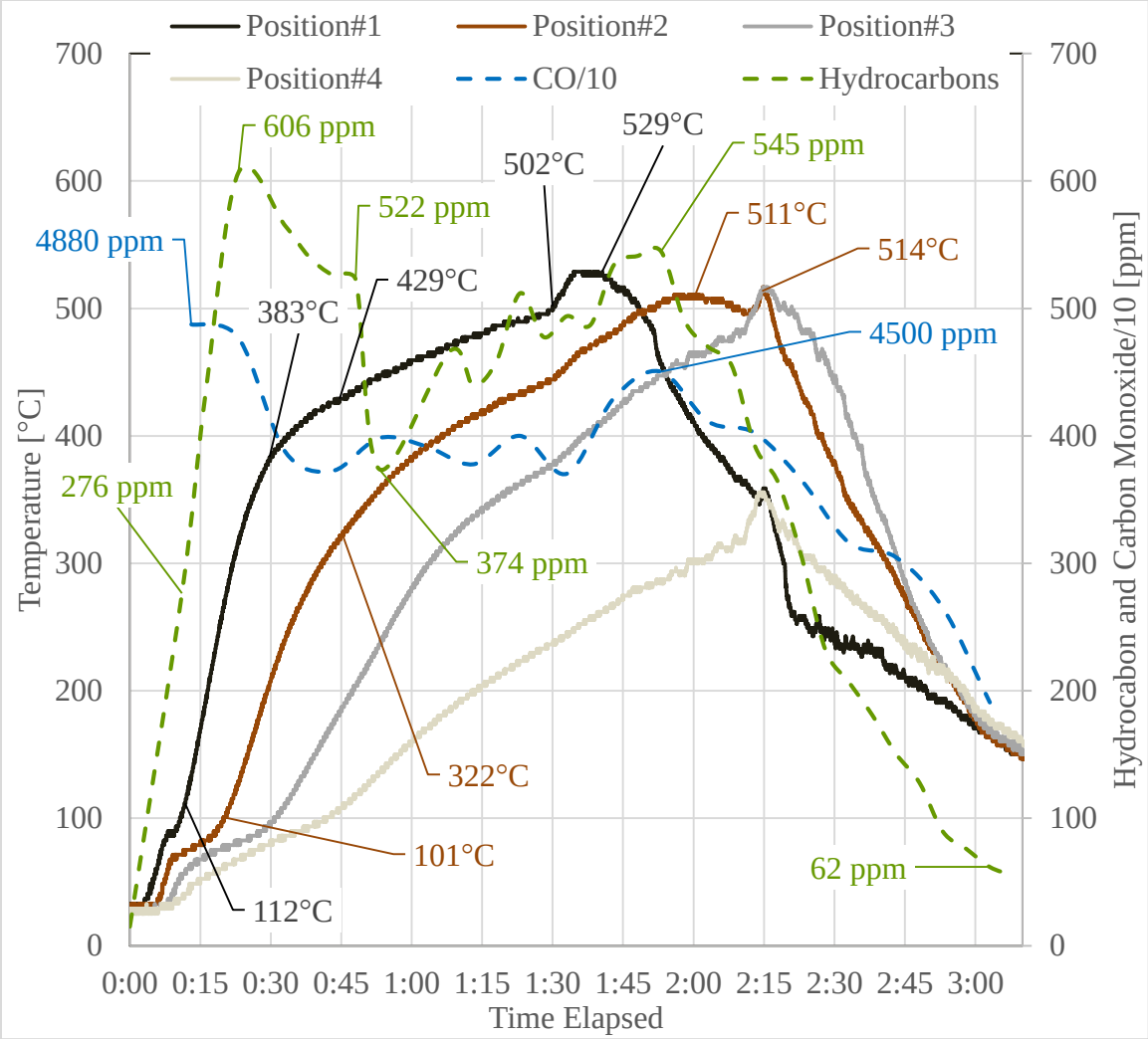

Figure 34: Temperature, CO, and HC data for walnut sawdust with airflow of 3 lpm and chimney; Positions 1-4 correspond to the innermost to outermost thermocouple, with position#1 being innermost. HC and CO data corresponds to the right vertical axis. CO has been reduced by a factor of 10.

The slope of the temperature between 10 and 30 mins for thermocouple position#1 was ~13°C/min, between 30 and 45 mins ~3°C/min, and between 45 mins and 1 hr and 30 mins ~2°C/min. The temperature rose rapidly to its peak of ~530°C at 1 hr and 40 mins, after which the temperature declined for the remainder of the experiment. For position#2 the slope between 20 mins and 45 mins, ~9°C/min, indicates the conversion of raw wood

to char ~4cm radially from the mesh interface. The slope between 45 mins and 2 hrs was ~2-3°C/min. After the initial peak at ~2 hrs, 511°C, the temperature remains within a few degrees of this value for 15 mins after which the thermocouple becomes exposed to air and the temperature declines rapidly. Position #4 also peaked at 2 hrs and 15 mins. This suggests that the bed had decreased in volume, uniformly across the bed, along the area of the thermocouple array, which subsequently exposed the thermocouples for positions 2, 3, and 4 at approximately the same time. Video data also supports this conclusion. As the bed approaches 2 hrs and 15 mins, the video suggests that an ember formed near the location of thermocouple positions 2 and 3. After the ember is no longer visible ~2 hrs and 16 mins, the temperature profiles all uniformly decrease as they measure the air temperature within the chamber.

The HC emissions saw an immediate increase associated with the initial rise in temperature at thermocouple position#1. The slope of the HC concentration increased between 13 mins to 23 mins at a rate of ~29 ppm/min. The peak at 23 mins is associated with the initial propagation of the wave and its conversion of raw sawdust to char between 3-4 cm away from the mesh interface as confirmed by both the temperature slope transitions at positions 1 and 2 along with the video data. The HC emission then begins a decline to 374 ppm at 53 mins, after which begins another increase to 545 ppm at 1 hr and 53 mins. This increase occurs along the same time span as the final decomposition of the remaining unburnt sawdust in the bed and the conversion of char to ash, as confirmed by the temperature profile and the video data. After 1 hr and 53 mins, the HC emission decreased steadily at a rate of ~7 ppm/min. This decrease was associated with the full conversion to a bed that is majority ash in composition, as observed in the video data.

The CO emissions peaked at 13 mins (the first measurement taken after adding the chimney) with a concentration of 4880 ppm. After which it settles out between 3900 and

4000 ppm between 33 mins and 1 hr and 43 mins. The CO concentration then increased to 4500 ppm at 1 hr and 53 mins after which it steadily declined at a rate of ~38 ppm/min. It is worth noting that the HC and CO's second peak occurred at the same time of 1 hr and 53 mins. It is not apparent from the video or temperature data why the second peak may have occurred at this time.

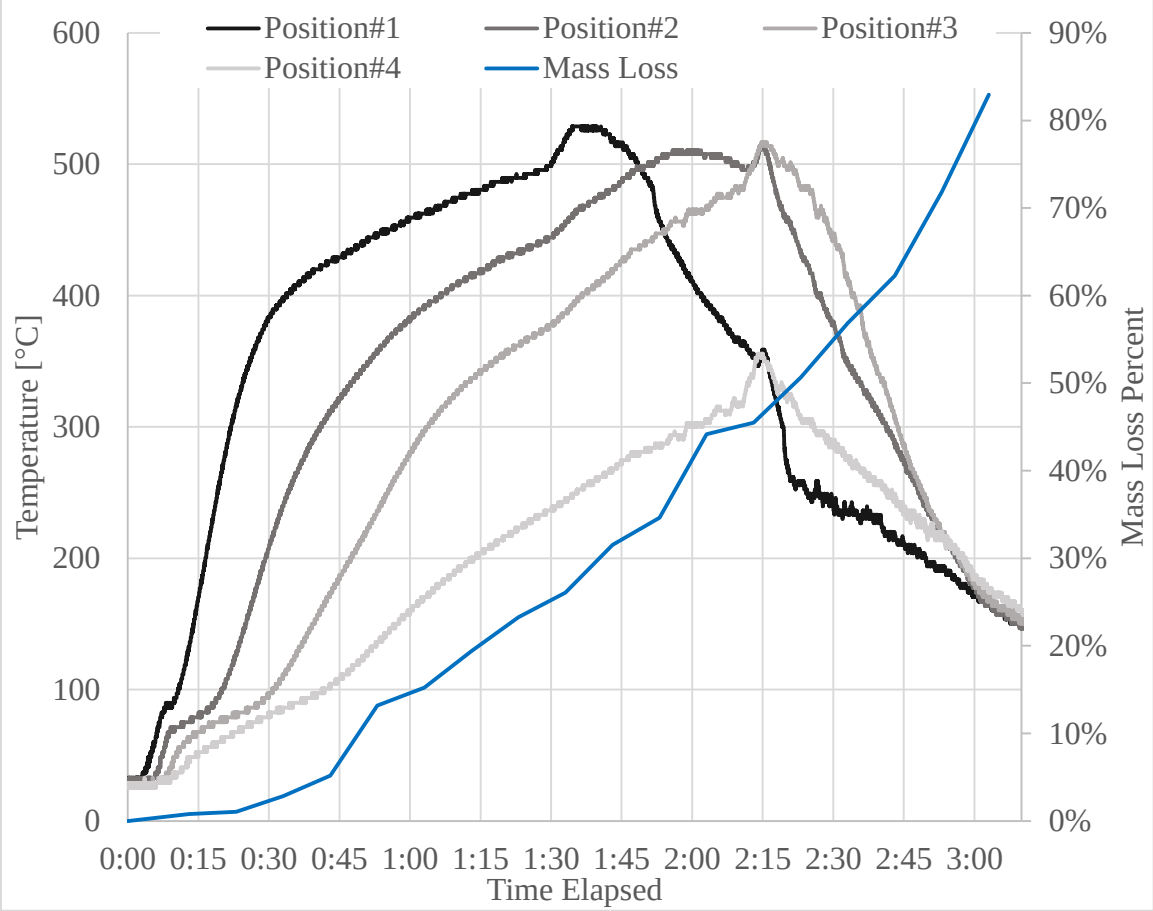

Figure 35: Temperature and mass loss data for Walnut sawdust with chimney and airflow of 3 lpm air; Positions 1-4 correspond to the innermost to outermost thermocouple, with position#1 being innermost. Mass loss is expressed in mass percent on right vertical axis.

The mass loss occurred more rapidly near 2 hrs and 43 mins. Before that, the mass loss remained fairly consistent with a loss of ~1-2 grams/min. Whereas, after 2 hrs and 43

mins, the mass loss occurred at a rate of ~4 grams/min. At 3 hrs, over 80% of the original mass had been consumed.

4.6.2.2 Walnut with Vitiated Air

Tests with walnut sawdust were conducted with vitiated air consisting of 1.5 lpm air and 1.5 lpm N_2 (11% O_2). The initial mass of the sawdust within the packed bed was 404 grams which equated to 6750 mL of sawdust at a depth of ~15cm. The thermocouple arrangement was consistent with previous testing. The ignition coil was removed after 9 mins and airflow was introduced at 10 mins. The chimney was added after the addition of airflow ~10 mins. The results of the temperature, HC, and CO data are shown in Figure 36.

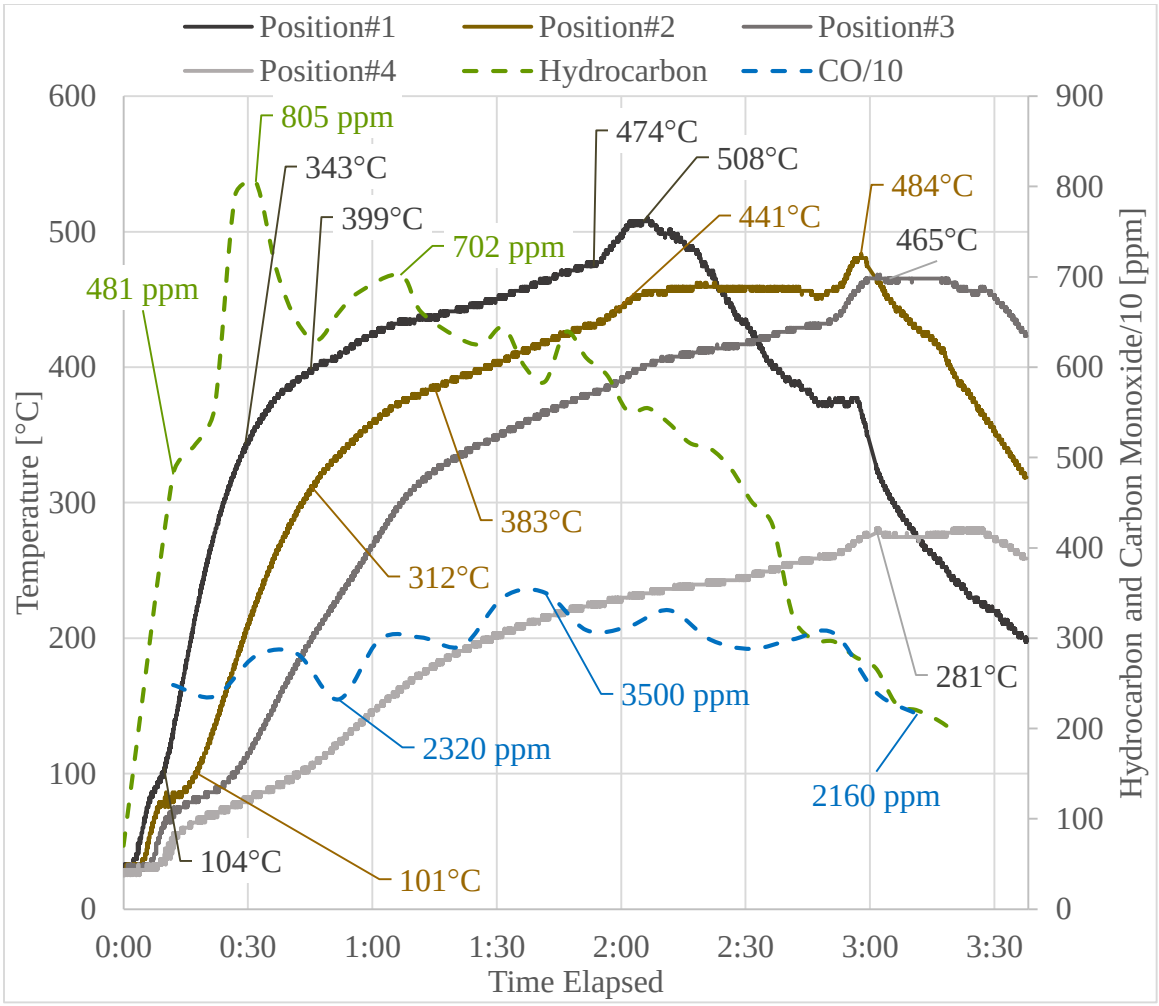

Figure 36: Temperature, CO, and HC data for walnut sawdust with chimney and vitiated airflow of 1.5 lpm N_2 and 1.5 lpm air; Positions 1-4 correspond to the innermost to outermost thermocouple, with position#1 being innermost. HC and CO data corresponds to the right vertical axis. CO has been reduced by a factor of 10.

After the removal of the ignition coil, the temperature increased from 10 mins to 30 mins at a rate of ~12°C/min. Between 30 mins and 45 mins the slope was ~4°C/min. this time period, the char begins to be converted to ash. The temperature increase between 45 mins and 1 hr and 50 mins maintained a mostly linear increase at a rate of ~1°C/min. At 1 hr and 53 mins, the temperature rapidly increased at a rate between 3-4°C/min to the

peak temperature for position#1, 508°C. After which the temperature decreased through the remainder of the experiment, indicating that the thermocouple had become exposed to the temperature of the air within the chamber.

For position#2 the slope between 16 mins and 45 mins, ~7-8°C/min, indicated the conversion of raw wood to char at ~4cm radially from the mesh interface. The slope between 45 mins and 1 hr and 15 mins was ~3-4°C/min. From 1 hr and 15 mins to ~2 hrs the temperature increased at a rate of ~1-2°C/min. A peak temperature of 484°C was recorded at 2 hrs and 58 mins into the experiment. After the initial peak at ~3 hrs the temperature for position #2 began to decline. Position#3's peak temperature response occurred at 3 hrs and 2 mins, 468°C, followed by a slow decrease, and then a rapid decline associated with thermocouple exposure. Position#4's peak temperature of 281°C occurred at 3 hrs and 2 mins, as well, and displayed similar temperature decreases to that of thermocouple position#3. The result indicates that the outer radius of the bed decreased in height at relatively the same rate, as the outer two thermocouples became exposed at approximately the same time ~3 hrs and 30 mins. The decrease in height is also verified in the video data. As the outer portions of the bed transitions from char to ash, the entire bed decreases in height at a relatively uniform rate. This is not unique to the vitiation result, but is best evidenced by the difference in temperatures between positions #3 and #4.

The HC concentration increased at a rate of ~20 ppm/min until a peak of 805 ppm at a time of 32 mins. The bed during this time is experiencing transition from raw wood to char at ~3 cm from the mesh interface. The HC emissions then decrease to between 600-700 ppm for the time span of 45 mins and 1 hr and 50 mins, after which the HC emission continually decreases for the remainder of the experiment. The 1 hr 50 min mark also indicates the conclusion of the conversion of the raw sawdust to char for the remaining sawdust along the outer wall. After the conversion of raw wood to char is complete, the

HC concentration experiences a downward trend corresponding to the bed transition to mostly ash.

CO concentrations were averaged over 20 seconds. The concentration oscillated between 2300 and 3000 ppm until an increase to the highest concentrations at between 1 hr and 32 mins to 1 hr and 52 mins at 3504 and 3500 ppm, respectively. The minimum measured CO, at 3 hrs and 12 mins, was 2160 ppm. The values decreased after the peak at ~1 hr and 52 mins as the bed was converted to primarily ash. The CO data did not seem to follow a broader trend within the smoldering combustion conversions.

Due to a malfunction within the scale, mass loss measurements were not available for comparison over the entirety of the experiment. However, initial indications of mass loss suggested similar behavior to that of the standard air result for walnut.

Results for walnut with vitiated air produced similar temperature trends to those of the 3 lpm airflow case. The shifts in time with regard to when the thermocouple registered temperature slopes can be attributed to initial ignition inconsistencies or minor deviations in the location of the tip of the thermocouple. The prolonged peaks for the vitiated case's outer thermocouples did however produce a different result than that of the air. The sustained peaks cannot be isolated to whether this was due to vitiation or the effects of bed compaction around the thermocouples. Vitiation can be assumed to have been a limiting factor on the smoldering within the region around the outer thermocouples. The HC peaks differed by ~200 ppm and the vitiated case did not experience a significant second peak as compared to the airflow result.

CO emissions varied by ~1300 ppm at peaks and on average varied by ~1600ppm. This result is not necessarily indicative of the effects of vitiation, as other tests produced results more closely related to that of the "pure" air case for the walnut bed.

4.6.3 Species Comparison

The results for the two species, poplar and walnut, are compared in this section. The comparisons are made for the cases with air at 3 lpm shown in Figure 28 and Figure 34 and those with vitiated air of, 1.5 lpm N_2 and 1.5 lpm air shown in Figure 32 and Figure 36. The temperature, HC and CO data are compared across the four tests 3 hr time spans. Data were taken for the experiment with poplar sawdust and vitiated air for only 2 hrs and 45 mins while all other tests in the comparison met or exceeded this time. The initial mass for each test was 387 grams for the walnut with air, 404 grams for walnut with vitiated air, 860 grams for the poplar with air, and 782 grams for the poplar with vitiated air. All of the beds were filled to a depth ~15 cm of sawdust. The times for ignition coil removal and addition of the chimney varied by no more than 1 min across the four tests.

The particle distribution for the respective species are shown in Table 10.

	Poplar	Walnut	Poplar	Walnut
Bin Range	Mass Percent		Frequency/bin	
20-4 mm	7.7%	17.5%	0.5	1.1
4-2.38 mm	29.9%	30.2%	18.5	18.6
2.38-1.68 mm	14.5%	20.6%	20.8	29.5
1.68-.354 mm	32.5%	30.2%	24.5	22.7
.354-.297 mm	5.1%	0.3%	90.0	5.6
.297-.250 mm	0.4%	0.3%	9.1	6.8
.250-.177 mm	4.3%	0.2%	58.5	3.3
.177-.125 mm	0.9%	0.2%	16.4	4.6
.125-.088 mm	0.9%	0.0%	23.1	0.0
.088-.053 mm	0.9%	0.0%	24.4	0.0

Table 10: Dried particle size concentrations for dried poplar and walnut samples. Left side of the table is size of mesh aperture. Frequency of particles weighted by bin size with mass mean diameter of each species.

The particle size for the walnut sample was concentrated around the larger particle sizes far more so than that of the poplar. The particle size distribution with respect to bin

weighted frequencies of the walnut sawdust showed that ~53% of the particles were greater than 1.68 mm as compared to poplar's ~14%. The frequency of particles below .354 mm was higher than that of walnut, which indicates that the density of the walnut bed was less than that of the poplar bed. This is based on the knowledge that the bed was filled to the same height, the mass of walnut added was half that of the poplar.

The results of the temperature measurements are shown for the innermost and outermost thermocouple in Figure 37.

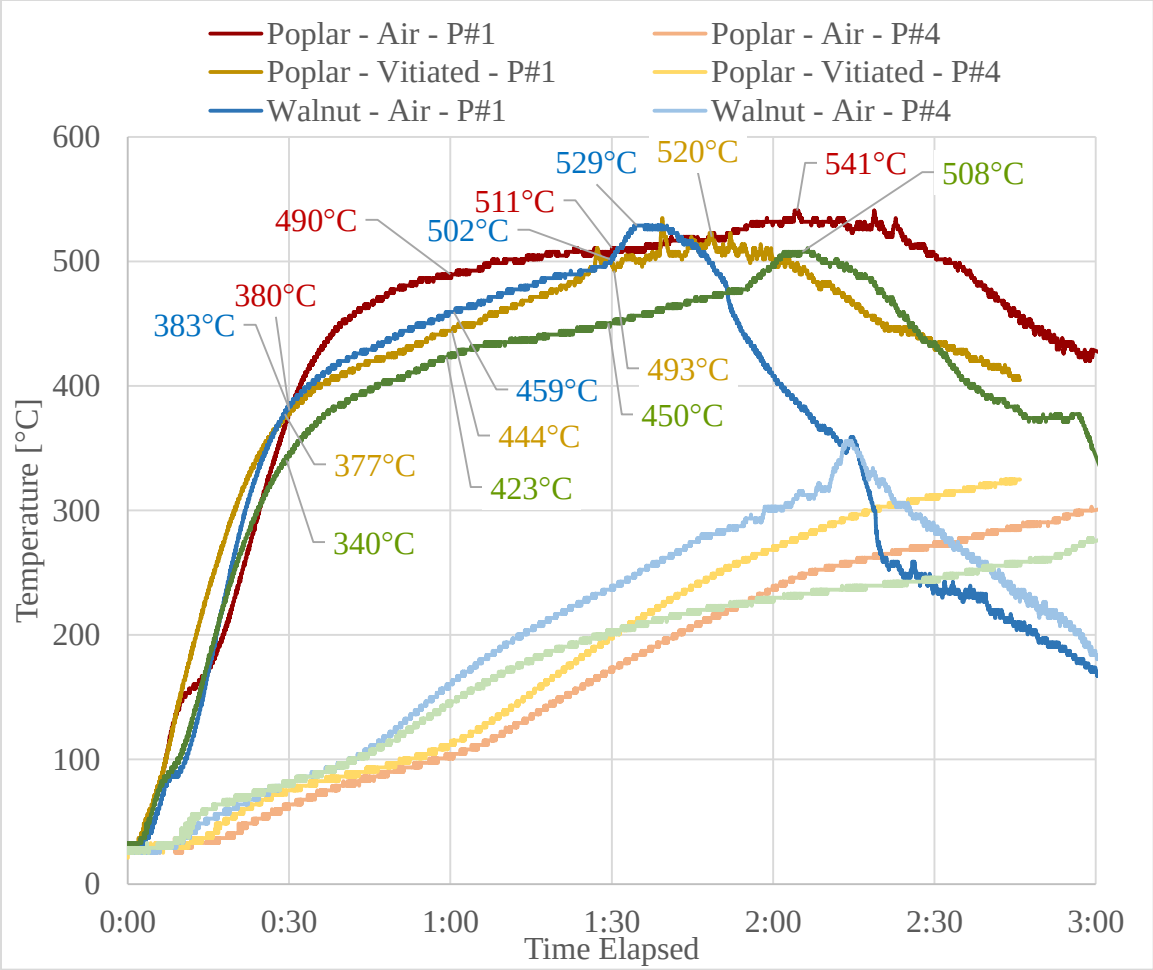

Figure 37: Temperature comparison for innermost (P#1) and outermost (P#4) thermocouples for standard and vitiated airflows in poplar and walnut sawdust beds with chimney

The initial temperature slopes for the two species with both air and vitiated air show similar trends of increase ~12-13°C/min at position#1 of the thermocouple array. The temperature profile most evidently diverges after 30 mins into the experiments. The variation of slopes are shown in Table 11.

Range of Time	Poplar Air	Poplar Vitiated	Walnut Air	Walnut Vitiated
0:30-1:00	4 °C/min	2 °C/min	3 °C/min	3 °C/min
1:00-1:30	1 °C/min	2 °C/min	1 °C/min	1 °C/min
Peak Temps	**541 °C**	**535 °C**	**529 °C**	**511 °C**

Table 11: Temperature profile slopes for position#1 in °C/min over 30 min time ranges in poplar and walnut sawdust beds using vitiated and standard airflows

The slope variations happen most dramatically in the range of 30 mins to 1 hr. After 1 hr, the slopes are all relatively the same. This is an expected result based on the known characteristics of the ashing phase. The higher slope for the poplar with air is also indicative of the relatively higher peak temperature, 541°C, as compared to the walnut.

The temperature of the smoldering walnut sawdust with air appears to decline much faster than that of the other three tests. This would indicate that the bed decreased in volume faster than the three other cases, due to exposing the thermocouples to the air within the combustion chamber sooner.

The HC and mass loss data were compared across the four test cases in Figure 38.

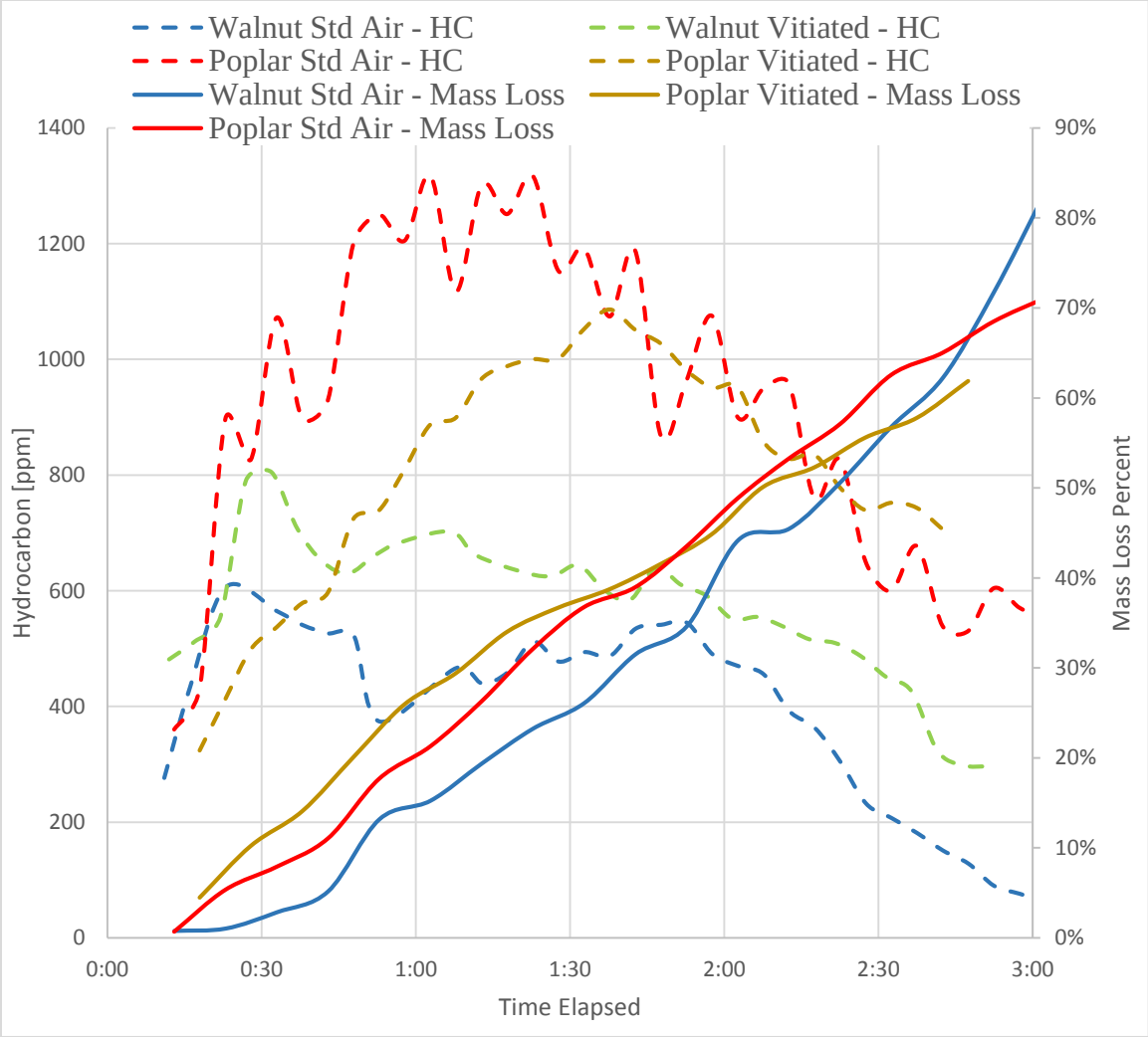

Figure 38: Comparison of mass loss and HC emission for standard and vitiated airflows in poplar and walnut sawdust beds with chimney

The HC emissions for poplar follow more of a parabolic pattern with a peak of ~1315 ppm occurring between 1 hr and 1 hr and 30 mins for the standard airflow case, and a peak of ~1070 ppm just after 1 hr and 30 mins for the poplar with vitiated air. The walnut emissions peaked at approximately 30 mins at ~610 ppm and ~830 ppm for standard and vitiated air, respectively, during the initial charring wave front propagation. The difference in walnut and poplar emission may be attributed to the dramatic difference in particle size

distribution. The less dense walnut bed is assumed to also be more porous than the poplar bed. This could therefore support higher oxygen transport to the propagating front in the outer portions of the bed which would then afford more complete combustion reactions, reducing volatile emissions. The mass loss does not produce a species specific trend.

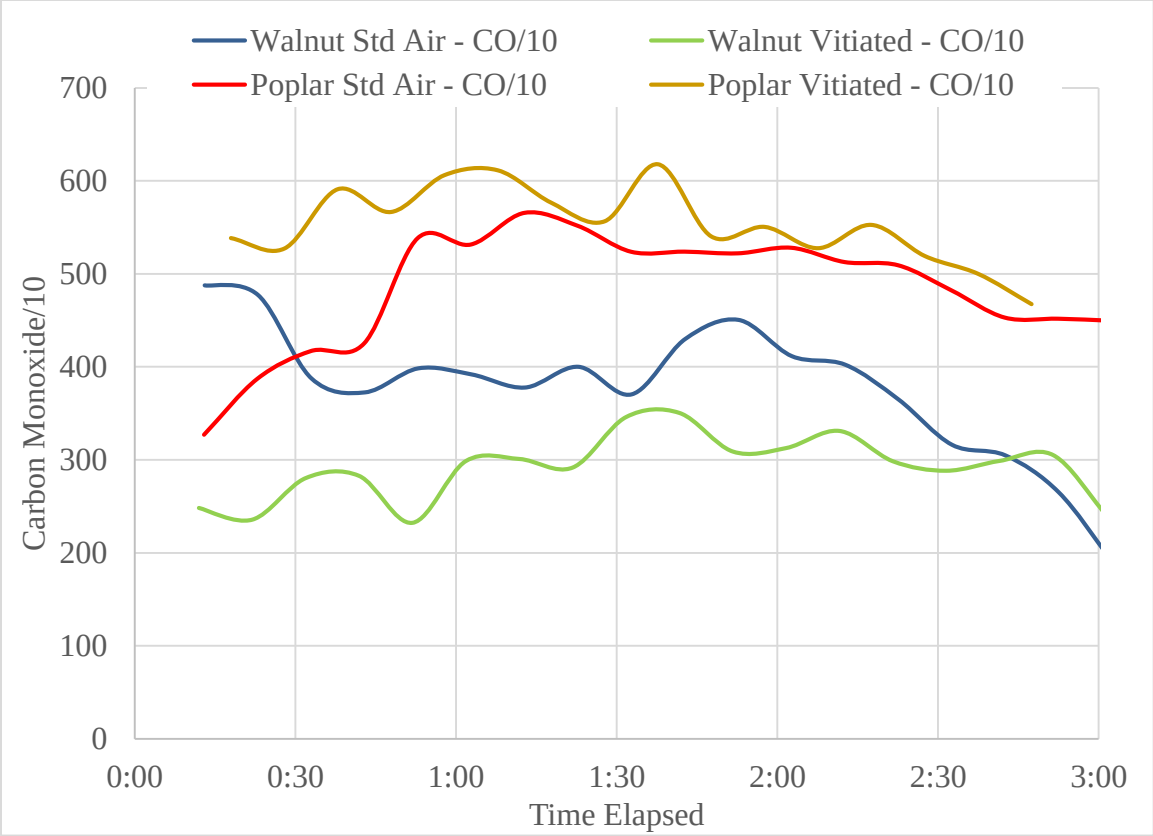

Figure 39: Comparison of CO emission for standard and vitiated airflows in poplar and walnut sawdust beds with chimney. CO has been reduced by a factor of 10

The CO emissions are higher for the poplar species than those for the walnut. The emissions of CO from poplar with air increases from ~3200 ppm initially, to between 5000-6000 ppm after 45 mins, until the decrease associated with the conversion to ash at 2 hrs and 30 mins. The CO emissions from poplar with vitiated air oscillate between ~5200-6200 ppm over the entirety of the experiment, until 2 hrs and 30 mins, until the bed is primarily

ash. The CO emissions for walnut with air peaks initially after which it oscillates between ~3700-4000 ppm before another spike at 1 hr and 50 mins, which gives way to a decrease associated with the conversion to ash. The CO emission for the walnut with vitiated air remain the lowest compared to the other results and peak just after 1 hr and 30 mins at ~3500 ppm. Outside of the initial peak it remains fairly constant with an average ppm around ~3000 ppm. A species specific trend exists for the CO emission but is not isolated to just specie differences. The reduced emissions from the walnut may be influenced by the effects of oxidation along the smoldering front with the more porous bed producing less CO.

Chapter 5: Conclusions and Recommendations

5.1 SUMMARY

The smoldering combustion within a cylindrical sawdust bed has distinct fronts that propagate radially outward from an ignition source. The front can be initialized without flaming, and is self-sustaining from 2-5 hrs, depending on the oxygen content within the bed. Temperature peaks within the inner radius (inner ~3cm of the sawdust bed) occur between 1 hr and 1 hr and 45 mins. As the front moves into the outer radii of the combustion chamber, the combustion characteristics and temperature become dependent on the exposure to oxidative effects. The decomposition of the inner structure, and the rate at which it becomes porous, depends on the exposure to airflow, which promote oxidative effects, leading to the ashing front that follows the initial char front propagation.

The charring and ashing fronts have characteristic temperature profiles and produce HCs in their respective conversions of either the raw wood or char. HC emissions are most prevalent as the bed transitions from fuel to char. After the bed has entirely transitioned to char, the HC concentration in the emission stream begins to decrease indicating that the process of converting char to ash, while a HC emitter, emits less than that of the charring process. The CO production characterizes neither the charring nor the ashing front's conversion processes, but does indicate that a process of fuel conversion is taking place within the overall bed. The ignition process often yields the highest CO output, with a decreasing trend as the fuel and char constituents are converted ultimately to ash.

The data are evidence of smoldering production characteristics for a laboratory designed combustion chamber. Improvement and efficiency modifications were not considered and the reported data within the emission stream at the chimney outlet is meant to observe combustion characteristics in the lab environment.

5.2 Particle Size and Temperature Conclusions and Recommendations

The sizing data and the available temperature results, for the corresponding days, contributed to the assertion that particle sizes could affect the wave front propagations in radial smoldering combustion. However, a direct correlation was not available based on the data collected.

A more extensive study with more experiments utilizing the comparison between particle sizes, and the temperature and front propagations, could potentially yield results that support the assumption that radially propagating smoldering has a relationship to the size of the particles. A conclusion could be drawn with regard to surface to mass ratio effects having a more substantial impact on the rate of smoldering propagation, than that of the convective effects found in environments with the same particle sizes.

Future recommendations are to perform tests utilizing sieve separation and taking particle sizes above .420 mm (to delineate between medium and large particle sizes) that can be used to compact the sawdust bed. Adding more trays to fill in the regions above and below .420 mm would likely result in a reduced standard deviation, as well. The analysis would then compare the effective speed at which the smoldering front propagates, laterally. The hypothesis being that, due to the smaller particles having an increased exposed surface area to smoldering and oxidative effects, combustion can propagate quicker through the bed.

5.3 Transition to Flaming Conclusions and Recommendations

A transition to flaming was observed when the sawdust bed was initially exposed to convective and oxidative effects of increasing airflow followed by the termination of the airflow. Furthermore, if the ignition coil was left exposed to the sawdust bed longer than ten minutes, transition to flaming sometimes occurred. The innermost thermocouple in the array, ~2-3 cm from the ignition coil and mesh interface, would range from ~100-120°C.

Further study should be done to identify the underlying cause of transition while the ignition coil is still in place. It is undetermined whether the result is from auto-ignition of HC volatiles, or a combination of ember production within the mesh and sawdust interface that ignites the volatiles within the forward propagating fuel to char conversion.

Future recommendations are to utilize the HC analyzer placed inside of the chamber, just above the sawdust bed, while the chimney is attached, to better understand the HC loads that are present, within the chamber, before transition occurs. Other operations could include using a "bagging" technique at different heights and radii above and across, respectively, the sawdust bed. This would lend a better understanding of localized effects of HC loads and verify that the flame is following the path of the HC emissions.

5.4 Combustion Characteristics Conclusions and Recommendations

Airflow speeds within the core, from 0.011 to 0.037 m/s, do not appear to be the limiting reactant for the combustion reactions. Greater air speeds did decrease the amount of time the temperature profiles would take to reach their peak temperatures, due to an increased speed of front propagation. CO values follow a decreasing profile after a peak concentration during the initialization. Only the trends are compared due to the variability in dilution across the range of airflow conditions.

In analyzing the emission product from the conversion processes within the bed, the emission at the chimney output was assumed to represent the characteristic of the entire bed. This however is not actually a good indication of localized processes within the radially propagating fuel conversions. Future work could attempt to bag emissions in localized areas of the combustion chamber to more precisely characterize bed transition effects on emissions.

Experiments with vitiated air in which the oxygen concentration was 7% or 11% were conducted. Vitiation at 11% produced a slower front propagation lending to Ohlemiller's assertion that oxidative effects are essential to front propagation [16]. Furthermore, the vitiated air still produced a front very similar to the unmodified airflow case with respect to charring and ashing propagation. Oxygen constituent within the air supply greater than 11% only effected the speed of front propagation for smoldering combustion. Below 7% oxygen content, the smoldering reaction did not have a self-sustaining operation. This is due to the endothermic energy consumption by pyrolysis, and a lack of exothermic oxidation to support further smoldering combustion.

Future work could focus on reducing the range of combustion versus no combustion from 7-11%. This could be accomplished by having a more precise control over the supply air and nitrogen constituent. Taking a stepwise reduction from 11% constituent oxygen could result in an improved accuracy with regard to the limit of self-sustaining combustion reactions within the sawdust bed.

Appendices

APPENDIX A : SEM PARTICLE IMAGE SIZES

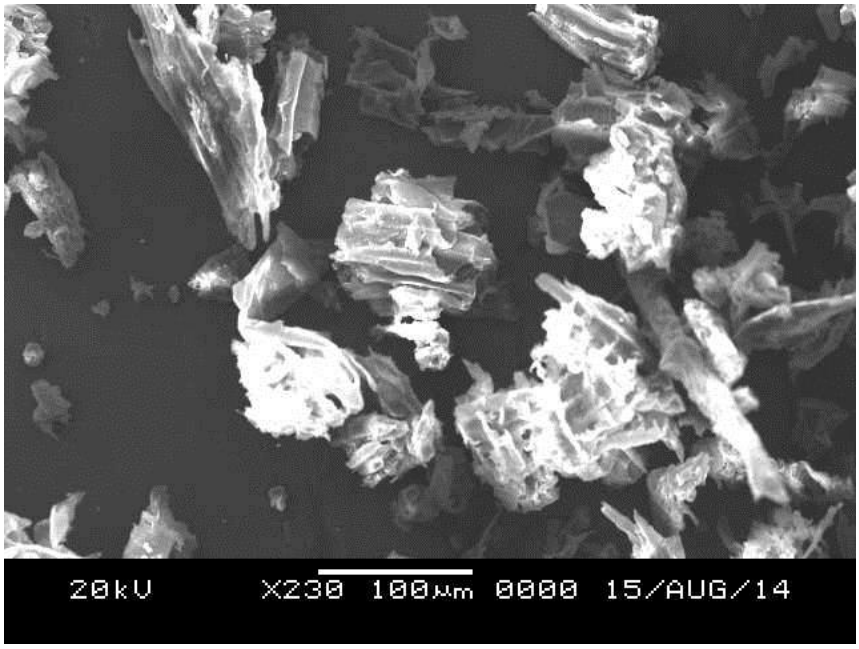

Figure 40: SEM 100 micron scale

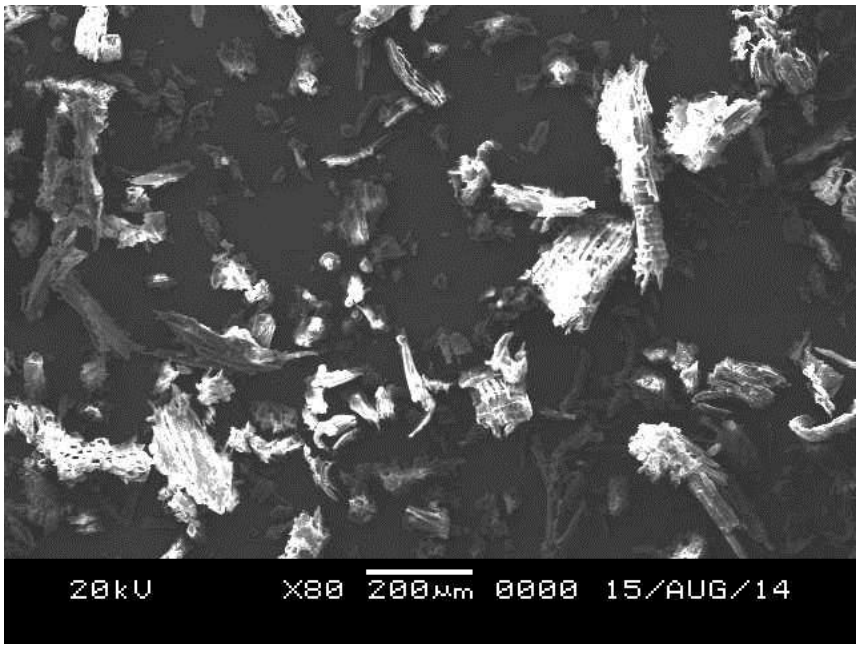

Figure 41: SEM 200 Micron Scale

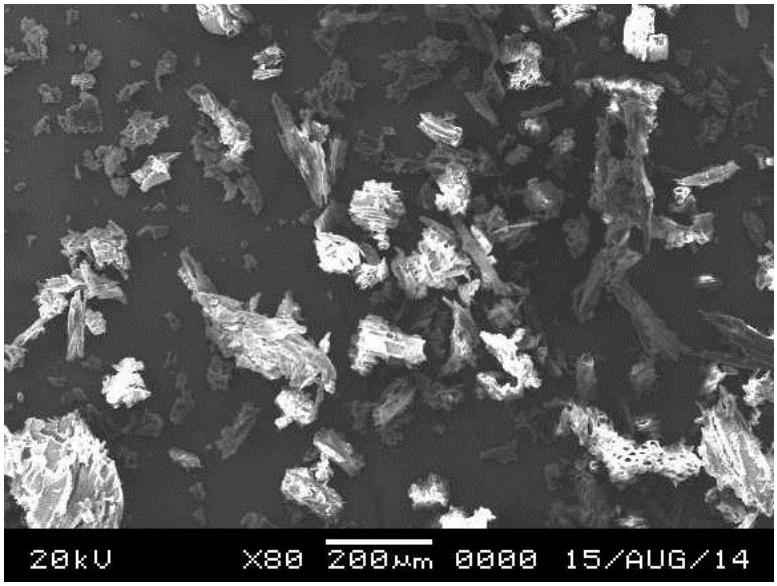

Figure 42: SEM 200 Micron Scale

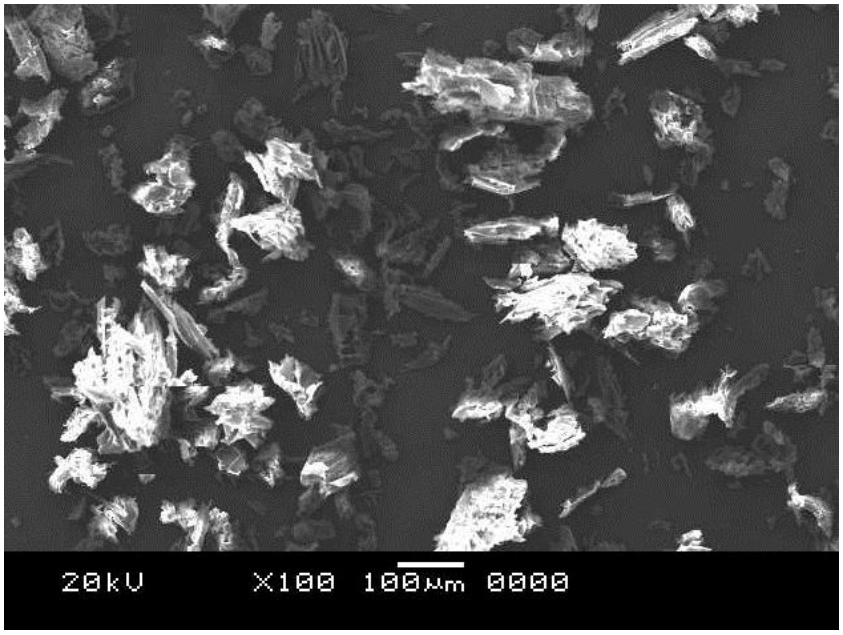

Figure 43: SEM 100 Micron Scale

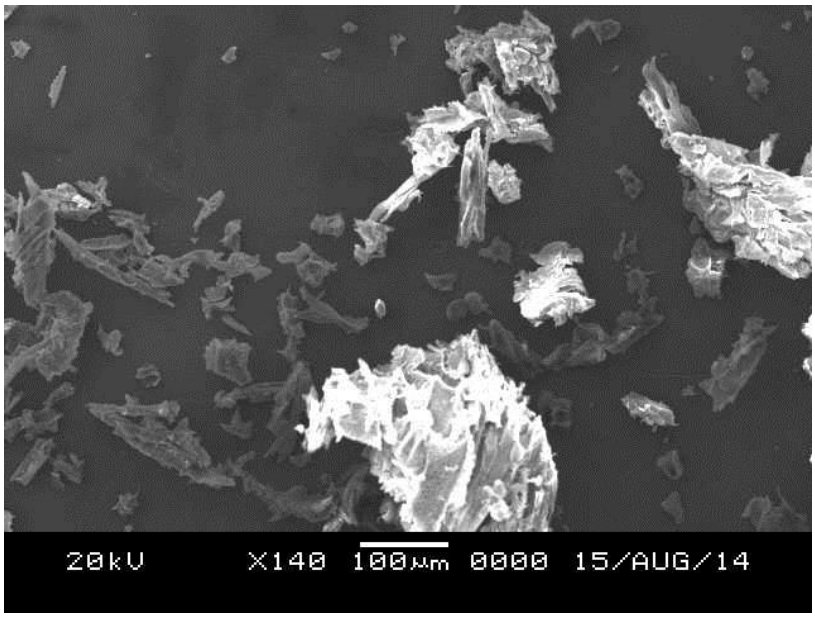

Figure 44: SEM 100 Micron Scale

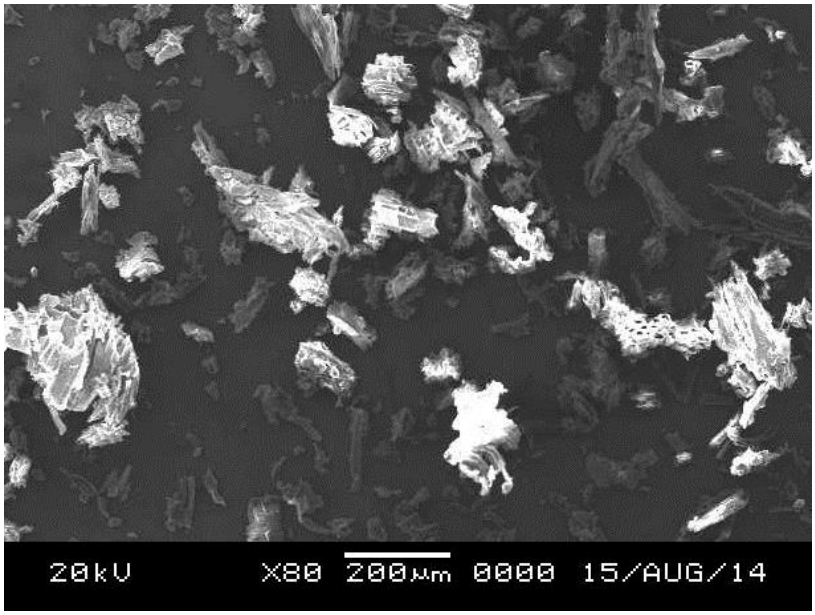

Figure 45: SEM 200 Micron Scale

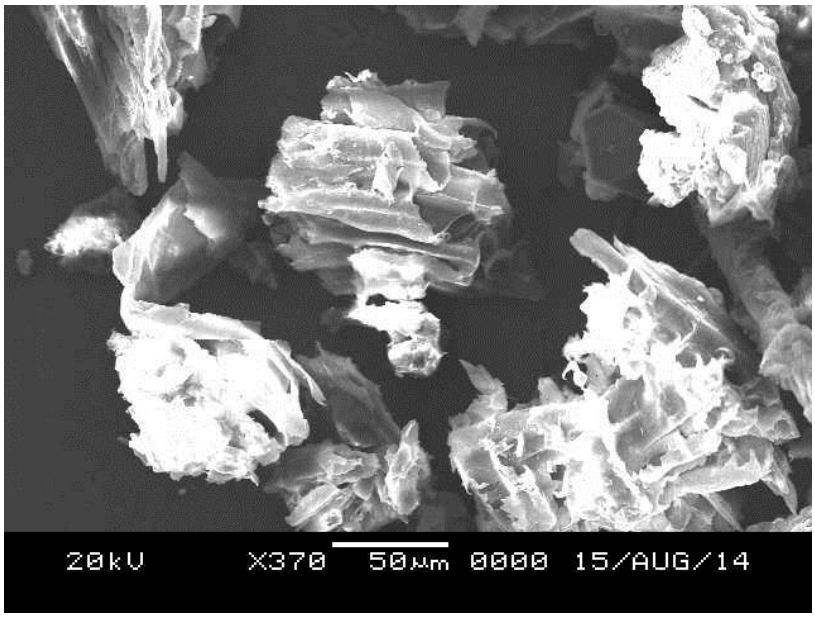

Figure 46: SEM 50 Micron Scale

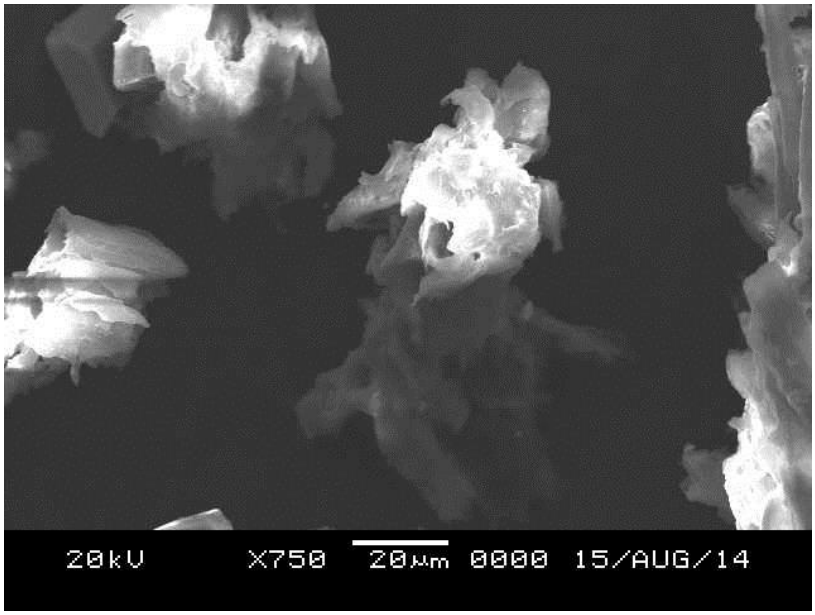

Figure 47: SEM 20 Micron Scale

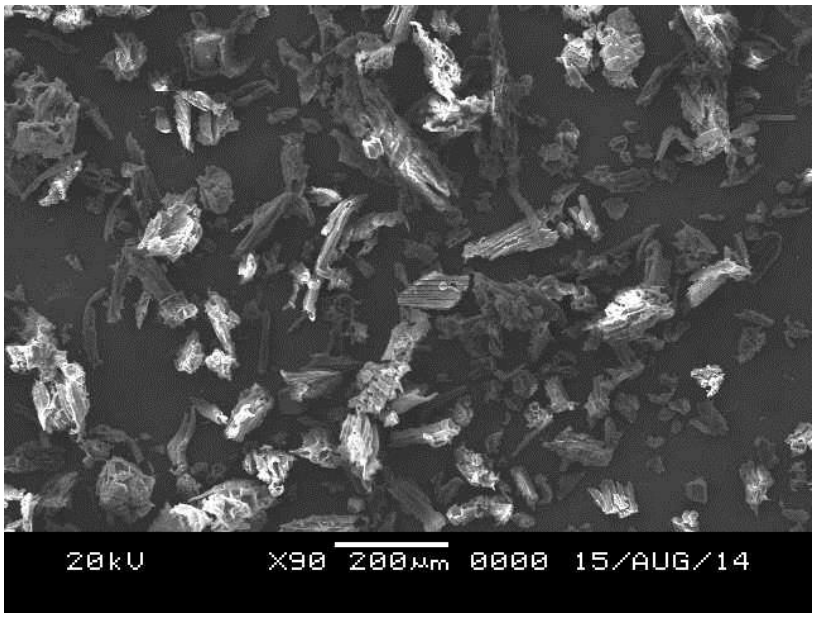

Figure 48: SEM 200 Micron Scale

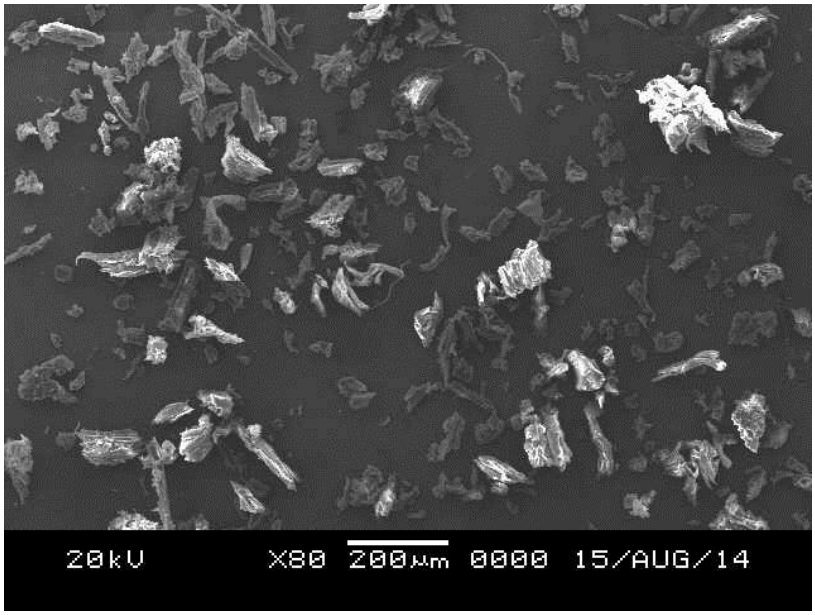

Figure 49: SEM 200 Micron Scale

APPENDIX B : LABVIEW BACK-END

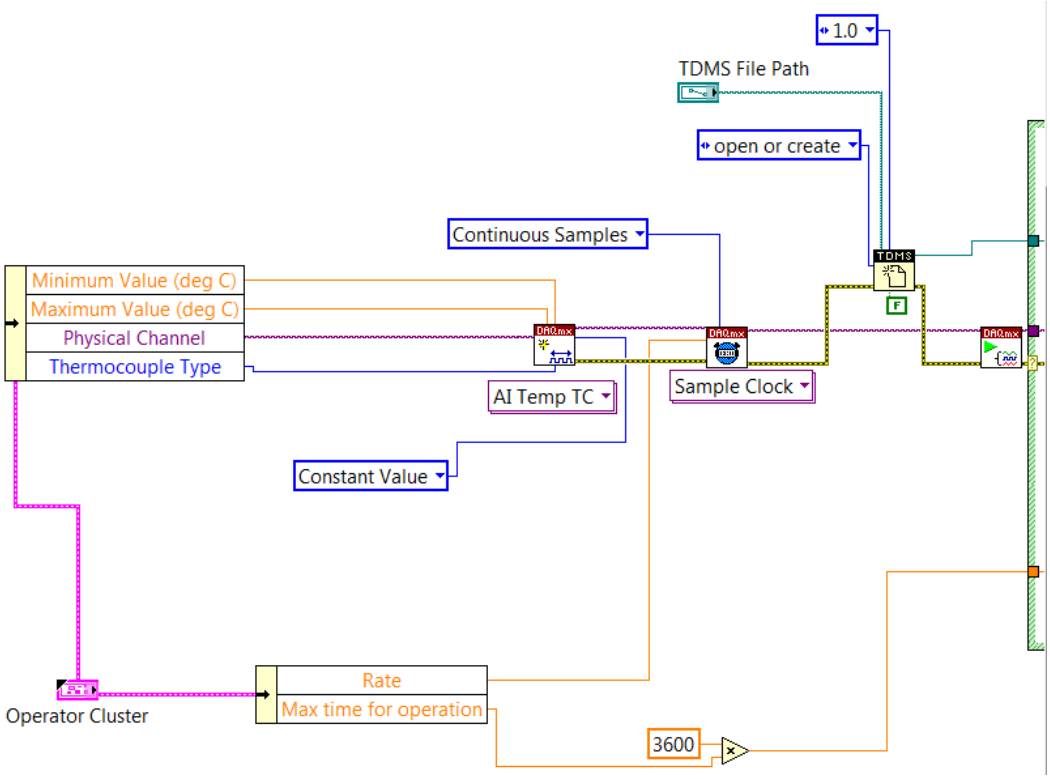

Figure 50: Back-end of LABVIEW coding environment, view of inputs

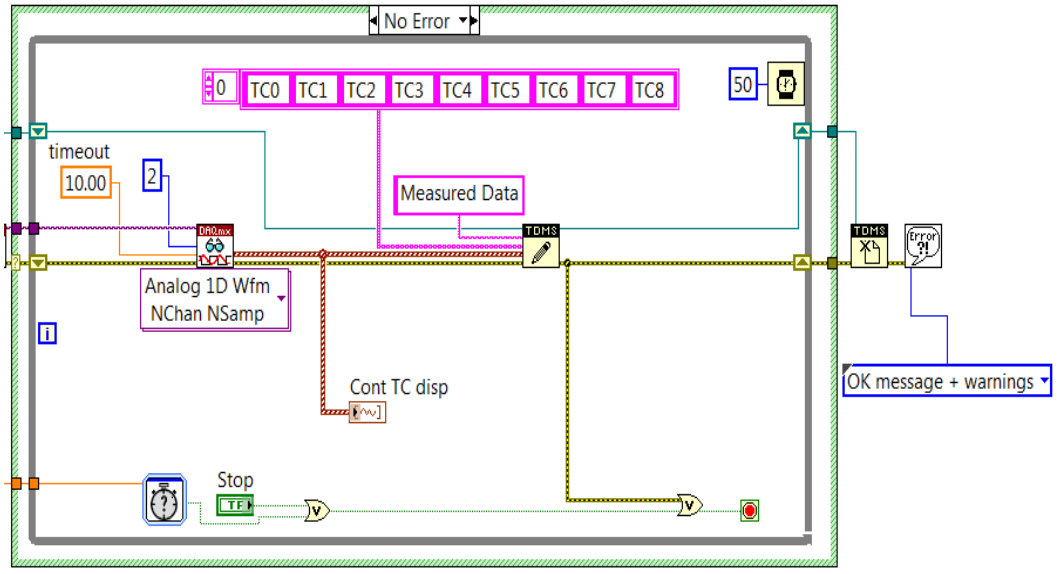

Figure 51: Back-end of LABVIEW coding environment, internal thermocouple processes

References

[1] E. Rehfuess, “Fuel for Life: Household Energy and Health,” Geneva, 2006.

[2] D. Haluza, A. Kaiser, H. Moshammer, C. Flandorfer, M. Kundi, and M. Neuberger, “Estimated health impact of a shift from light fuel to residential wood-burning in Upper Austria.,” *J. Expo. Sci. Environ. Epidemiol.*, vol. 22, no. 4, pp. 339–43, 2012.

[3] E. Hedberg, A. Kristensson, M. Ohlsson, C. Johansson, P. Å. Johansson, E. Swietlicki, V. Vesely, U. Wideqvist, and R. Westerholm, “Chemical and physical characterization of emissions from birch wood combustion in a wood stove,” *Atmos. Environ.*, vol. 36, no. 30, pp. 4823–4837, 2002.

[4] M. E. M, A. Lopez, A. Rodgers, S. Vander Hoorn, and C. Murray, “Selected major risk factors and global and regional burden of disease.,” *Lancet*, vol. 360, no. 9343, pp. 1347–1360, 2002.

[5] C. for D. C. and Prevention, “Centers for Disease Control and Prevention: Carbon Monoxide,” 1994. [Online]. Available: http://www.cdc.gov/niosh/idlh/630080.html. [Accessed: 01-Jan-2015].

[6] Environmental Protection Agency, “Overview of Greenhouse Gases: Methane Emissions.” [Online]. Available: http://www3.epa.gov/climatechange/ghgemissions/gases/ch4.html. [Accessed: 01-Jan-2015].

[7] R. M. Rowell and M. A. Dietenberger, “Thermal Combustion , and Fire Retardancy of Wood,” *Handb. Wood Chem. Wood Compos.*, pp. 127–149, 2013.

[8] B. Y. J. A. D. Ahlman and W. C. Harlie, “Sawdust Cookstove,” no. 239, 2001.

[9] M. Ortega, “Improved combustion in wood stoves,” no. August, 2008.

[10] J. J. Jetter and P. Kariher, “Solid-fuel household cook stoves: Characterization of

performance and emissions," *Biomass and Bioenergy*, vol. 33, no. 2, pp. 294–305, Feb. 2009.

[11] A. F. Roberts, "A review of kinetics data for the pyrolysis of wood and related substances," *Combust. Flame*, vol. 14, no. 2, pp. 261–272, 1970.

[12] H. Yang, R. Yan, H. Chen, D. H. Lee, and C. Zheng, "Characteristics of hemicellulose, cellulose and lignin pyrolysis," *Fuel*, vol. 86, no. 12–13, pp. 1781–1788, 2007.

[13] C. C. Lo, "Characteristics of Smoldering Combustion of Sawdust," University of Texas at Austin, 2013.

[14] K. W. Ragland, D. J. Aerts, and a. J. Baker, "Properties of wood for combustion analysis," *Bioresour. Technol.*, vol. 37, no. 2, pp. 161–168, 1991.

[15] T. J. Ohlemiller, "Modeling of smoldering combustion propagation.pdf," *Prog. Energy Combust. Sci.*, vol. 11, no. 4, pp. 277–310, 1985.

[16] T. J. Ohlemiller, "Smoldering Combustion," *SFPE Handb. Fire Prot. Eng.*, pp. 200–210, 2002.

[17] William C. Hinds, *Aerosol technology*, vol. 14, no. 2. 1983.

[18] S. Mudgal, A. Turbe, and I. Kuwahara, "Preparatory Studies for Eco-design Requirements of Eups (II)," vol. 33, no. December, pp. 1–100, 2009.

[19] I. Manual, "Model 400A Hydrocarbon Analyzer," no. December, 2008.

[20] T. L. B. Yelverton, A. L. Holder, and J. Pavlovic, "Emissions removal efficiency from diesel gensets using aftermarket PM controls," *Clean Technol. Environ. Policy*, vol. 17, no. 7, pp. 1861–1871, 2015.

[21] Environmental Protect Agency, "Method 202."

[22] F. Preto, “Pyrolysis, Char and Energy,” in *The Canadian Biochar Initiative, Inaugural Meeting*, 2008, p. 46pp.

[23] T. J. Ohlemiller, “Smoldering COMBUSTION,” pp. 171–179.

[24] C. Robinson and D. B. Smith, “The auto-ignition temperature of methane,” *J. Hazard. Mater.*, vol. 8, pp. 199–203, 1984.

[25] T. H. Greiner, “Carbon Monoxide Poisoning: Checking for Complete Combustion (AEN-175),” *Department of Agricultural and Biosystems Engineering, Iowa State University*, 1997. [Online]. Available: http://www.abe.iastate.edu/extension-and-outreach/carbon-monoxide-poisoning-checking-for-complete-combustion-aen-175/. [Accessed: 11-Nov-2015].